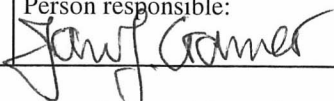


# GEOLOGI FOR SAMFUNNET

*GEOLOGY FOR SOCIETY*



Report no.: 2013.005		ISSN 0800-3416	Grading: Confidential until 31.12.2013	
Title: Sandwaves and sand transport on the Barents Sea continental margin				
Authors: Reidulv Bøe, Monica Winsborrow, Leif Rise, Margaret Dolan, Shyam Chand, Jochen Knies, Olav Walderhaug and Valerie Bellec			Client: Norwegian Deepwater Programme (NDP)	
County:			Commune:	
Map-sheet name (M=1:250.000)			Map-sheet no. and -name (M=1:50.000)	
Deposit name and grid-reference:			Number of pages: 85	Price (NOK): 300,-
			Map enclosures:	
Fieldwork carried out: 2012	Date of report: 31 <sup>st</sup> January 2013	Project no.: 342000	Person responsible: 	
<p>Summary:</p> <p>Sandwaves are common on many continental shelves indicating erosion, transport and deposition of sand by bottom currents. Their dynamic nature means that they can pose challenges to seafloor installations such as pipelines and other constructions on the seafloor. For studies of pollution and seabed resources (biological and geological) it is necessary to know where erosion and deposition occur. Detailed observations and descriptions of sandwaves as well as correct interpretation of their sedimentary environment are of importance for both industry and government for management of the ocean areas.</p> <p>Sandwaves occur at 500-800 m depth on the western Barents Sea continental margin and are most prolific in two areas. Video data acquired under the MAREANO programme (<a href="http://www.mareano.no">www.mareano.no</a>) indicated that the sandwaves are mainly composed of well-sorted sand, with some gravel occurring between sandwaves, but no samples for detailed studies of the sand and gravel were available prior to the present project. The well-sorted sand indicates a strong current (the North Atlantic Current, NAC) towards the NNW at this depth.</p> <p>A marine geological cruise to the south-western Barents Sea slope was carried out by R/V G.O. Sars in 2012 to acquire datasets for use in this project. The primary data collected were TOPAS and grab/gravity core samples. In addition, ADCP data was collected for analysis by the Institute for Marine Research (IMR). In total, 1144 km of TOPAS data were collected, along with sampling at 38 grab stations and 14 gravity core stations. During three other cruises in 2011-2012, by the University of Tromsø (UiT) (two cruises) and the Norwegian Defence Research Establishment (FFI), remapping of parts of the sandwave areas by multibeam echosounder was undertaken in order to compare these datasets with similar data collected by MAREANO in 2008-2009 and to study possible migration of sandwaves.</p> <p>This report, along with two earlier reports, summarizes project results obtained by NGU. The results are to be integrated with project results obtained by IMR and UiT and will be published in scientific journals.</p>				
Keywords: Marine geology	Sandwaves	Sand transport		
Gravity core	Grab	Seabed sediment		
Multibeam bathymetry	Mineralogy	Grain size		

## CONTENTS

1. INTRODUCTION.....	4
2. STUDY AREA.....	10
2.1 Geological setting .....	10
2.2 Oceanography .....	10
2.3 Bathymetry .....	11
3. METHODS.....	11
3.1 TOPAS sub-bottom profiler data.....	11
3.2 Sediment analyses.....	14
3.3 Multibeam data .....	15
3.3.1 MAREANO data .....	15
3.3.2 UiT data.....	16
3.3.3 FFI data .....	16
4. RESULTS.....	18
4.1 Seismic stratigraphy .....	18
4.2 Sand distribution and extent of sandwave fields .....	22
4.3 Sand thickness .....	22
4.4 Grain-size analysis.....	32
4.4.1 Grain-size distribution.....	32
4.4.2 Statistical analyses of grain-size distribution.....	36
4.4.3 Comparison of grain-size parameters within sandwave fields.....	38
4.5 Calcium carbonate content .....	39
4.6 Petrographic analysis .....	41
4.7 Physical and geotechnical properties.....	43
4.8 AMS <sup>14</sup> C dating .....	43
4.9 Multibeam data analysis .....	45
4.9.1 Comparison of bathymetric data quality .....	45
4.9.2 Terrain analysis of bathymetry data .....	48
4.9.3 Analysis of backscatter data.....	54
5. DISCUSSION OF SAND SOURCE AND TRANSPORT DIRECTION .....	57
6. SUMMARY AND FURTHER WORK .....	59
7. REFERENCES.....	61

## 1. INTRODUCTION

Sandwaves have been widely documented across continental shelves around the world, including Norway (Rise et al. 1996, Bøe et al. 2009), and to a lesser degree from slope and canyon environments (Faugères et al. 1999). Their formation requires the operation of strong currents to erode, transport and deposit sands, however, numerous local variations in topography, sediment availability, hydrodynamic regime and global variations in climate and sea-level will influence their formation, distribution and evolution. The dynamic nature of sandwaves can present a navigation hazard in shallow areas and poses difficulties for seafloor installations such as pipelines. Detailed studies of sandwaves in deepwater environments are limited, but with increasing availability of high resolution marine geophysical and oceanographic datasets, we now have the potential to gain a better understanding of how sandwaves form and evolve.

Sandwaves were identified on the Barents Sea continental margin, offshore Norway during the MAREANO programme ([www.mareano.no](http://www.mareano.no)) (Figs. 1 and 2). A Norwegian Deepwater Programme (NDP) project entitled “Sand waves and sand transport on the continental margin offshore Norway” (Contract No. 4502202750 between Statoil Petroleum AS and NGU) was initiated in 2011 to study these in greater detail. Project partners are NDP, NGU, IMR and UiT. Key objectives of the project are to investigate:

- Sedimentary processes leading to sandwave formation
- Mode of evolution of the sandwaves
- The role of seabed currents in the formation and maintenance of the sandwaves

The data discussed in this report were collected during cruises to the study area in 2012. A marine geological cruise with R/V G.O. Sars 11-18 April 2012 collected 1144 km TOPAS data and sampling was performed at 38 grab stations and 14 gravity core stations (Figs. 3-5). A full cruise report gives details of the equipment used and the datasets collected during the cruise (Winsborrow et al. 2012). Remapping of parts of the sandwave fields by multibeam echosounder to collect data for a study of sandwave migration was done during two cruises, one by UiT and one by FFI.

The first year of the project focused on using existing datasets collected by the MAREANO programme to characterize the morphology of the sandwave fields. This primarily involved statistical analysis of multibeam bathymetry, in addition to analyses of videos and limited sub-bottom profiler datasets (King et al. 2011). Based on the MAREANO multibeam bathymetry, the extent of sandwaves on the continental slope was mapped. Detailed morphometric description of the sandwaves was also carried out, and they were found to have a mean height of 0.7 m and a maximum of 5.5 m. The mean wavelength (measured from crest to crest) was estimated to 58 m, ranging from 15 m to 205 m.

Robust statistical analyses presented several indices which suggested a clustering or domains of bedforms which are somewhat tuned to the meso-morphology of the terrain in which they lie, a terrain inherited from glacial processes (King et al. 2011). This suggested that there is a much more complex hydrologic regime than a simple continuous northward contour current which drives the bedforms. Local steering, current acceleration and perhaps induced turbulence were suggested. An upward driving hydrologic component must be able to balance mid-term tendencies of down-slope grain migration. The complexity suggested provided support for the initial hypothesis that relatively unique and poorly understood oceanic conditions are at play, possibly including tidal-wave driven internal waves channelled on the thermocline and tied to interaction with the slope near the shelf break. All indications suggested active bedform mobility.

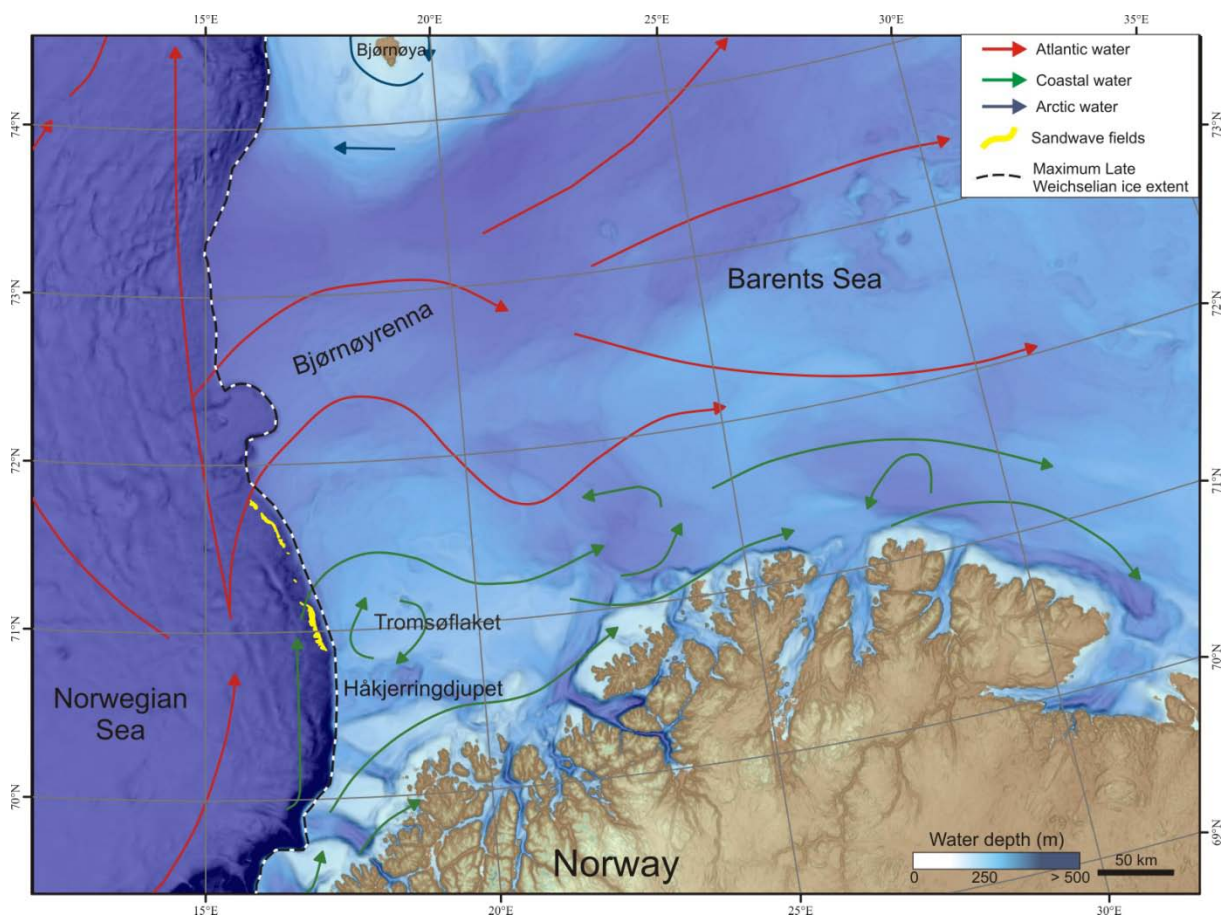
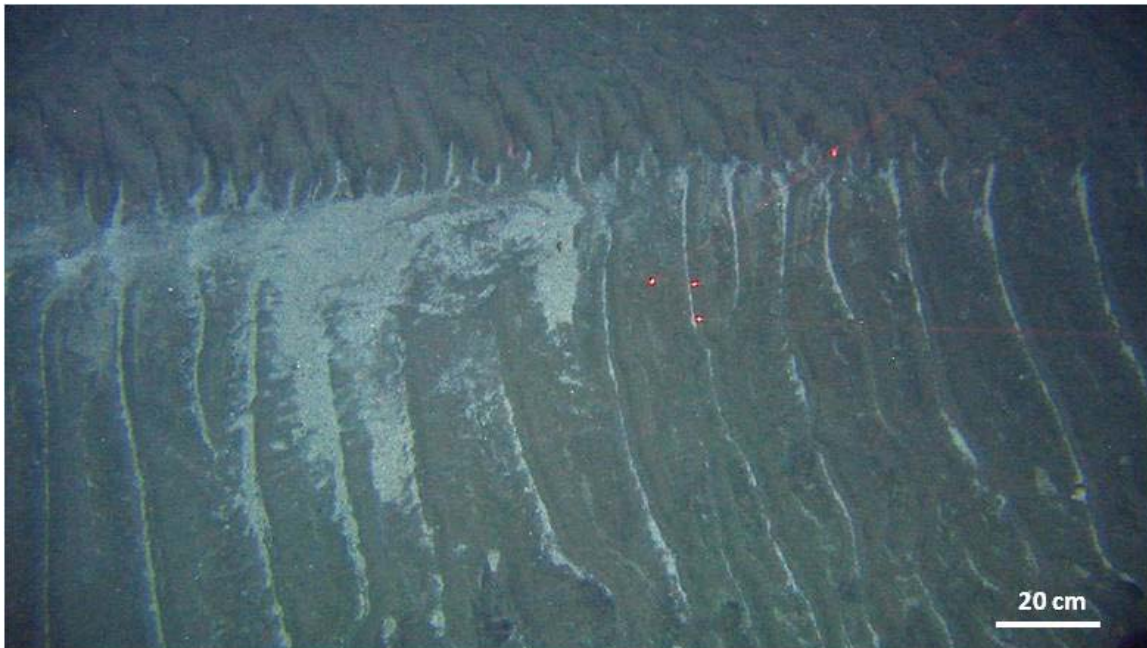


Figure 1. Bathymetric map of the south-western Barents Sea and continental slope showing the location of the sandwave fields and the approximate distribution of surface ocean currents. Surface currents from [www.mareano.no](http://www.mareano.no), ice extent from Svendsen et al. (2004).

A major component of the present project is mapping and modelling of bottom currents. IMR is responsible for development of 800 m and 160 m bottom current modelling grids, oceanographic measurements including current measurements with rigs on the seabed in the sandwave area, and current modelling based on these data. The results are underway and will

be published in reports and integrated with the geological data during the last phase of the project in 2013.



*Figure 2. Still image from CAMPOD video transect within the N1 sandwave field. This shows the crest of a sandwave with superimposed sand ripples (wavelengths approximately 10 cm), semi-perpendicular to the sandwave crest. Shells (white) are seen accumulated on the leeward side of sand ripples. Distance between red laser dots is 10 cm. Source: MAREANO ([www.mareano.no](http://www.mareano.no)). See Fig. 3 for location.*

An additional activity in this project has involved University of Tromsø (UiT) using their Geosystems 3D P-Cable seismic system to acquire 3D seismic data in two target areas. The acquisition of high-resolution 3D seismic data ideally complements the survey activities of NGU in that it supplements and allows a 3-dimensional characterization of sand waves and the subsurface geology. It was envisaged that this would provide a better understanding of the development, dynamics and depositional setting of the sandwaves. Several cruises have been undertaken and one masters thesis has been published (Waage 2012). The results of the studies will be integrated with NGU's and IMR's results during the last phase of this project.

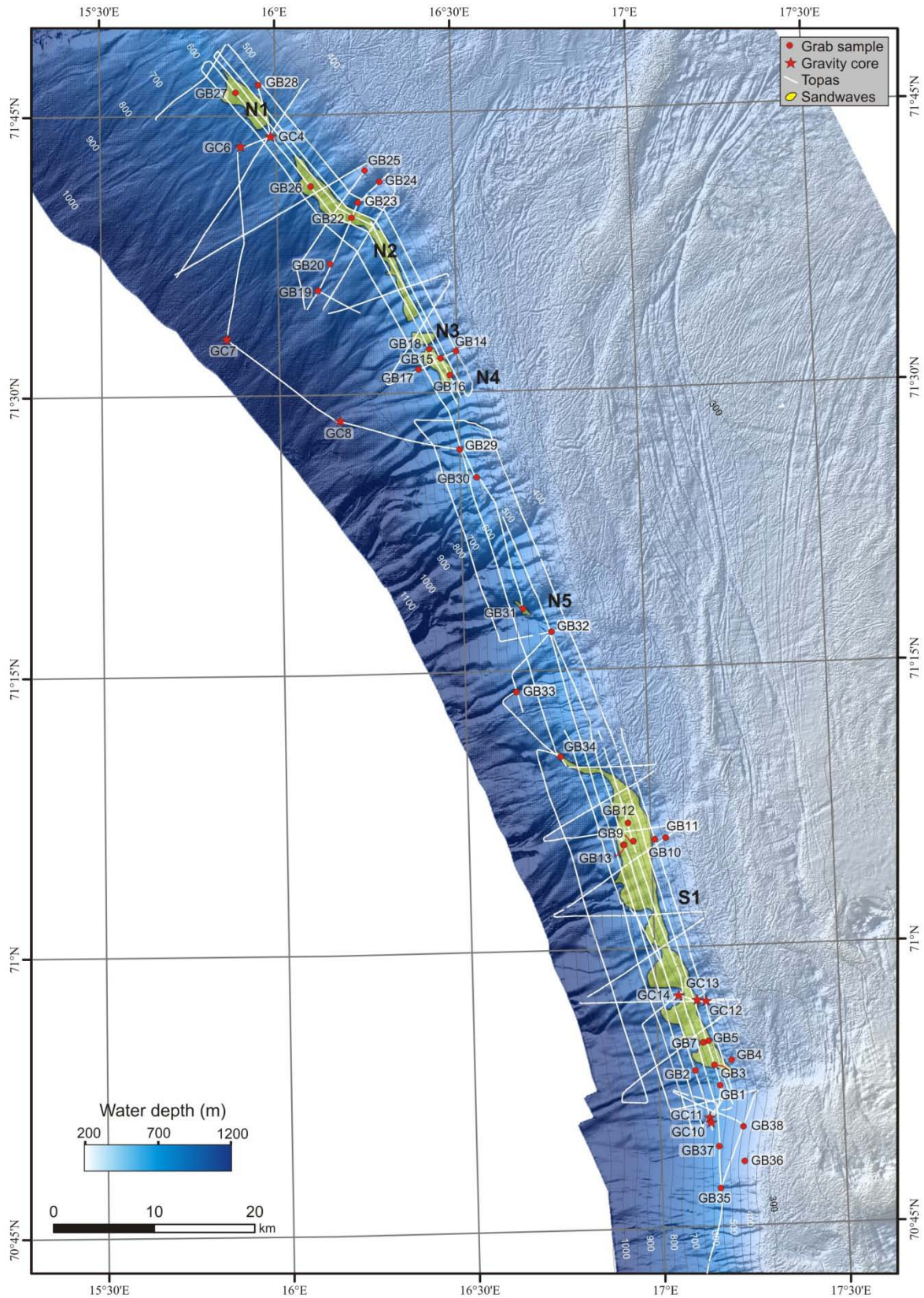


Figure 3. Datasets sub-bottom profiler, grab samples and gravity cores analyzed in this report. From MAREANO's multibeam bathymetry, five separate fields were mapped. These were named N1, N2, N3, N4 and S1 by King et al. (2011) and the same names will be used in this report.

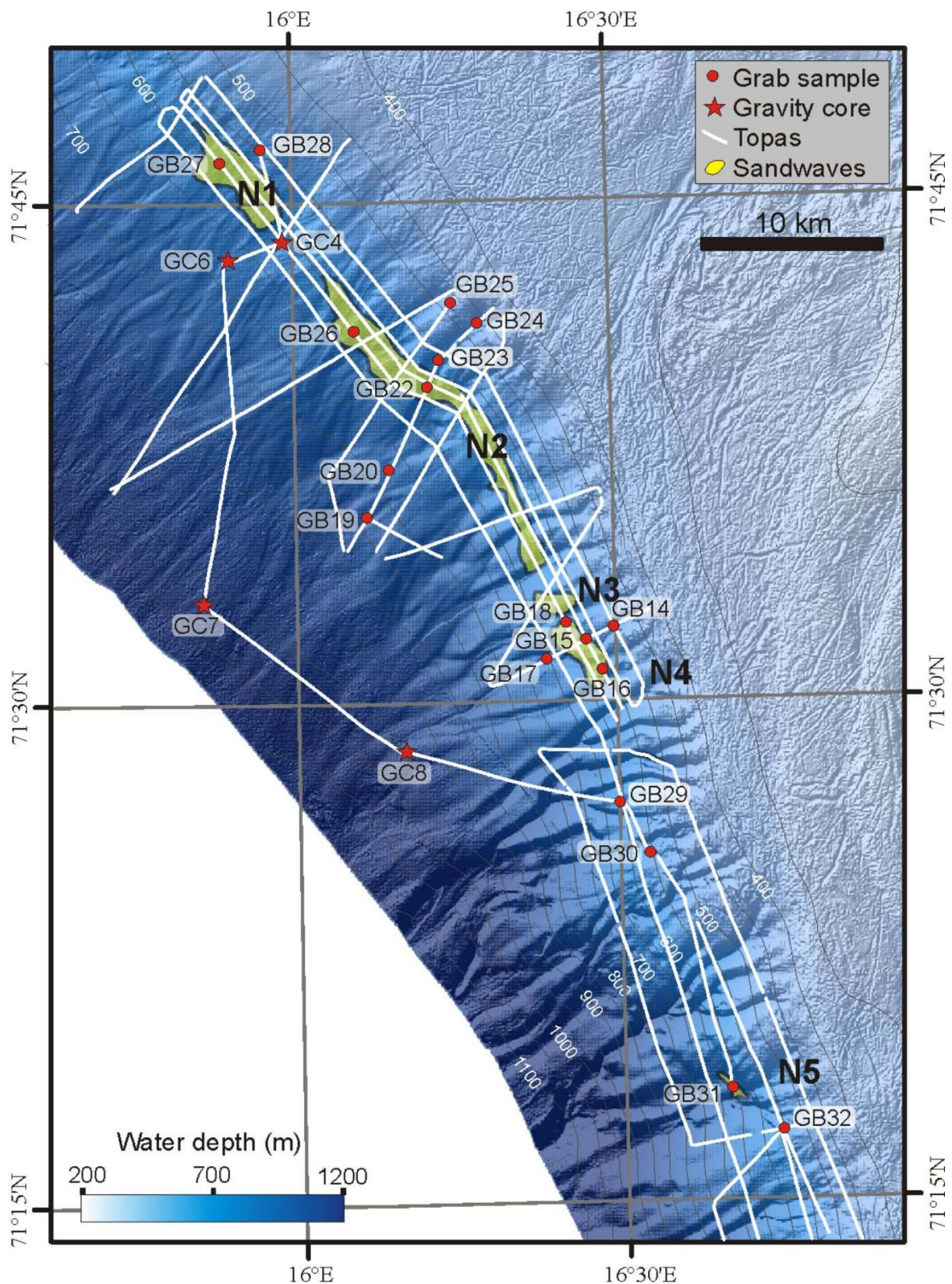


Figure 4. Datasets sub-bottom profiler, grab samples and gravity cores from the northern part of the study area.



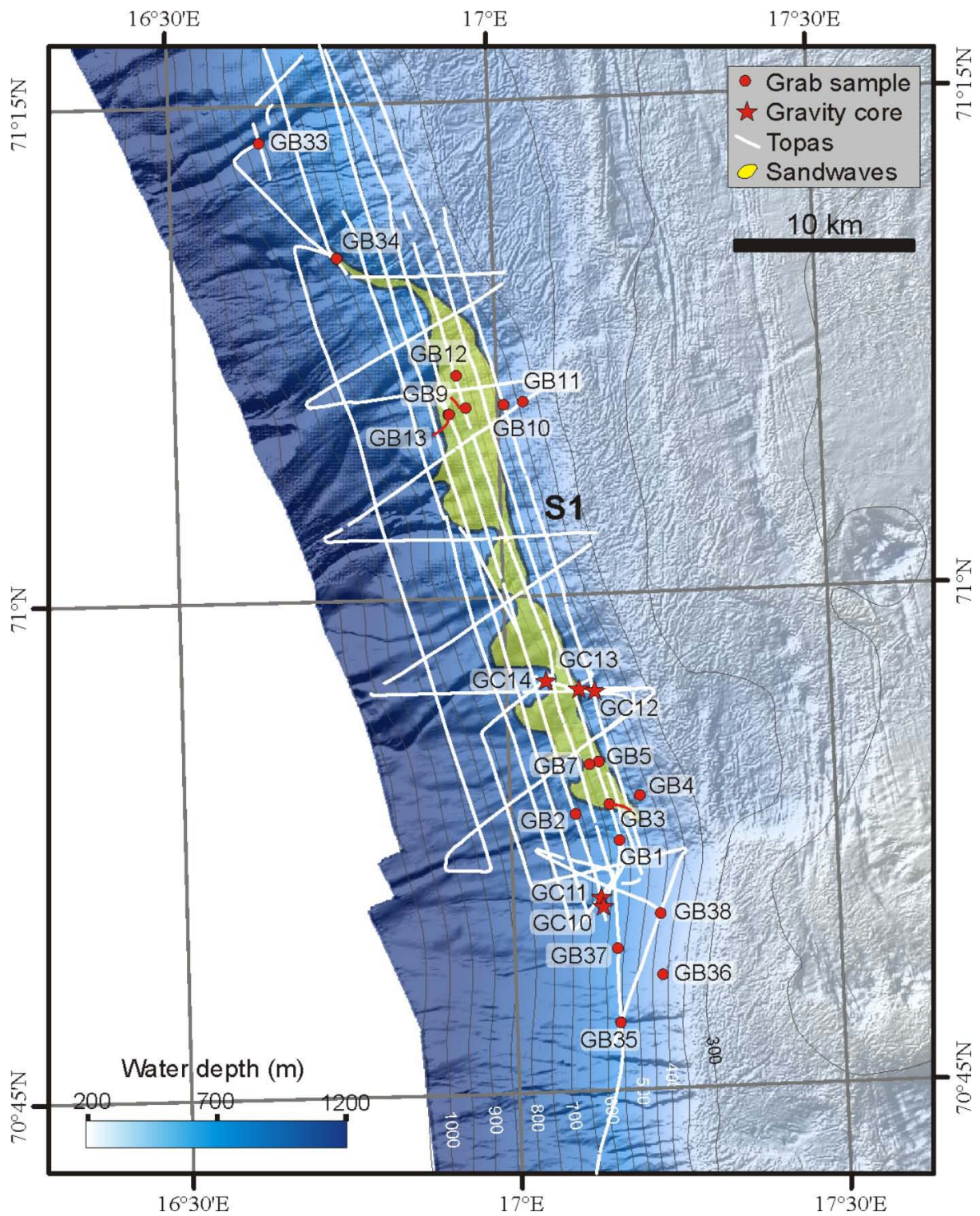


Figure 5. Datasets sub-bottom profiler, grab samples and gravity cores from the southern part of the study area.

## **2. STUDY AREA**

### **2.1 Geological setting**

The sandwave fields are located on the upper part of the continental slope in the south-western Barents Sea, between 500 m and 800 m water depth (Fig. 1). This area marks the transition from the deep Norwegian Sea to the epicontinental Barents Sea. The continental shelf offshore northern Norway has been glaciated multiple times during the Late Cenozoic (Vorren et al. 1988, Sættem et al. 1992), and during the most recent glaciation (late Weichselian) it lay at the confluence of the Fennoscandian and Barents Sea ice sheets (Vorren and Kristoffersen 1986, Landvik et al. 1998, Winsborrow et al. 2010). During maximum glaciation, the ice sheets covered the entire continental shelf, reaching the shelf edge. Major ice streams operated in cross-shelf troughs including Bjørnøyrenna and Håkjerringdjupet at this time (Fig. 1), discharging large volumes of sediment and meltwater (Vorren and Laberg 1996, Ottesen et al. 2008, Winsborrow et al. 2010). Chronological control is limited, however the few available dates suggest that initial ice retreat from the shelf edge occurred prior to c. 17 100-16 600 calendar years before present (cal. BP) (Rüther et al. 2011).

The south-western Barents Sea continental slope is characterized by multiple buried and seafloor downslope channels (Laberg and Vorren 1995, Laberg et al. 2010) (Fig. 3). These document glacial debris flow and meltwater discharge during glacial periods, as well as slides and mass-movement activity. Sandwave fields N1 and N2 are located in a relatively smooth part of the slope (Fig. 4), with fewer channels and slide activity. In contrast, sandwave fields N3, N4, N5 and S1 are located in a part of the slope which is steeper with more abundant channels and slide scars (Figs. 4, 5).

### **2.2 Oceanography**

Three ocean current systems occupy the south-western Barents Sea continental slope. The Norwegian Current flows north-easterly along the coastline of northern Norway at depths of 50-100 m (Fig. 1). This carries coastal water which is relatively fresh and exhibits large seasonal temperature variation. Outside and beneath this coastal water is Atlantic water, brought in by the North Atlantic Current. This water mass is more saline and has a relatively high temperature with little seasonal variation. Beneath this is the cooler, fresher intermediate water. The sandwaves lie at the water depth range where a marked (and migrating) thermocline marks the boundary between the main contour currents (King et al. 2011). Preliminary oceanographic modeling by the Institute of Marine Research (IMR) indicates considerable variability in bottom current strength, with the strongest current flowing northwards along the upper continental slope (Ådlandsvik and Ostrowski 2010).

A more detailed numerical modeling of current variability, calibrated using new observational datasets is an essential part of this project. A three month time series of current data, from the depth interval 80-250 m above seabed, existed prior to the initiation of this project. In addition, as part of this project, moored rigs were set out within sandwave field N2 to measure current profiles in the lower 50-100 m above the seafloor. The oceanographic data are being interpreted by IMR and will be integrated with the geological data during the final part of the project.

### **2.3 Bathymetry**

The continental shelf break occurs at around 400 m water depth in the study area (Figs. 1 and 3-5). In the south, the distance between the shelf break and the glacial bank Tromsøflaket, to the east, is only a few kilometres. Northwards the distance increases. Water depths on Tromsøflaket vary from 115 m in the shallowest area in the south to c. 350 m in the north. The western margin of Tromsøflaket is characterized by N-S-trending very long and elevated moraine ridges.

The Bjørnøya Trough stretches eastwards from the shelf break in the north, with water depths on the shelf of 300-400 m. The slide escarpments of the Bjørnøya Slide (Fig. 3), that cuts into the shelf, are up to 100 m high. West of the shelf break, water depths increase gradually. The chutes on the slope west of Tromsøflaket are 30-40 m deep, while the braided and anastomosing channels on the sea bed further north are generally less than 1 m deep. Slide escarpments on the slope exhibit up to 50 m relief.

## **3. METHODS**

### **3.1 TOPAS sub-bottom profiler data**

The TOPAS sub-bottom profiler data were acquired with R/V G.O. Sars in 2012. Full methodological details of the data acquisition set-up are provided in the cruise report (Winsborrow et al., 2012). Herein is information on the methods used for data processing and interpretation.

Standard processing of TOPAS data involved the application of techniques for increasing gain with depth (TVG) and filtering and conversion to segy-format using TOPAS software. The data were then processed further using NGU software SEGY\_MOD to remove the water column delay introduced by the TOPAS system and to convert the location coordinates from geographic units to metres in UTM coordinate system. The data was converted from segy to jp2-format using segyjp2 developed by Bob Courtney at the Geological Survey of Canada

GSC). After these processing steps the data were ready for interpretation using Promax and a seismic viewer software (SegyJP2Viewer) also developed by B. Courtney a GSC. The TOPAS data are observed to have diffraction related noise within the sandwave areas (Fig. 6).

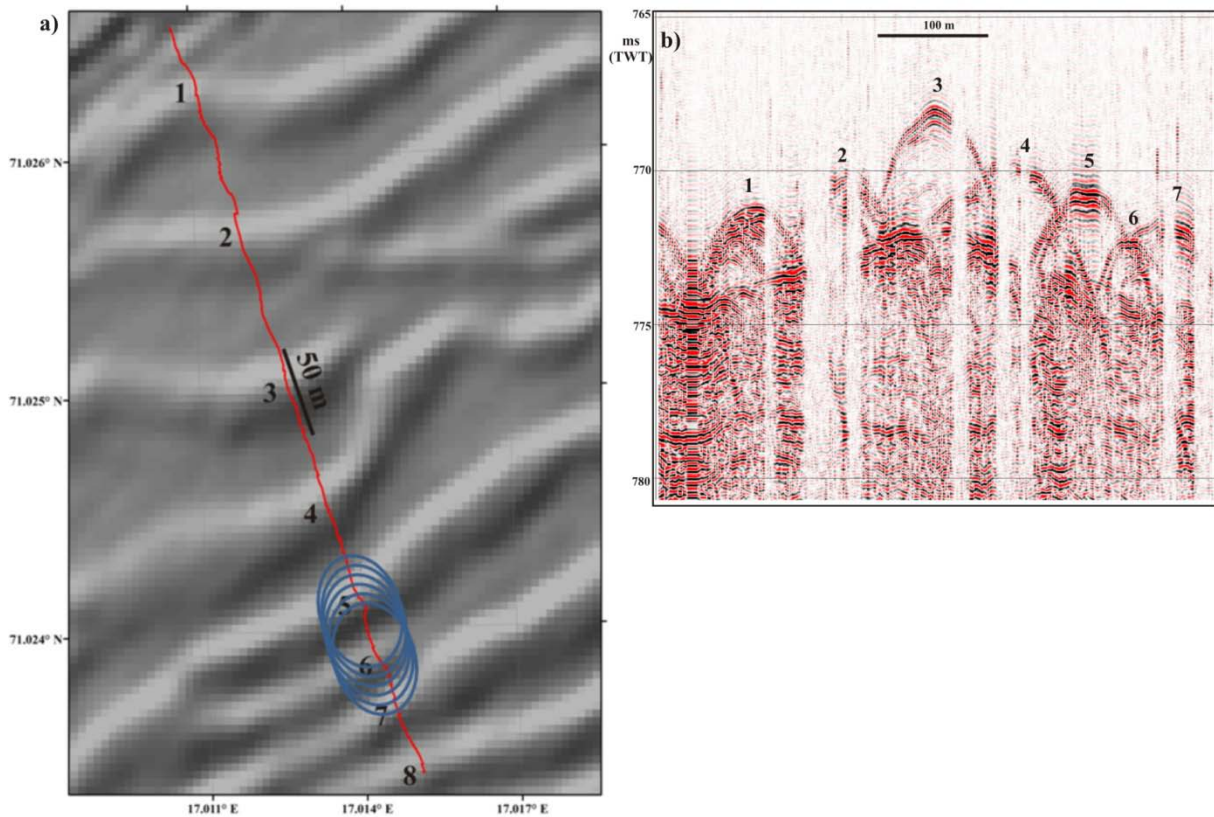


Figure 6. a) Multibeam bathymetry and TOPAS profile used for the special processing. Notice wave lengths (trough to trough distance) of sandwaves and also footprints of the TOPAS system (blue ellipses). b) TOPAS profile showing the sandwaves. Notice wide troughs observed in multibeam data which are not seen in TOPAS data due to diffractions.

The reasons for these hyperbolic reflections were investigated and special processing flows were designed in VISTA seismic processing software. The steps involved were as follows: 1) a TOPAS profile was selected in an area where the multibeam data showed large sandwaves (Fig. 6), 2) the TOPAS data were deconvolved using a spiking deconvolution filter, 3) as case 1, the deconvolved TOPAS data were migrated using a constant velocity model (1500 m/s) using different migration apertures, 4) as case 2, the deconvolved TOPAS data were migrated using a layered velocity model using different apertures.

The results indicate that the TOPAS data cannot be improved very much by migration since diffraction hyperbolas occur due to large footprint (60 x 40 m) of the TOPAS system at these water depths (~575 m). The footprints are comparable to the wavelengths of the sandwaves. The large across track footprint (40 m), though narrower than along track footprint (60 m), introduces diffractions from the sides of the sandwaves. This is especially apparent when the TOPAS line is not perpendicular to the sandwave and when the sandwave width changes

along its length. Along track diffractions are removed by migration, but due to the interaction between along and across track diffractions, the TOPAS data appear diffuse (Fig. 7). Comparisons between MAREANO multibeam bathymetry and TOPAS data show that sandwave crests occur at the same locations in the two datasets and that these can be used for estimating sand thickness.

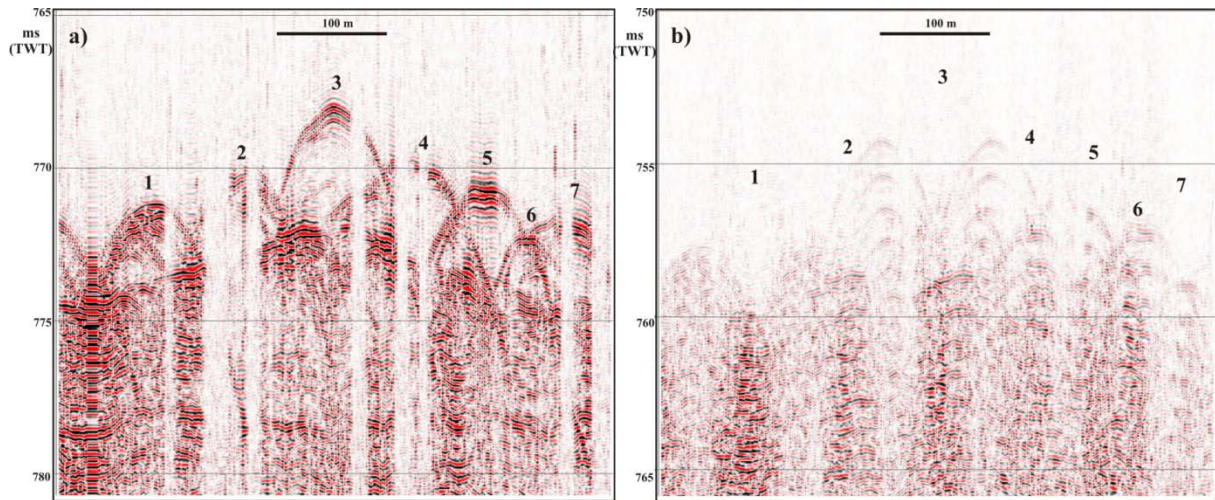


Figure 7. a) Unmigrated and b) migrated TOPAS seismic across sandwaves using migration aperture of 25 traces on both sides of sandwaves and increasing velocities with depth.

Interpretation of TOPAS data was carried out in Petrel and SegyJP2Viewer. The base of the sand layer was interpreted manually in Petrel. Mapping had to be carried out individually for each line, and this mapping could not be combined for the whole dataset, due to problems with correcting the dataset for tidal variations. Sand thickness was then estimated manually every 250 m along all seismic lines in Petrel (Fig. 8), assuming a sound velocity of  $1550 \text{ ms}^{-1}$ . These data were then input in ArcGIS for analysis and comparison with other datasets.

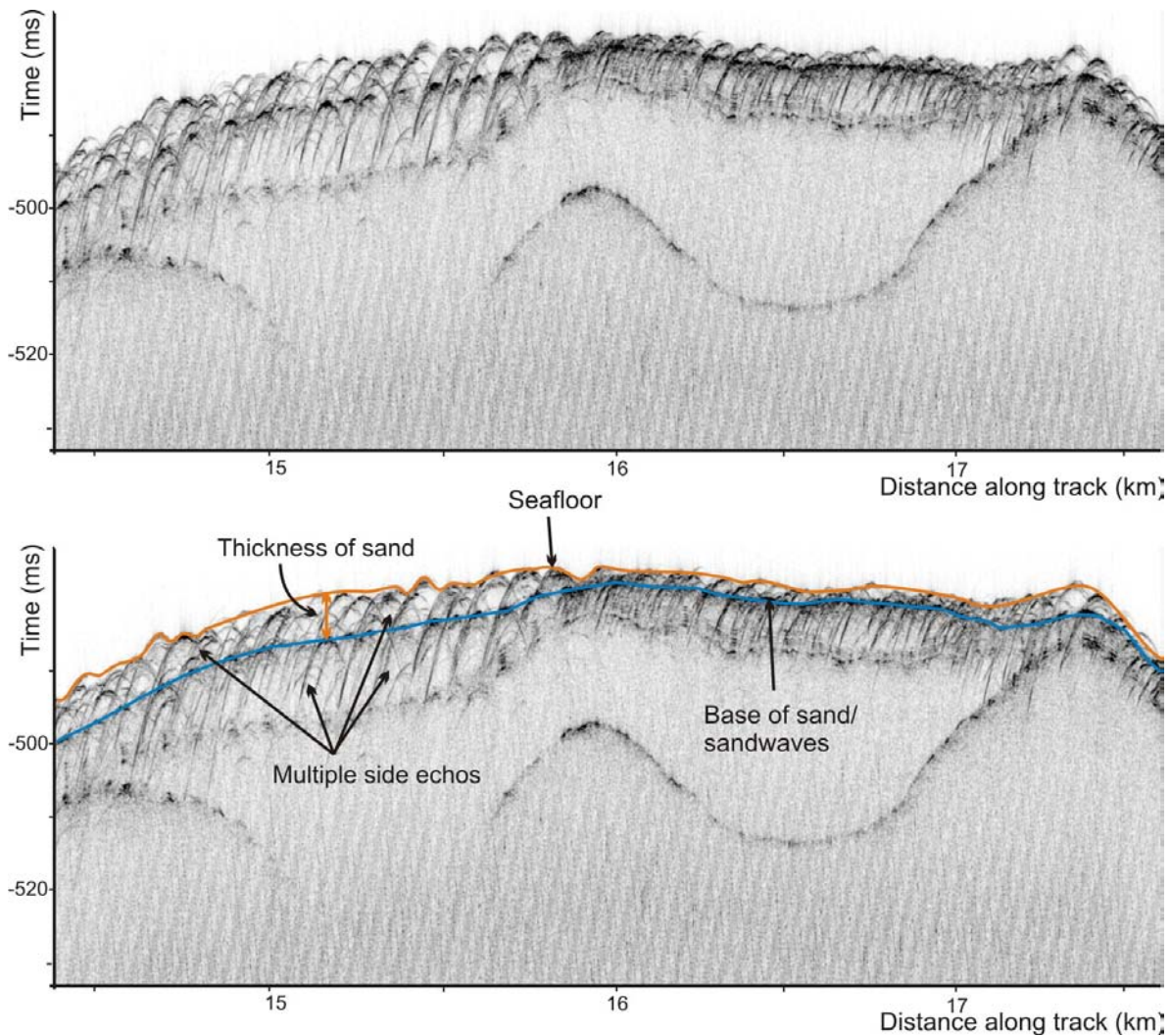


Figure 8. Example of TOPAS data collected in the sandwave area, and the way in which TOPAS data were used to estimate sand thickness. The upper image shows data without interpretation and the lower shows data with interpretation of seafloor and base of sand layer. In some locations, interpretation was not straight forward due to multiple side echos.

### 3.2 Sediment analyses

Analyses were carried out on 35 grab samples (GB) and 9 gravity cores (GC). All grab samples were described onboard according to NGU classification standards (SOSI-classification). Full details of acquisition methodology and logs for all grab samples are found in Winsborrow et al. (2012). Prior to opening the gravity cores, physical properties of the sediments (wet bulk density and magnetic susceptibility) were measured in the lab at NGU with a Multi Sensor Core Logger (MSCL). The cores were then opened, described, X-rayed and measured for undrained shear strength and water content (see Appendix 1 for core logs).

Undrained shear strength measurements were taken at selected intervals using the Swedish fall cone method. Weight and apex angle of the cone were determined by the expected undrained shear strength of the material. The fall cone was suspended just above the sediment

and then released. Depth of penetration of the cone into the material was then converted to kPa using a standard conversion table. Water content was determined by taking wet sediment samples at selected intervals throughout the core. These were weighed and then put into a drying oven at 105 °C for 24 hours, before weighing again. The water content is the weight of the water in percentage of the sediment's dry weight.

Particle size analysis was carried out on 35 grab samples and on 15 subsamples removed from the top layer of GC 4, 6, 7, 8, 10, 11 and 14. Analysis was carried out using a combination of wet sieving and Coulter laser particle counter. Coulter LS 200 at the NGU lab was used to determine particle size in the range 0.4-500 µm. For the fraction greater than 500 µm, wet sieving was used, with mesh sizes of 1, 2, 4 and 8 mm.

LECO analysis was carried out on 35 grab samples and 3 subsamples from the top layer of GC 4, 10 and 14. This analysis measures total organic carbon and total carbon content, and from this, calcium carbonate content was calculated using the following formula: (total carbon content - total organic carbon) x 8.33. This is based on the assumption that all inorganic carbon has been carbonated by marine life.

Visible shell fragments were removed for AMS <sup>14</sup>C dating at the <sup>14</sup>C CHRONO Centre, Queens University, Belfast. Gravity cores 10, 11, 14 had datable material at or close to the base of the sand unit. Due to uncertainties in the dating results, one extra sample was dated using foraminifera.

Petrographic thin sections were made from 14 grab samples collected within the sandwave fields (Figs. 3-5) (see Appendix 2 for photomicrographs). The thin section work has been done at Statoil.

### **3.3 Multibeam data**

#### **3.3.1 MAREANO data**

Multibeam data acquired by MAREANO provided the baseline data for this project (Fig. 9). The multibeam data include bathymetry and backscatter collected by the Norwegian Mapping Authority (NMA) and contractors during 2008-2009 using 3 different survey vessels – ‘Hydrograf’ (NMA), ‘Victor Hensen’ (FOSAE) and ‘Franklin’ (MMT). Each survey vessel was equipped with Kongsberg EM710 multibeam systems which were operated according to the NMA standards for multibeam mapping in MAREANO ([www.mareano.no](http://www.mareano.no)). Post-processing of the bathymetry data also followed these standards while backscatter data were processed by NGU using custom software from GSC (some data were later reprocessed using QPS-Fledermaus FMGT for comparison with FFI data - see below). Both bathymetry and backscatter data were of sufficient density to produce raster grids at 5 m resolution. It was

these data that facilitated initial identification of the sandwave fields that motivated this project. Following the MAREANO surveys, further multibeam datasets were acquired in 2011 and 2012 by UiT and FFI, giving a time series of comparable data in selected parts of the study area.

### 3.3.2 UiT data

Multibeam data were acquired in part of the northern sandwave study area (N2) by UiT in 2011 using their research vessel 'Helmer Hansen' (Fig. 9). These data were acquired opportunistically using a Kongsberg EM300 multibeam echosounder during a 3D P-Cable seismic survey of the area. In order to optimize seismic data quality, the survey operated at low survey speed and tight line spacing with the result that multibeam data density was superior to that normally obtained with an EM300 in these water depths. Following data cleaning (Kongsberg Neptune) these data were also of sufficient density for gridding at 5 m raster resolution (GMT). In 2012, UiT acquired more multibeam data in the southern sandwave study area (S1) using the same survey approach as in 2011. The bathymetry data were cleaned and gridded at 5 m resolution. Backscatter from the UiT surveys were not considered for comparative studies. This was due to the fact that a different multibeam echosounder was used, which operates with different beam geometry and at a lower frequency, thereby obtaining a different view of the seabed's acoustic response (backscatter).

### 3.3.3 FFI data

FFI conducted a multibeam survey specifically for this project in 2012 (Fig. 9). The survey collected data in both the northern and southern sandwave fields using a Kongsberg EM710 multibeam echosounder on board the research vessel 'H.U. Sverdrup'. The survey acquired good quality bathymetry and backscatter data that could be directly compared with the MAREANO data from 2008-2009. Bathymetry data were cleaned by FFI and gridded to 5 m resolution by NGU. Backscatter data were processed by NGU using QPS-Fledermaus FMGT to produce raster mosaics at 3 m resolution.

All available multibeam bathymetry data were assessed for data quality and subject to terrain analysis to derive morphometric indices (e.g. slope, curvature) and feature classifications that could be used to assess detectable changes in the sandwaves between datasets. Backscatter data were also assessed for the MAREANO and FFI datasets.



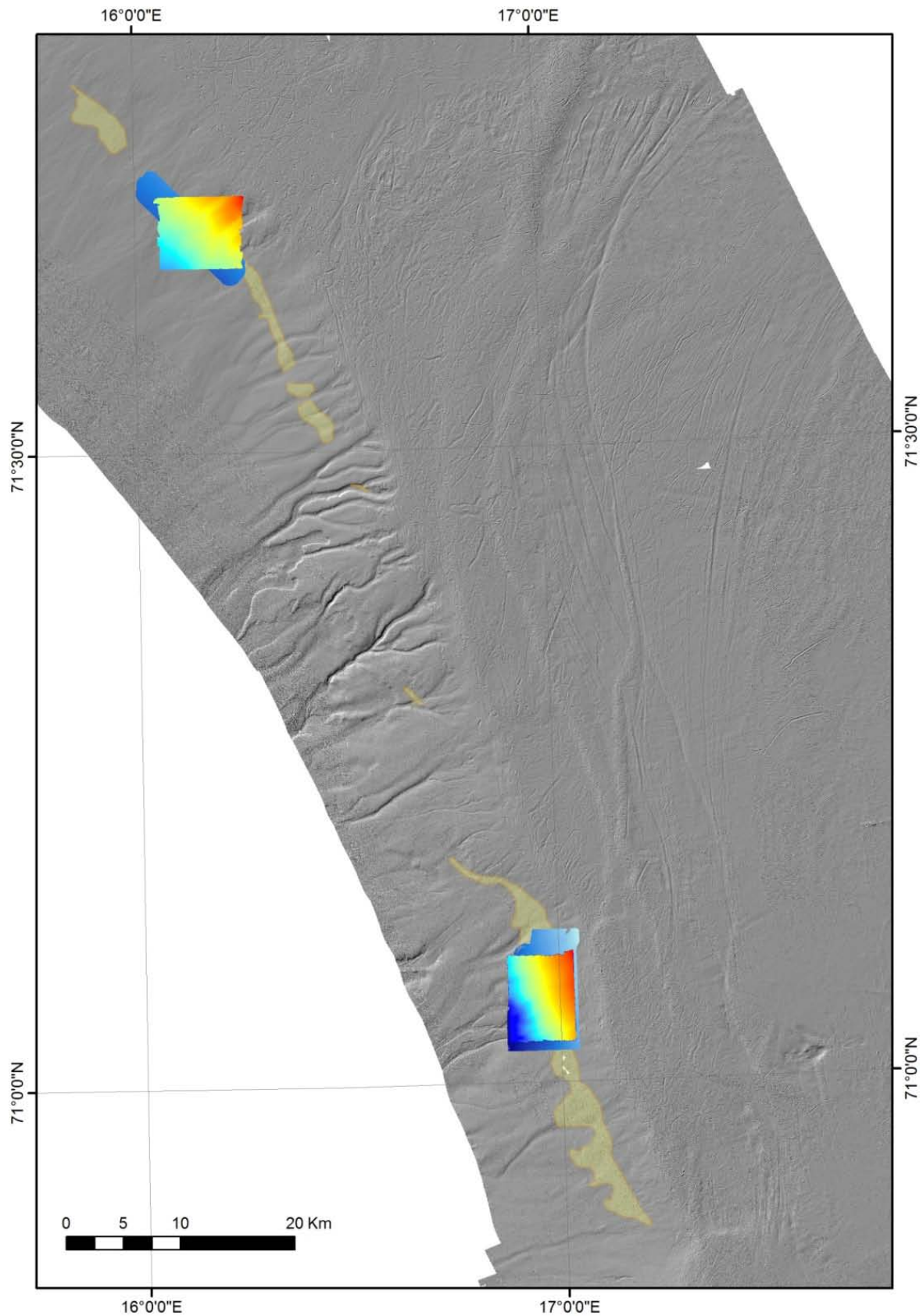


*Figure 9. Multibeam (bathymetry and backscatter) data acquisition locations showing bathymetry data. MAREANO data are shown as grayscale shaded relief. UiT data are depth shaded in blue, while FFI data are depth shaded in rainbow scale. Sandwave fields are indicated in yellow.*

## 4. RESULTS

### 4.1 Seismic stratigraphy

Sandwaves were readily identifiable on the sub-bottom profiler data despite the difficulties encountered in removing the abundant side-echoes. It was however, difficult in some instances to identify the base of the sand layer. Below are examples from each of the sandwave fields showing the stratigraphic setting of the bedforms (Figs. 10-13).

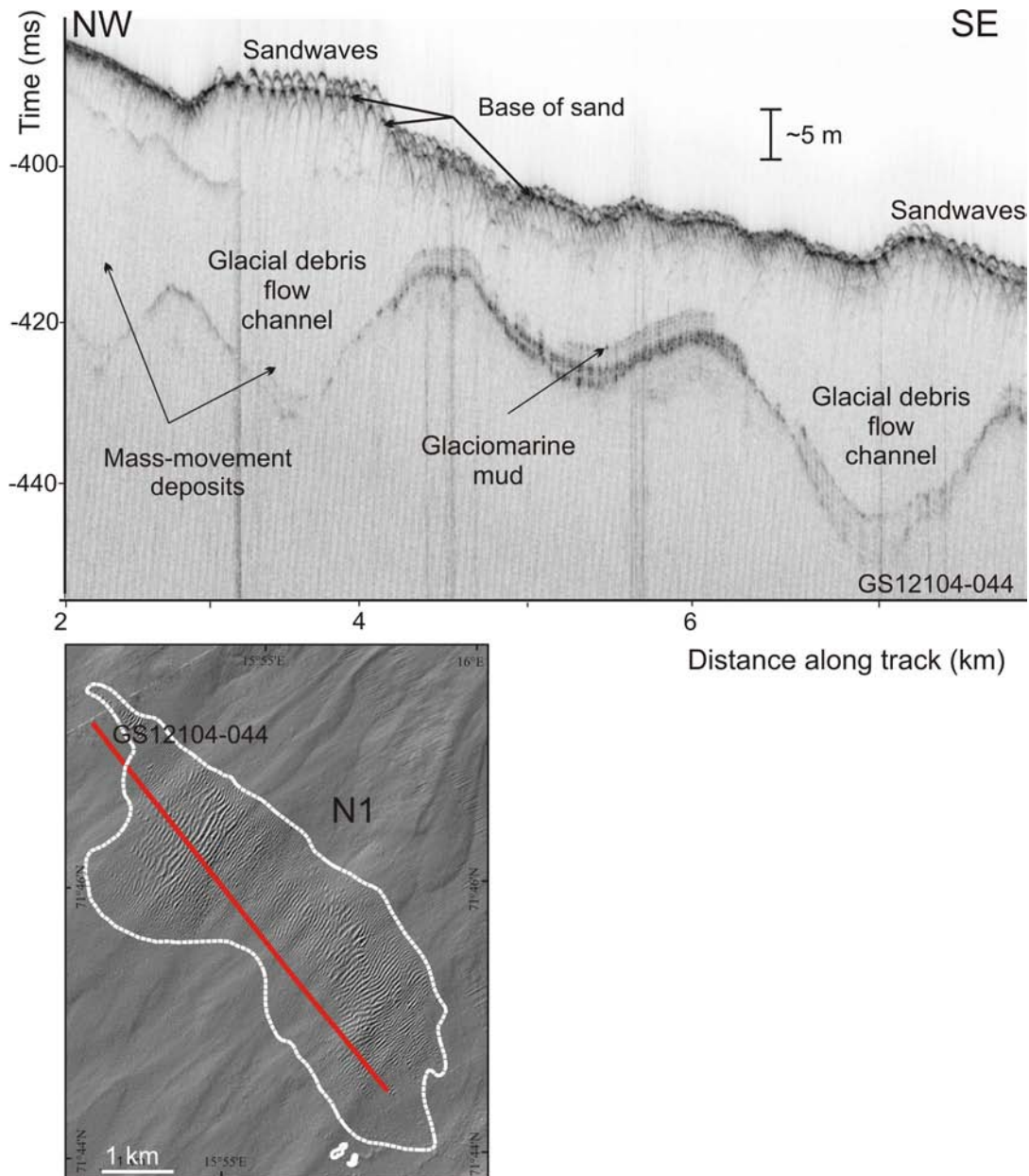


Figure 10. TOPAS profile and shaded relief images showing sandwaves within the N1 sandwave field. Multiple glacial debris flow channels are in-filled with mass-movement debris and laminated glaciomarine muds.

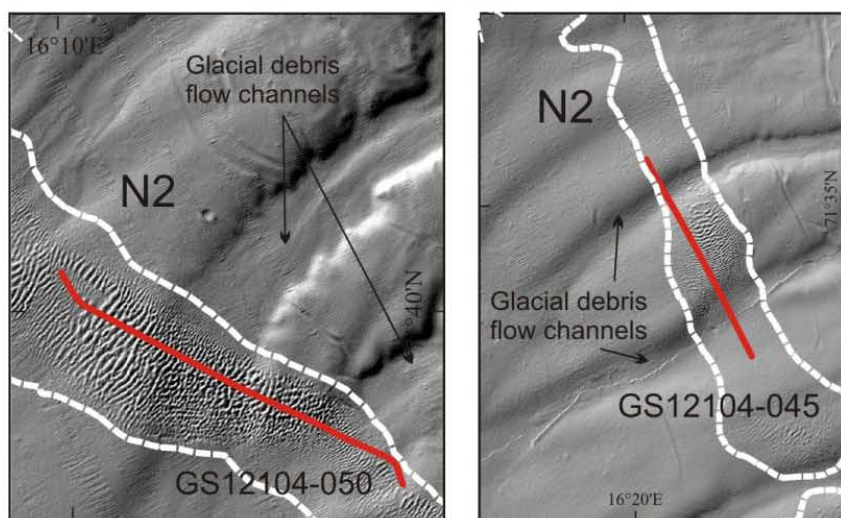
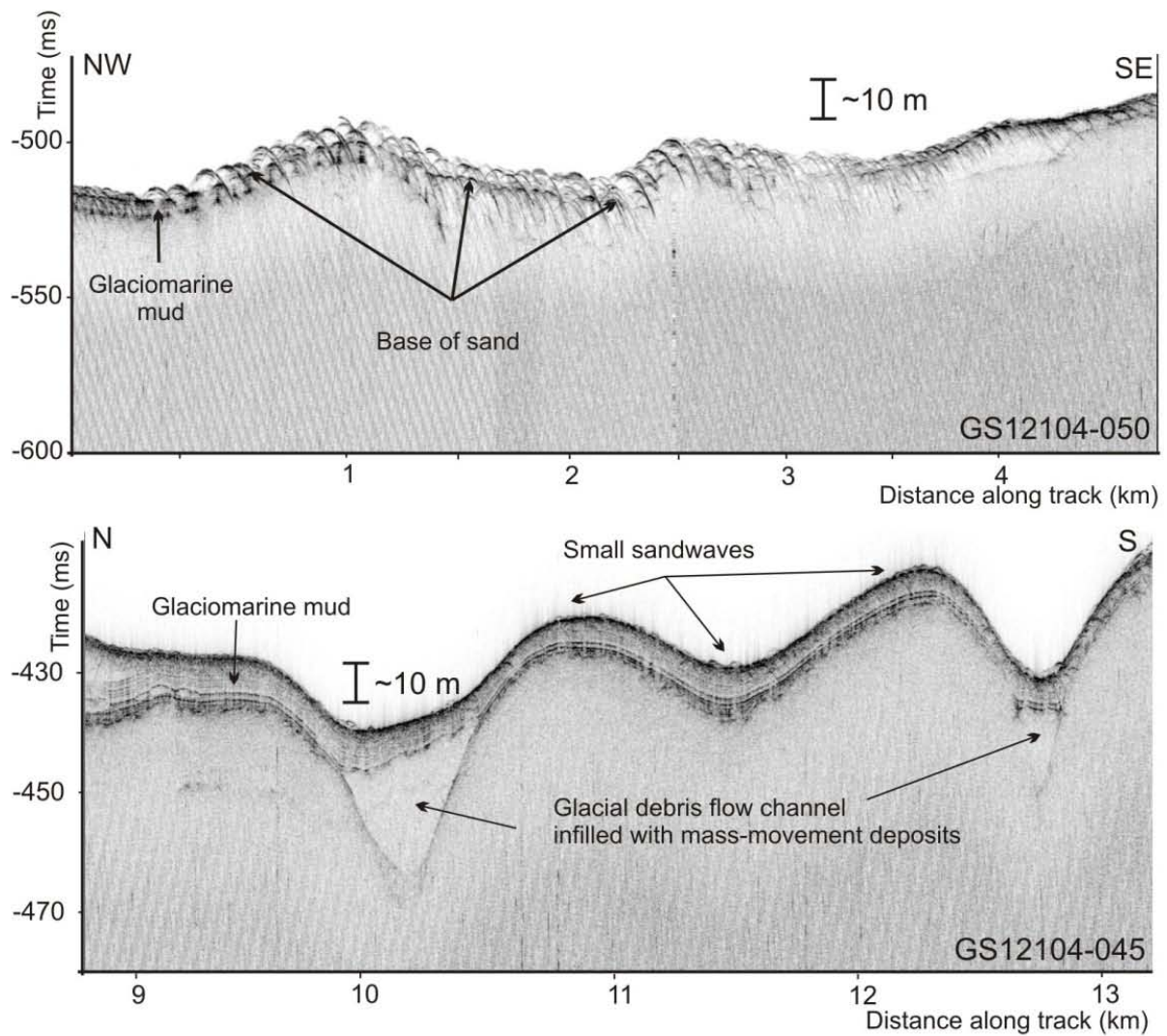


Figure 11. TOPAS profiler and shaded relief images showing small sandwaves within the N2 sandwave field. In the lower image, a thin sand layer overlies laminated glaciomarine sediments which in turn overlie channels in-filled with mass-movement deposits.

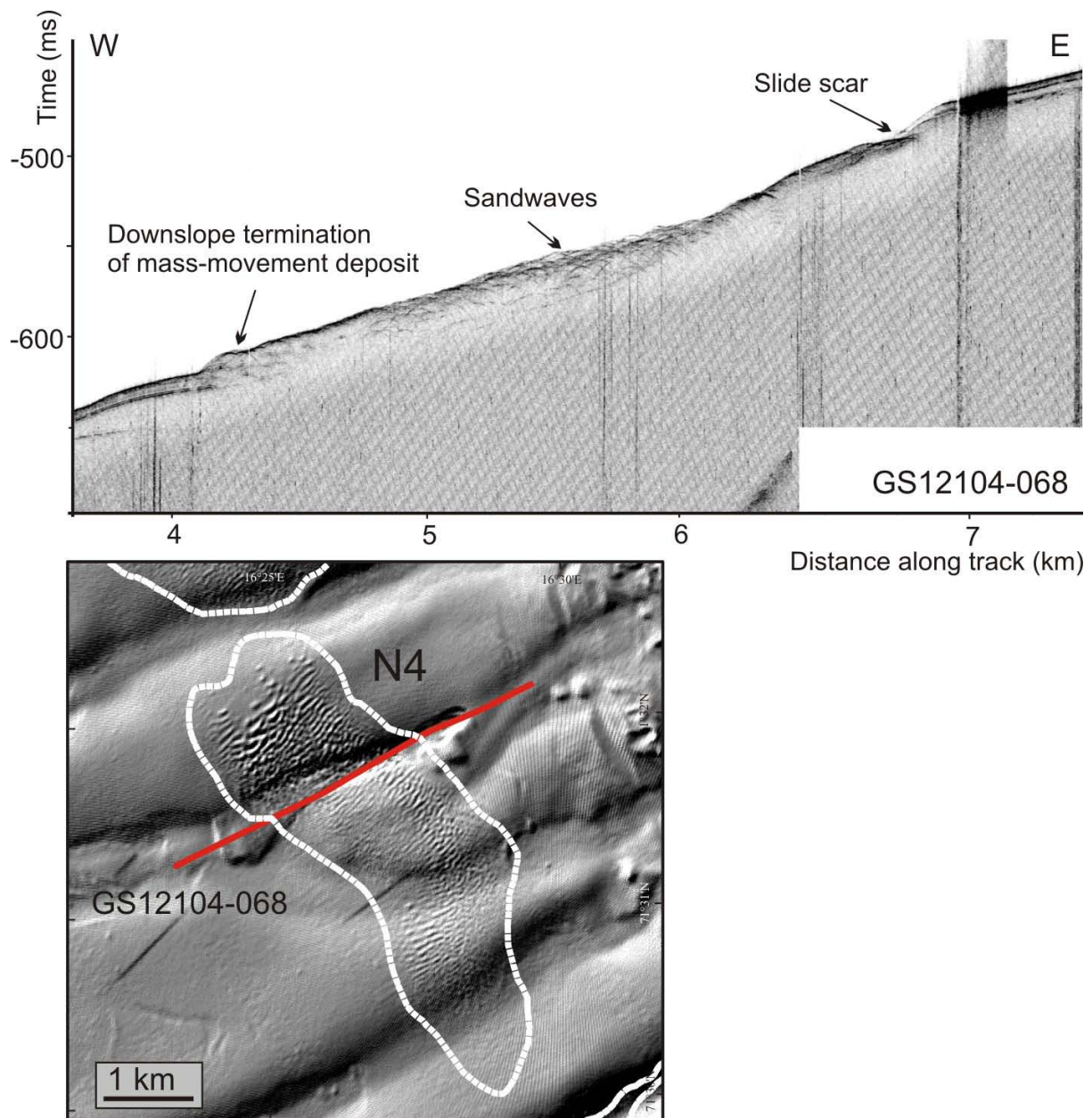
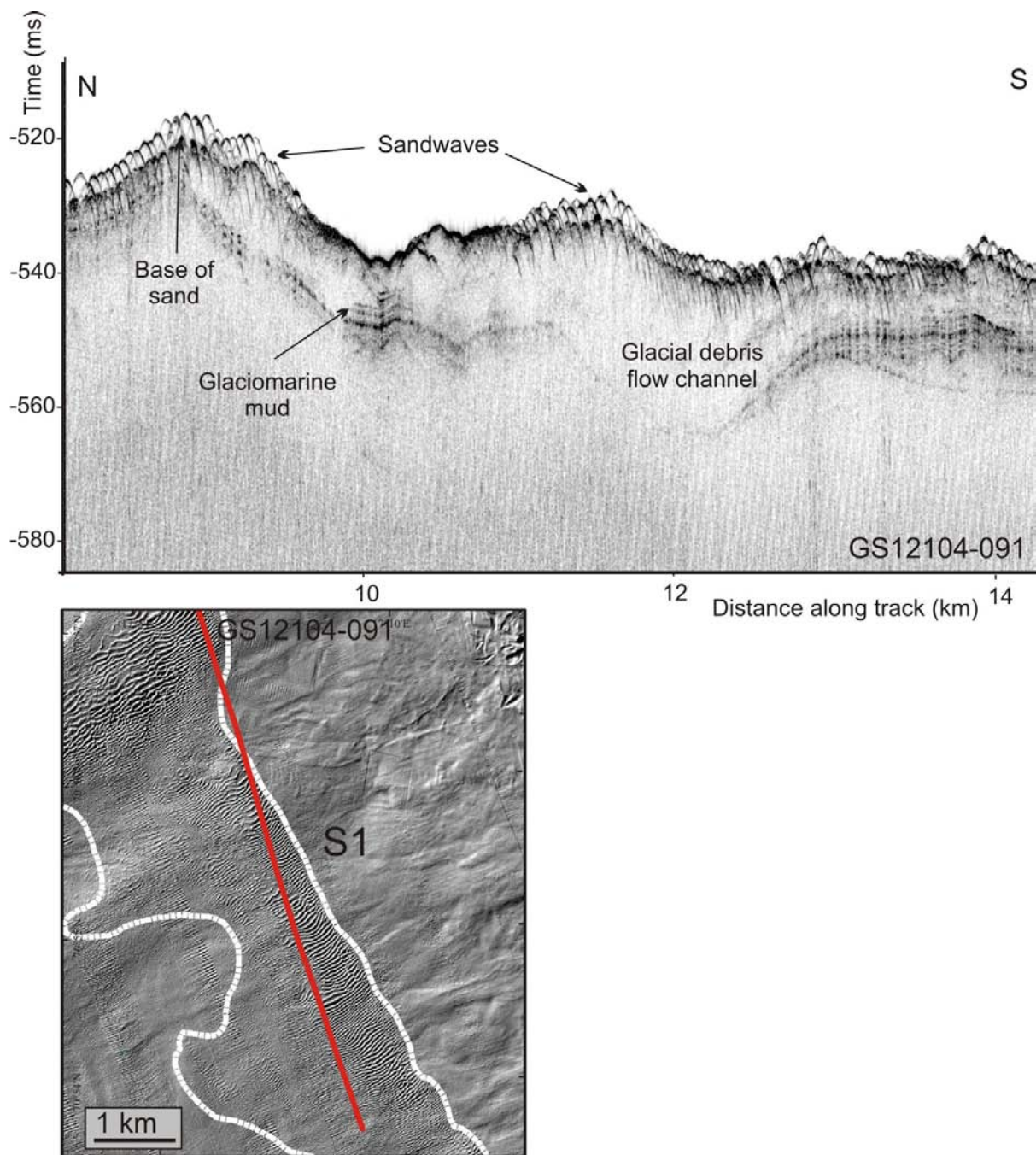


Figure 12. Sandwave field N4 is located within an area of multiple glacial debris flow channels. The sandwaves cross these channels with no sign of disturbance. This indicates that the sand was deposited after the most active phase of channel formation and also suggests that the channels are not the primary source of sand. The sandwaves also cross a later slide feature with no apparent interruption, indicating that the sandwaves formed after this mass-movement event.



*Figure 13. The southern part of the S1 sandwave field. Large sandwaves overlie laminated glaciomarine muds and glacial debris flow channels in-filled with mass-movement debris. There is no clear relationship between the location/formation/morphology of sandwaves and the location of seafloor channels. The sandwave fields cross channels and mass-movement deposits without any apparent change in sandwave field dimensions, sand thickness or bedform morphology.*

From the sub-bottom profiler dataset we see no indication of a sand layer beneath the sandwaves, nor do we see buried or partially buried sandwaves. Where present, the sandwave unit is the uppermost sedimentary deposit. The sandwaves frequently overlie a complex sequence of glaciomarine muds, mass-movement deposits and in-filled glacial debris flow channels.

## **4.2 Sand distribution and extent of sandwave fields**

The extents of the sandwave fields mapped by King et al. (2011) based on MAREANO multibeam bathymetry and mapped in this study based on sub-bottom profiler data are shown in Figs. 14 and 15. Their extent mapped from the two different datasets/methods is broadly similar, however, the sub-bottom profiler dataset allows for identification of smaller sandwaves than are resolved by the multibeam bathymetry dataset. This has meant that the margins of all the sandwave fields have been extended slightly. The largest changes have been between fields N2 and N3, which based on multibeam swath bathymetry were mapped as two separate fields, but which are shown to be joined by small sandwaves visible on the sub-bottom profiler dataset (Fig. 16). A new, higher-resolution multibeam dataset acquired by FFI in the present project show that sand and sandwaves have an even wider extent (see section 4.9 below).

## **4.3 Sand thickness**

The sub-bottom profiler dataset was used to estimate the thickness of sand within the study area. Figs. 17-19 and Table 1 show the results of this work. No pervasive trends in sand thickness are observed. There is no observed trend in sand thickness with water depth or distance along the continental slope. A slight tendency for increasing sand thickness within the downslope channels is observed, in particular in sandwave field S1. There are however, channels where sand thickness is relatively low (e.g. the southern part of N2, Fig. 18) and shoulders between channels with thick sand (e.g. the northern part of N2, Fig. 17).

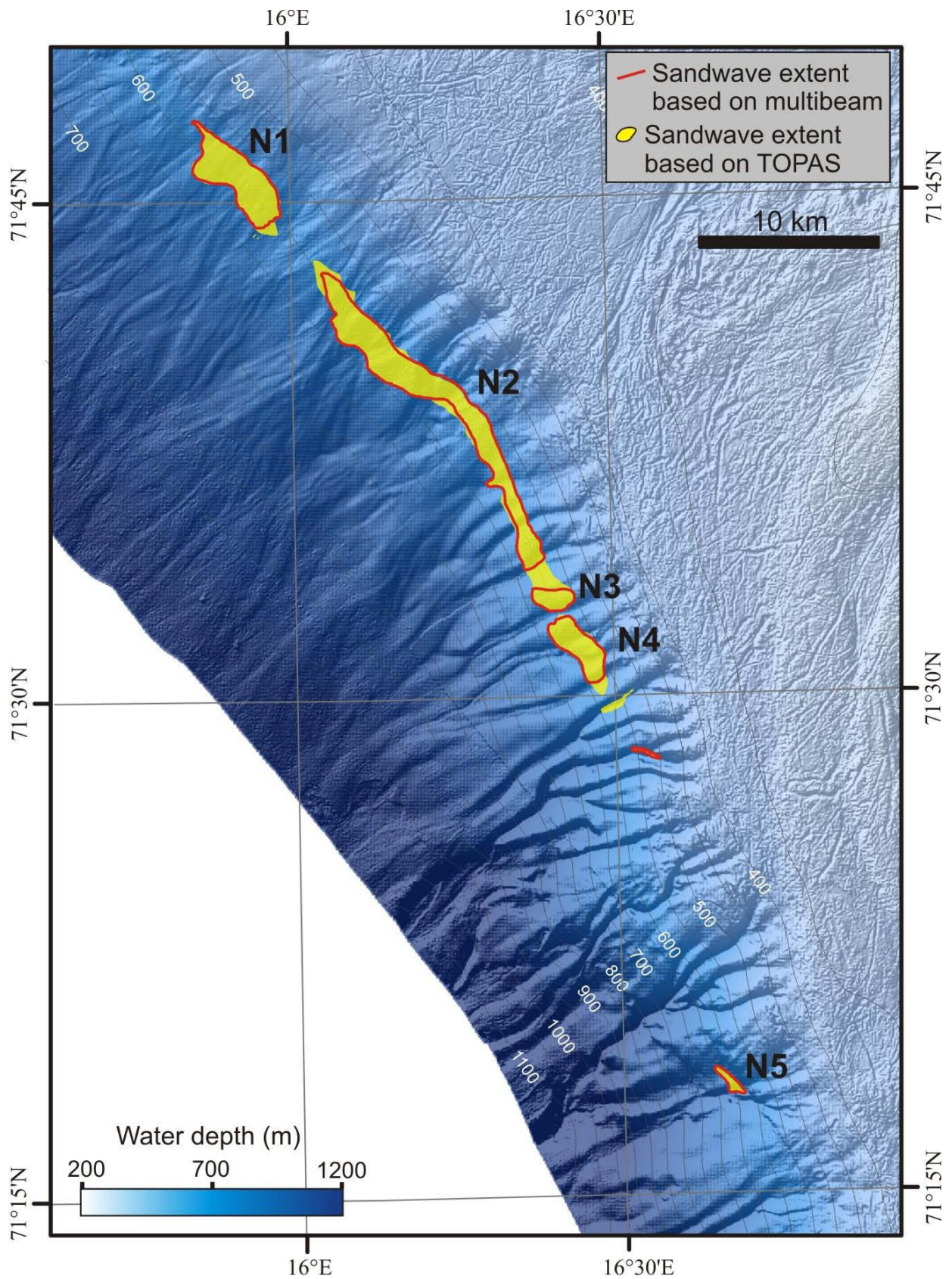


Figure 14. Extents of sandwave fields mapped in the northern part of the study area based on MAREANO multibeam bathymetry and TOPAS sub-bottom profiler data.

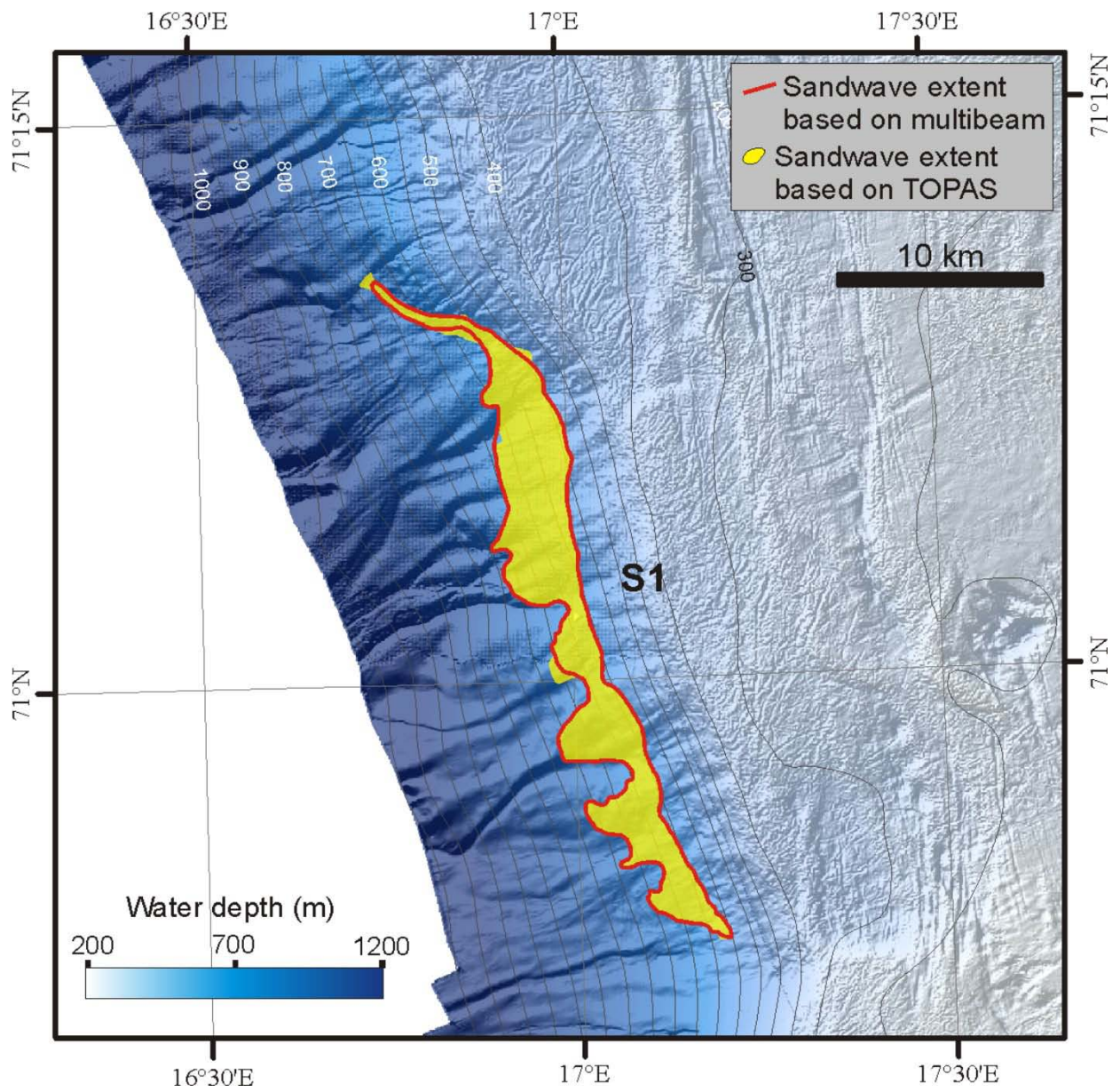


Figure 15. Extents of sandwave fields mapped in the southern part of the study area based on multibeam swath bathymetry and TOPAS sub-bottom profiler data.



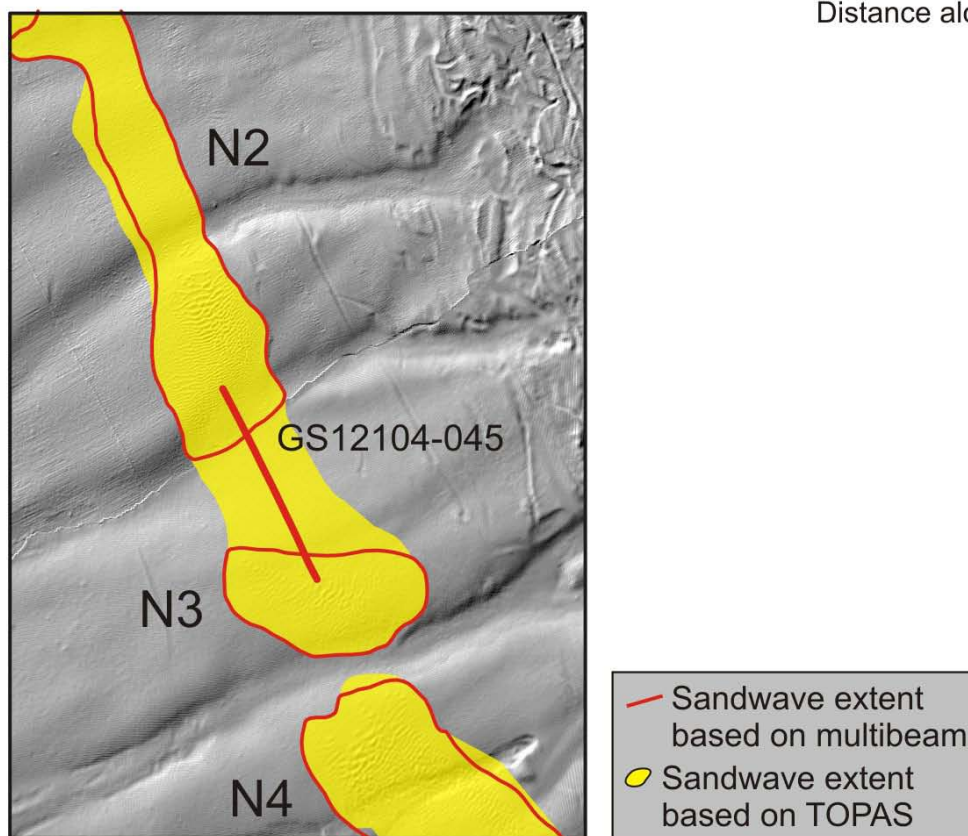
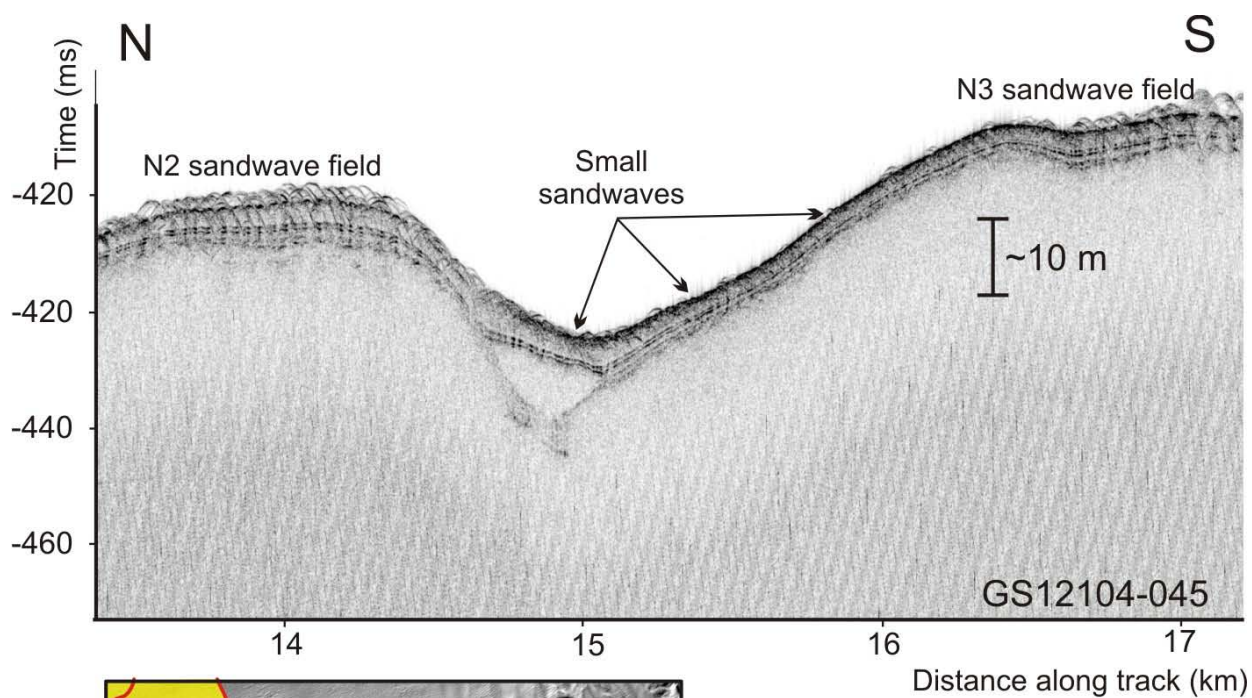


Figure 16. TOPAS profiler data are able to resolve smaller sandwaves than the multibeam swath bathymetry data, and show that sandwave fields N2 and N3 are in reality one sandwave field.

**Table 1. Estimated sand thickness within the different sandwave fields based on TOPAS sub-bottom profiler data.**

<b>Field</b>	<b>Mean sand thickness (m)</b>	<b>Maximum sand thickness (m)</b>	<b>Standard deviation in sand thickness (m)</b>
<b>All fields</b>	1.7	6.2	1.1
<b>N1</b>	1.2	2.8	0.7
<b>N2, N3, N4</b>	1.9	5.9	1.4
<b>S1</b>	1.6	5.0	0.9
<b>Channels south of N4</b>	2.3	6.2	1.9

No evidence was found in the sub-bottom profiler dataset for buried or partially buried sandwaves, thus only one sandwaves unit occurs. There is no evidence for a sand layer beneath the seafloor sandwaves. We would therefore expect sandwave heights measured from the multibeam bathymetry dataset by King et al. (2011) to show a good approximation for sand thickness in most instances. This is confirmed by Fig. 20 which shows a good correlation between sandwave thickness estimated from sub-bottom profiler data and sandwave height estimated from multibeam swath bathymetry by King et al. (2011).

In addition to the measurements from the sub-bottom profiler and multibeam datasets, sand thickness is known at locations where grab or gravity core samples penetrated the base of the sand unit. This occurred at 11 grabs stations (Fig. 21) which are all outside the sandwave fields (except GB 3, which is not considered further as total sample length recovered was only 3 cm). Sediments recovered where top layers of gravelly sand less than 15 cm thick. Sand was not identified on the sub-bottom profiler or multibeam datasets at these stations because of too low resolution/thickness. Within the sandwave fields all grab samples recovered a single sand unit. The recovery may be interpreted as minimum sand thickness.

Using the MAREANO multibeam bathymetry, King et al. (2011) estimate that the entire sandwave field area contains a minimum of 300 million cubic metres of sand. They calculated this based on sandwave distribution and height but express uncertainty given that they do not have information on the thickness of sand layer beneath the sandwaves. Based on the sub-bottom profiler data that is now available we can confirm that the height of sandwave is a fair assumption for sand thickness. It should be noted that neither the MAREANO multibeam data nor the TOPAS data recognize the small sandwaves in the outskirts of the sandwave fields (see below) and these sand volumes are thus not included.

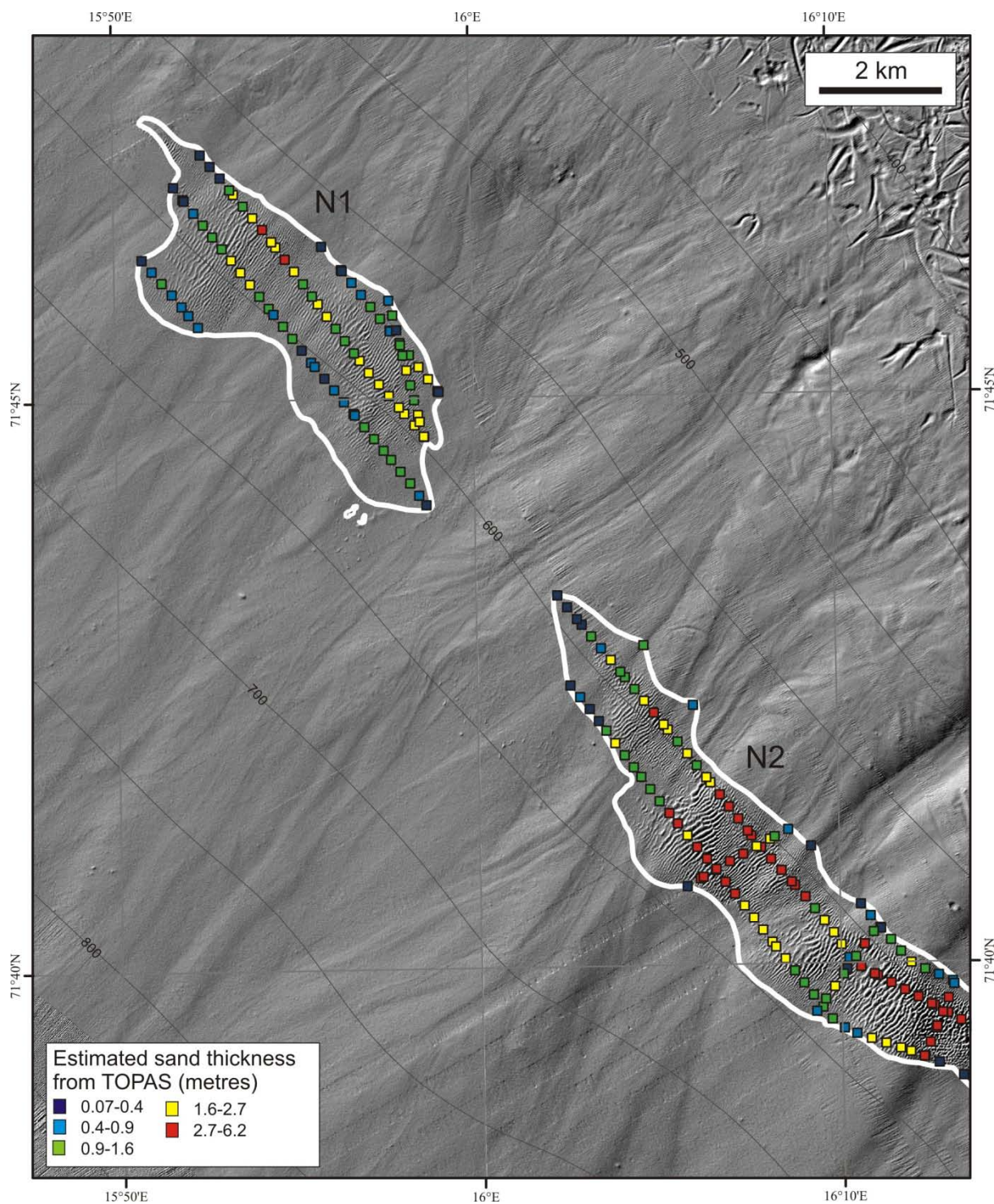


Figure 17. Thickness of sand in N1 and northern N2 sandwave fields estimated from sub-bottom profiler data.

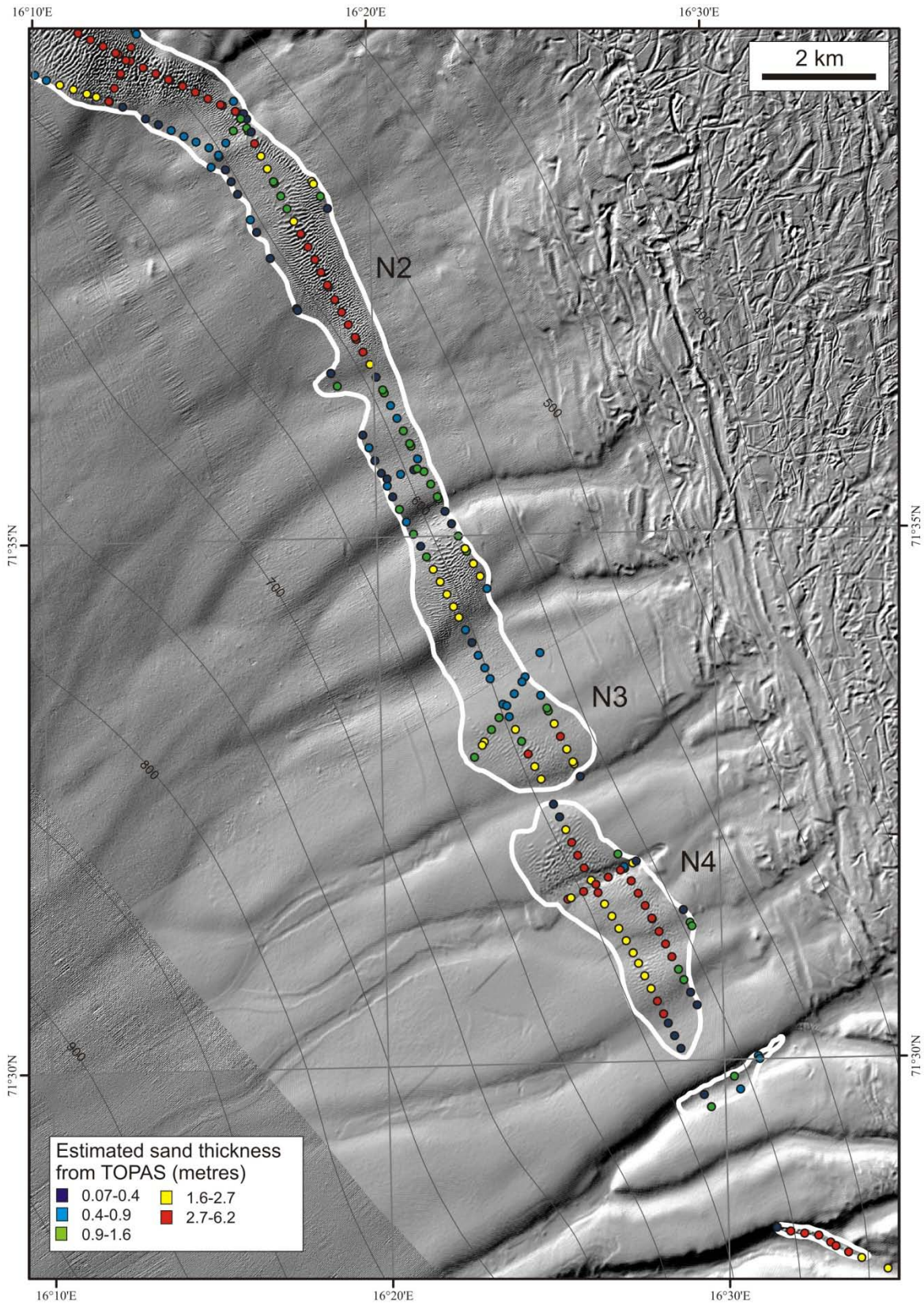


Figure 18. Thickness of sand in N2, N3 and N4 sandwave fields estimated from sub-bottom profiler data.

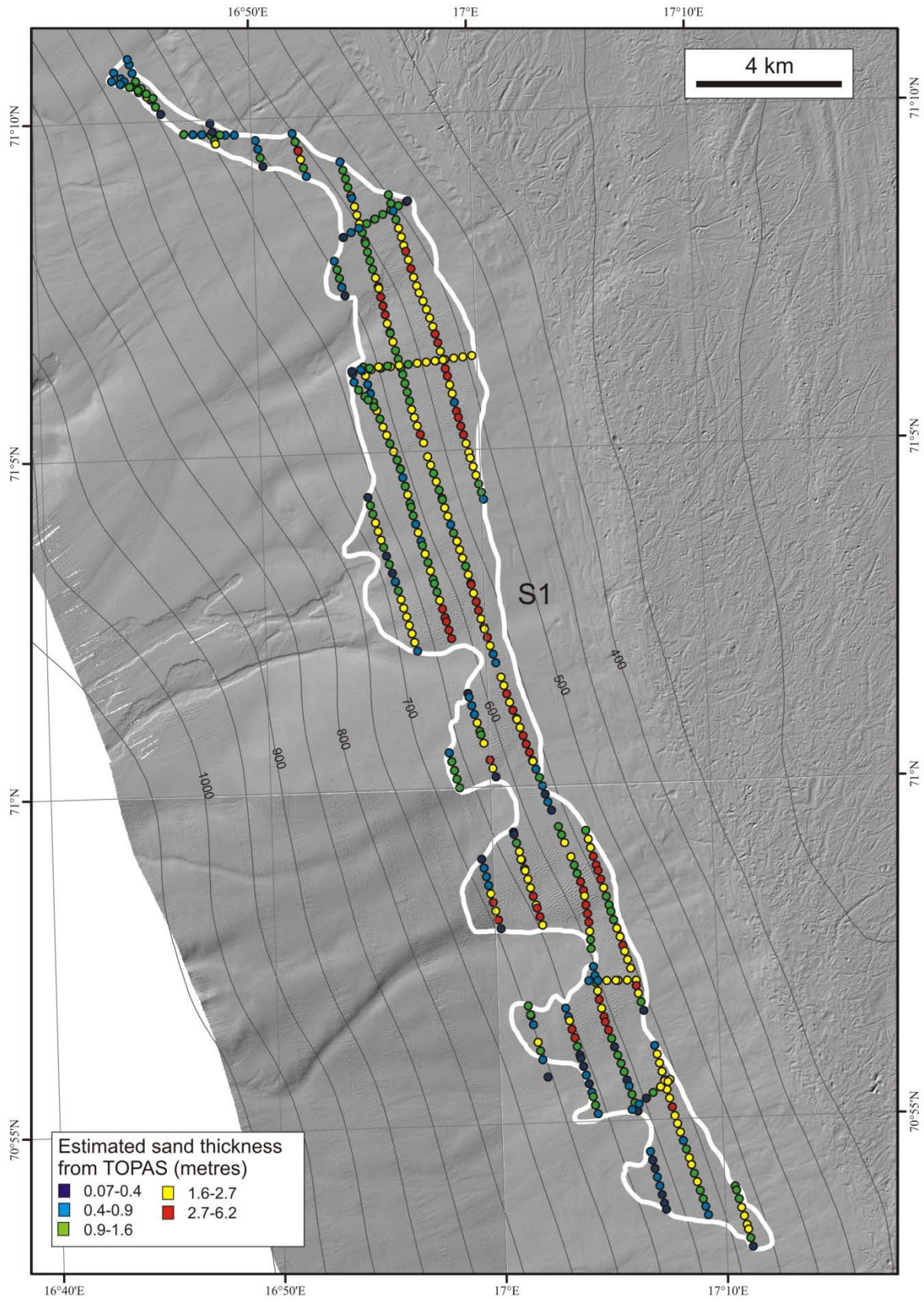


Figure 19. Thickness of sand in S1 sandwave field estimated from sub-bottom profiler data.

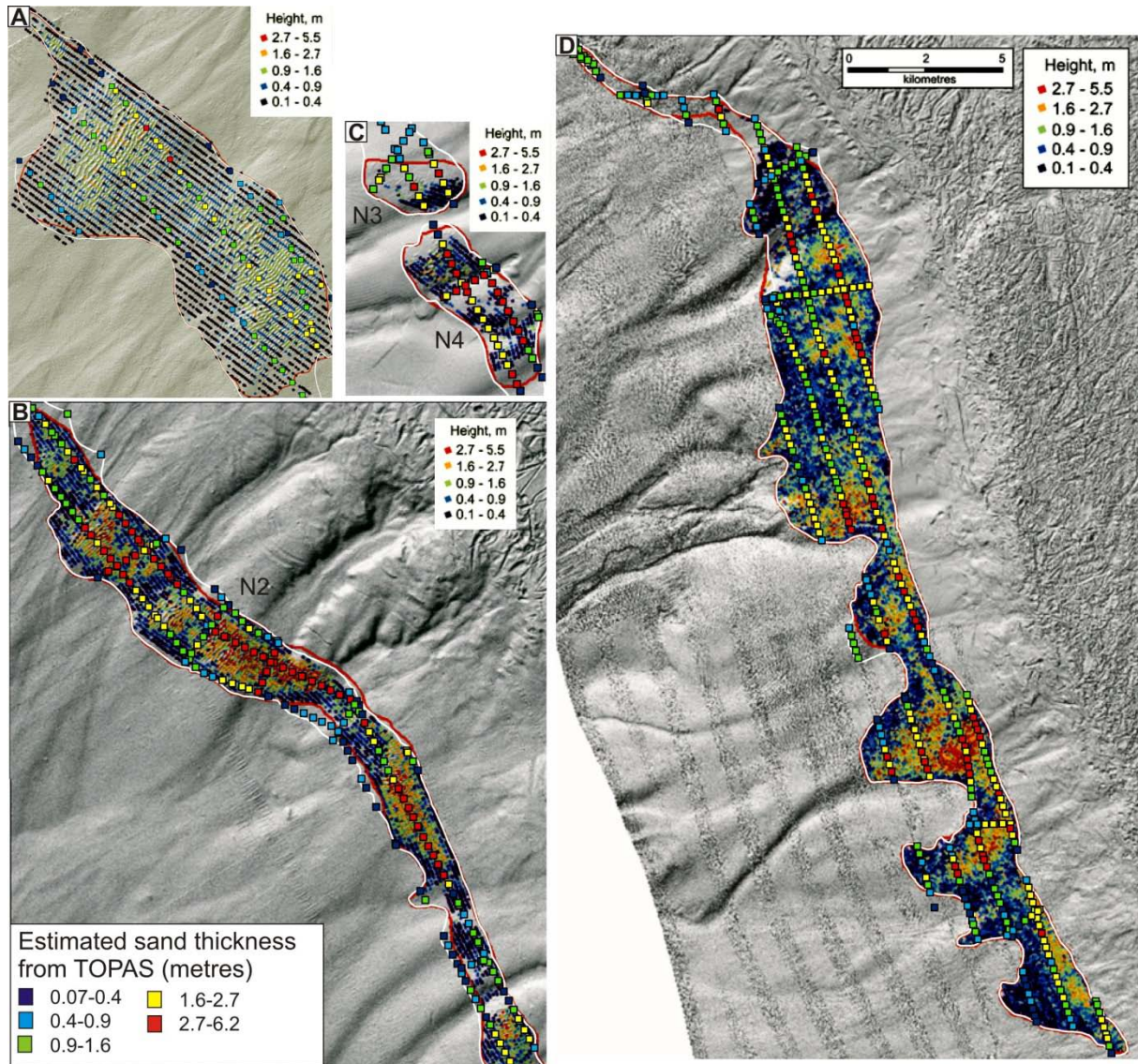


Figure 20. Comparison of estimated sand thickness based on TOPAS sub-bottom profiler data (large coloured squares) and sandwave heights calculated from MAREANO multibeam bathymetry for sandwave field N1 (A), N2 (B), N3 and N4 (C) and S1 (D). The red line shows the extent of the sandwave field based on multibeam bathymetry and the white line the extent based on sub-bottom profiler data.

All grab samples within the sandwave fields comprise well-sorted sand. The base of the sand was recovered in 11 grab samples and 7 gravity cores. Seven gravity cores penetrate the base of the sand unit. The top sand layer in all the gravity cores comprises silty gravelly sand with gravel. The thickness of this top layer varies from 3 to 25 cm. This is consistent with the seabed sediment composition described from MAREANO video lines (King et al. 2011).

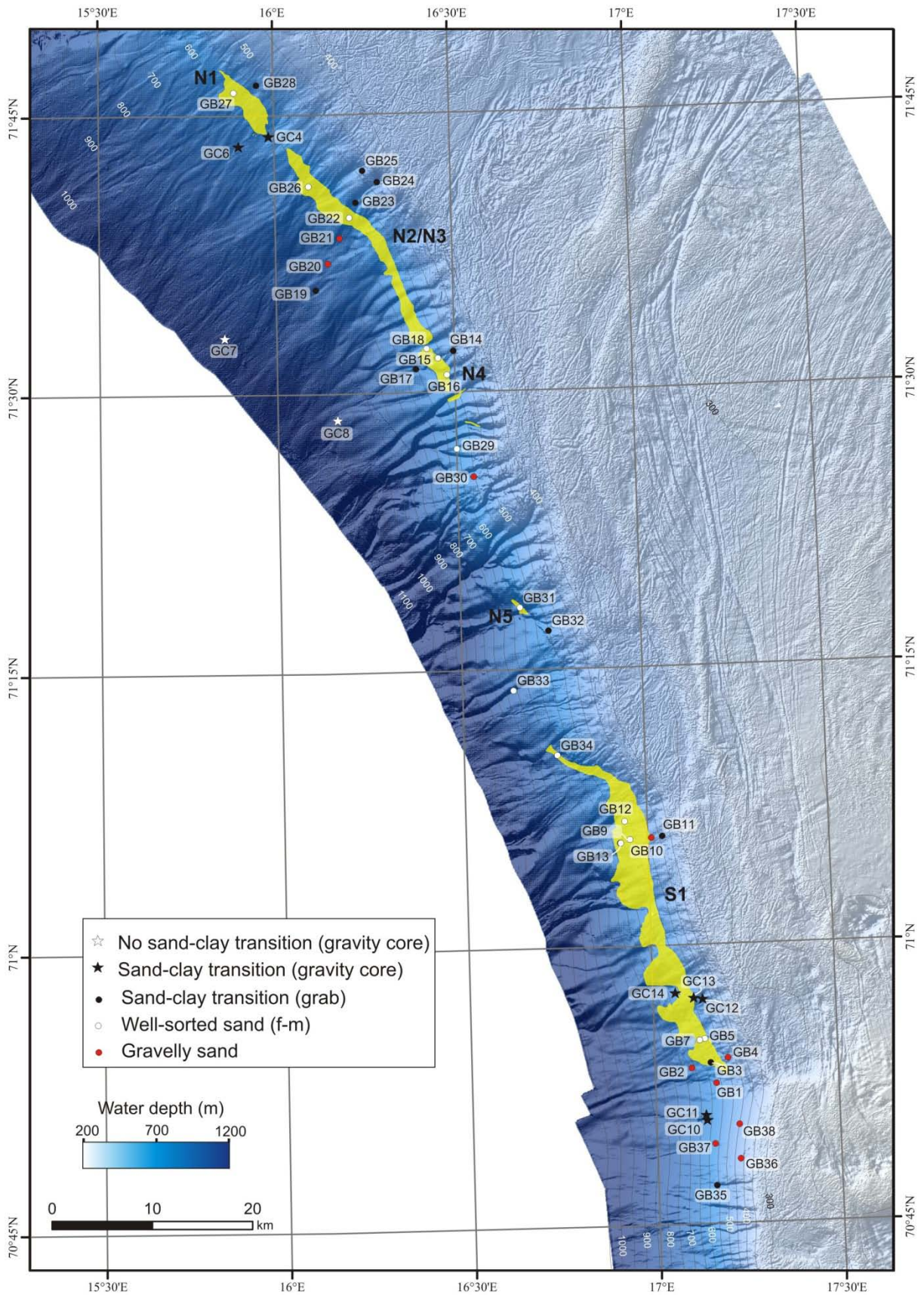


Figure 21. Seabed sediment composition from grabs and gravity cores.

## 4.4 Grain-size analysis

### 4.4.1 Grain-size distribution

Grain size distribution of seabed sediments (commonly sampled at 0-2 cm depth) was analyzed for all grab samples. Coarse top layers in gravity cores were also analyzed. Derived grain size distributions are presented as cumulative curves showing the volume percentage of grains finer than a certain particle diameter (i.e. x-axis of the diagrams display the equivalent diameter size in logarithmic scale) (Figs. 22-26). All curves show a small jump in distribution at 0.5 mm, reflecting the transition in the measuring method from Coulter laser particle counter to wet sieving.

In the sandwave fields, nearly 100% of the particles are in the sand fraction (0.063-2 mm) with the majority of grains being 0.2-0.4 mm in diameter (within the fraction medium-grained sand; i.e. 0.2-0.6 mm) (Figs. 22, 26).

The grain size distributions of the 7 grab samples in the S1 sandwave field (Fig. 22) are very different from the samples adjacent to, but outside the S1 sandwave field (Fig. 23, 24). The samples outside the sandwave field are less well-sorted, containing more coarse sand (0.6-2 mm) and gravel (2-20 mm). The best sorting (i.e. steepest part of the curve) occurs in medium-grained sand.

The seismic data and multibeam bathymetry show that there are two small sandwave fields between S1 and N4. One of the fields, N5, was sampled (GB 31). The grain-sized distribution for the sample is quite similar to the results from the other sandwave fields (Fig. 25), but it contains more silt (~4%). Five further samples were taken outside of the sandwave fields in this area, Three of them (GB 29, GB 32 and GB 33) have grain-size distributions similar to the sandwave samples (Fig. 25). GB 33 is located in a channel.

The grain-size distributions in the northern sandwave fields N4, N2 and N1 are shown in Fig. 26. Of these, the northernmost samples (GB 22, GB 26 and GB 27) are slightly more fine-grained than the sandwave samples further south, although all are well-sorted comprising predominantly medium-grained sand. In the north, outside the sandwave fields, large variations in grain size occur (Fig. 27). Samples GB 28 and GB 23, located slightly east of N1 and N2, have grain-size distribution similar to the samples within the fields, but somewhat higher coarse sand/fine gravel content.



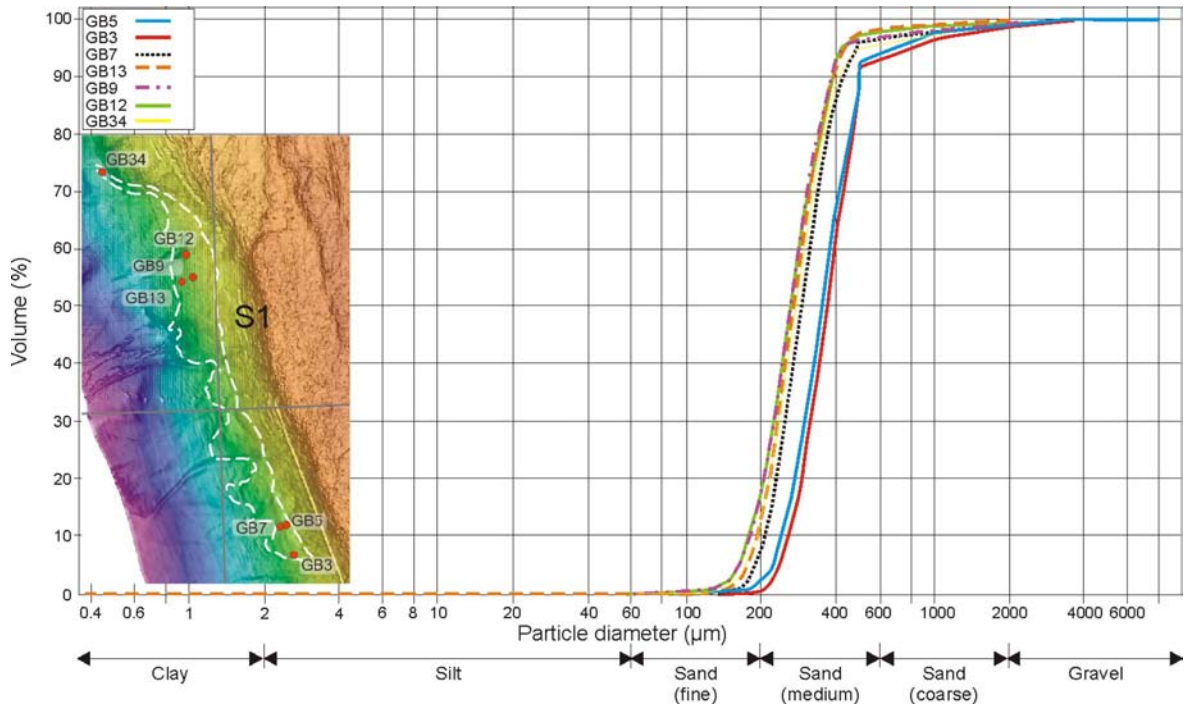


Figure 22. Grain-size distribution curves for grab samples within the S1 sandwave field.

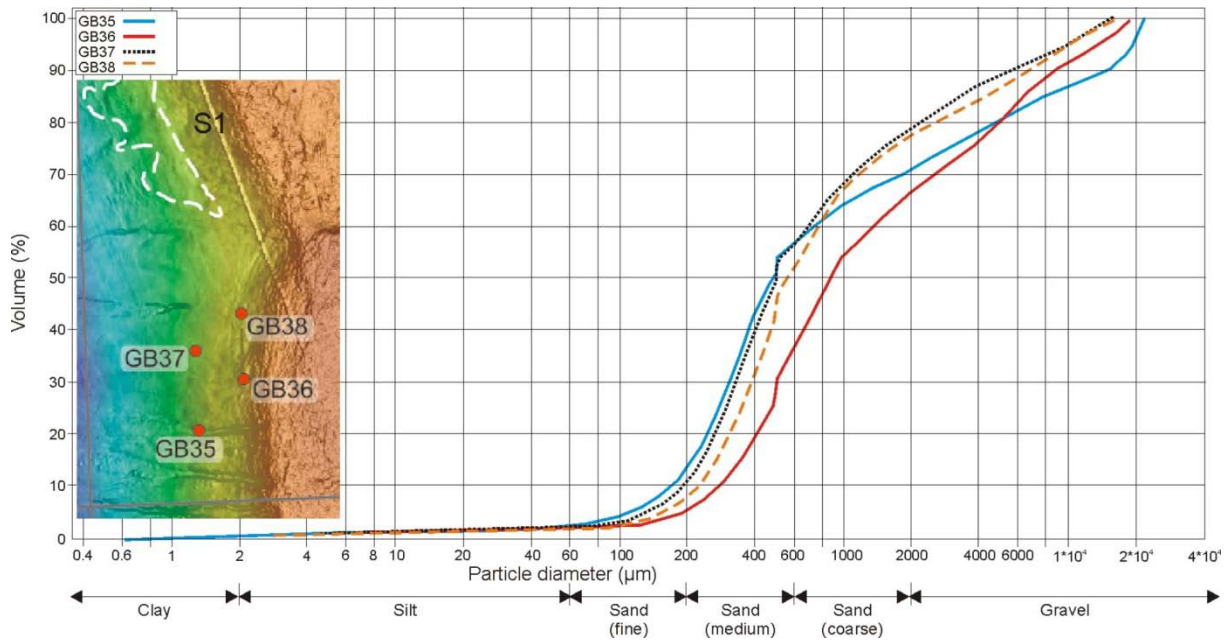


Figure 23. Grain-size distribution curves for grab samples on the continental slope west of Tromsøflaket (SSE of the S1 sandwave field).

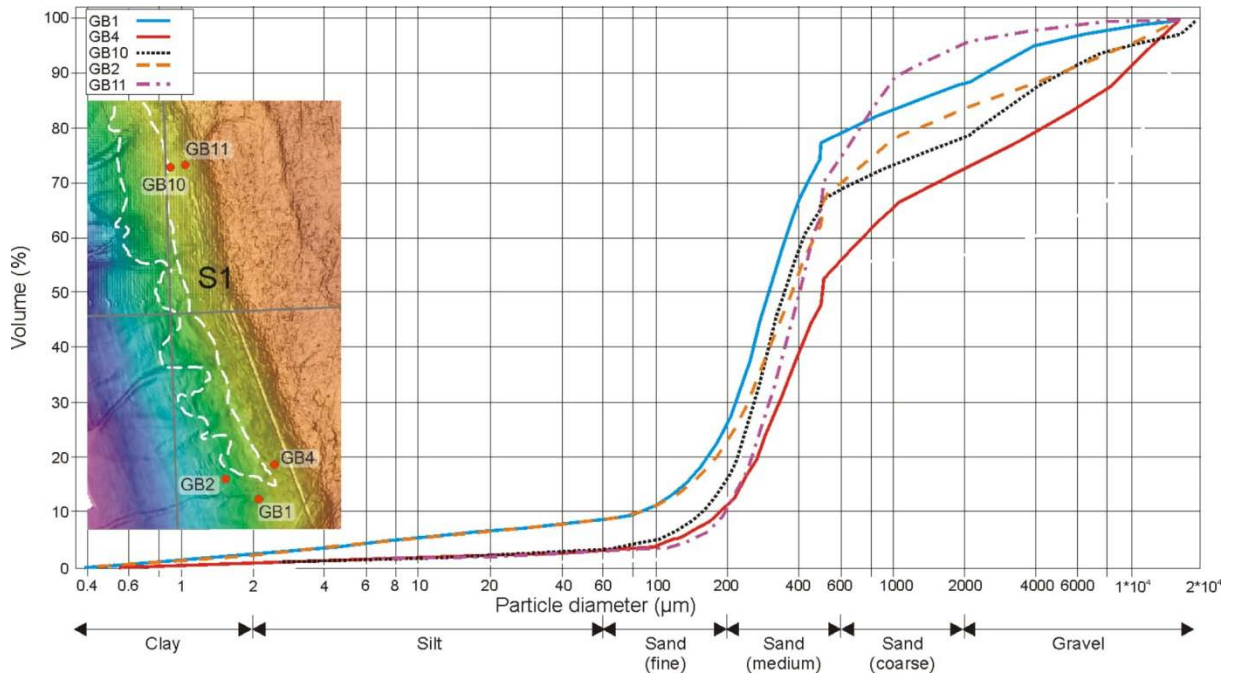


Figure 24. Grain-size distribution curves for grab samples outside sandwave field S1.

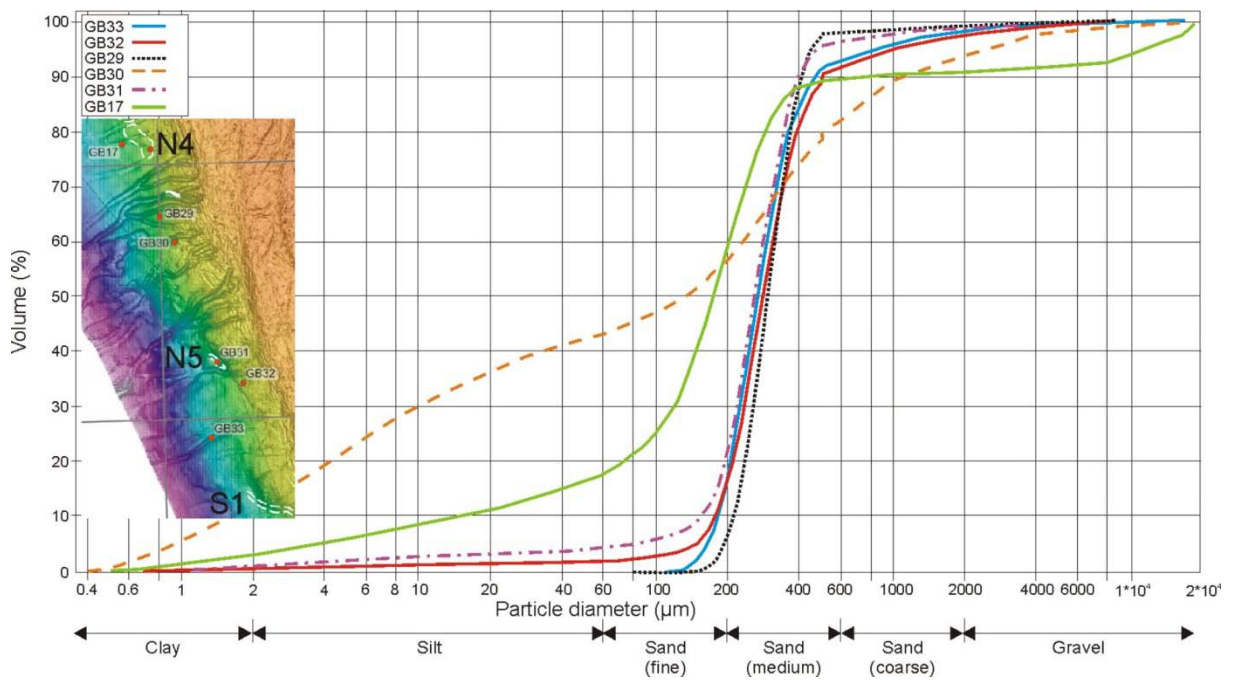


Figure 25. Grain-size distribution curves for grab samples between sandwave fields S1 and N5.

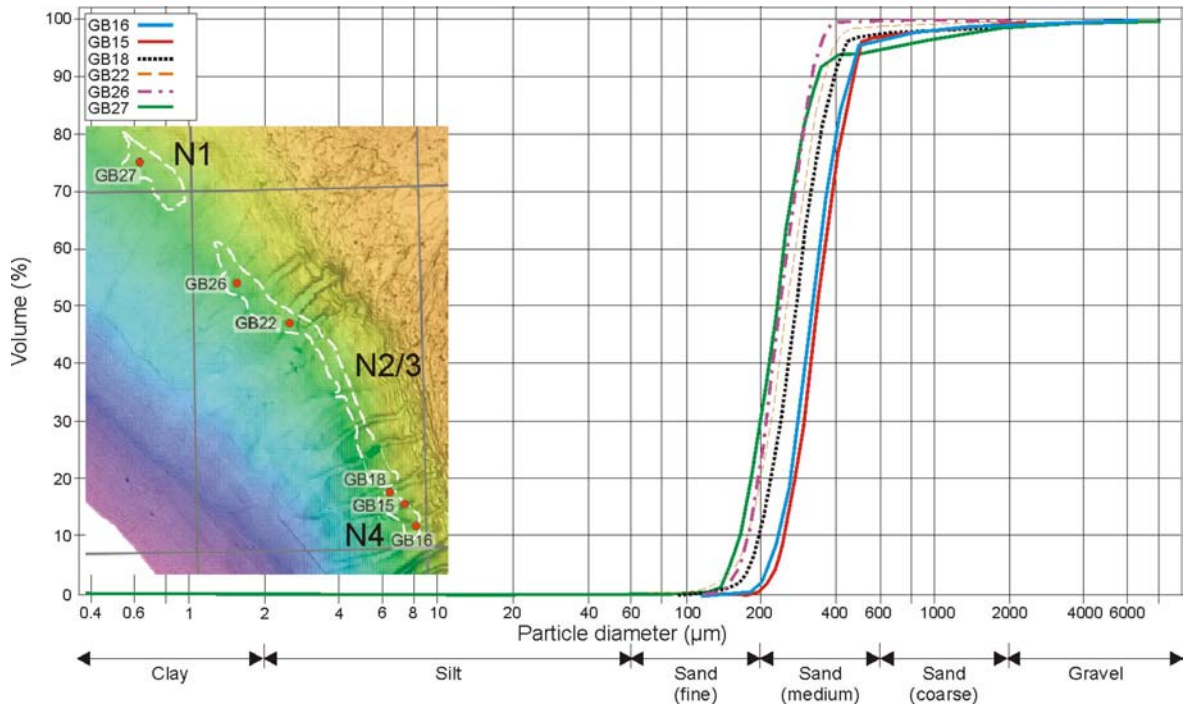


Figure 26. Grain-size distribution curves for grab samples within sandwave fields N1, N2, N3 and N4.

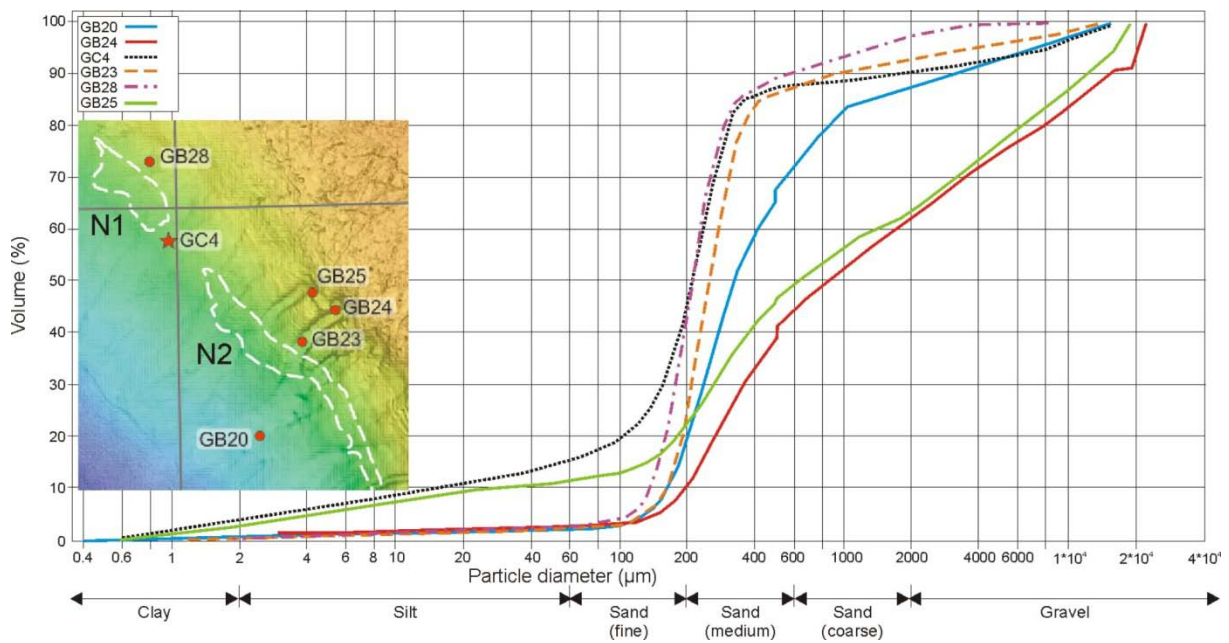


Figure 27. Grain-size distribution curves for grab and gravity core samples outside the northern sandwave fields.

#### 4.4.2 Statistical analyses of grain-size distribution

Parameters used to describe grain-size distribution are (a) average grain size, (b) spread (sorting) around the average, (c) symmetry or preferential spread (skewness) on one side of the average, and (d) degree of concentration of the grains relative to the average (kurtosis). Several formulas for calculation of grain-size parameters exist (Blott and Pye, 2001), but in this study we have chosen to make plots of the median grain size ( $d_{50}$ ) versus sorting (or standard deviation) as defined by Folk and Ward (1957). The median grain size ( $d_{50}$ ) is the particle diameter at which half of the distribution (volume or weight-percent) is larger and the other half is smaller. For the well-sorted sand in the sandwave fields the median is close to the mean grain size as defined by Folk and Ward (1957) (i.e.  $(d_{16}+d_{50}+d_{84})/3$ ; see Table 2). At the grain size  $d_{16}$ , 16 weight-percent of the grains are smaller.

In order not to put too much emphasis on coarse sediment and too little on fine particles, it is common in sedimentology to logarithmically transform particle diameters from millimeter scale into phi values ( $\phi$ ), using the expression  $\phi = -\log_2 d$ , where  $d$  is the grain size in millimeters. Folk and Ward (1957) defines the sorting (standard deviation) by the expression:  $\sigma = (\phi_{84} - \phi_{16})/4 + (\phi_{95} - \phi_5)/6.6$ .

All the samples from the sandwave fields cluster close together in the sorting versus median grain-size diagram (Fig. 28a), most being well-sorted ( $\sigma = 0.35$ - $0.50$ ) according to the classes proposed by Folk and Ward (1957). Figure 28b shows that three of the samples outside the sandwave fields (GB 29, GB 32 and GB 33) plot within or very near the same cluster. As mentioned earlier, these samples occur in the area between fields S1 and N4. The samples GB 28 and GB 23, slightly east of sandwave fields N2 and N1, have a well-sorted fine to medium-grained sand fraction, but are defined as moderately sorted according to Folk and Ward (1957) as the samples have a higher percentage of coarse sand and gravel.

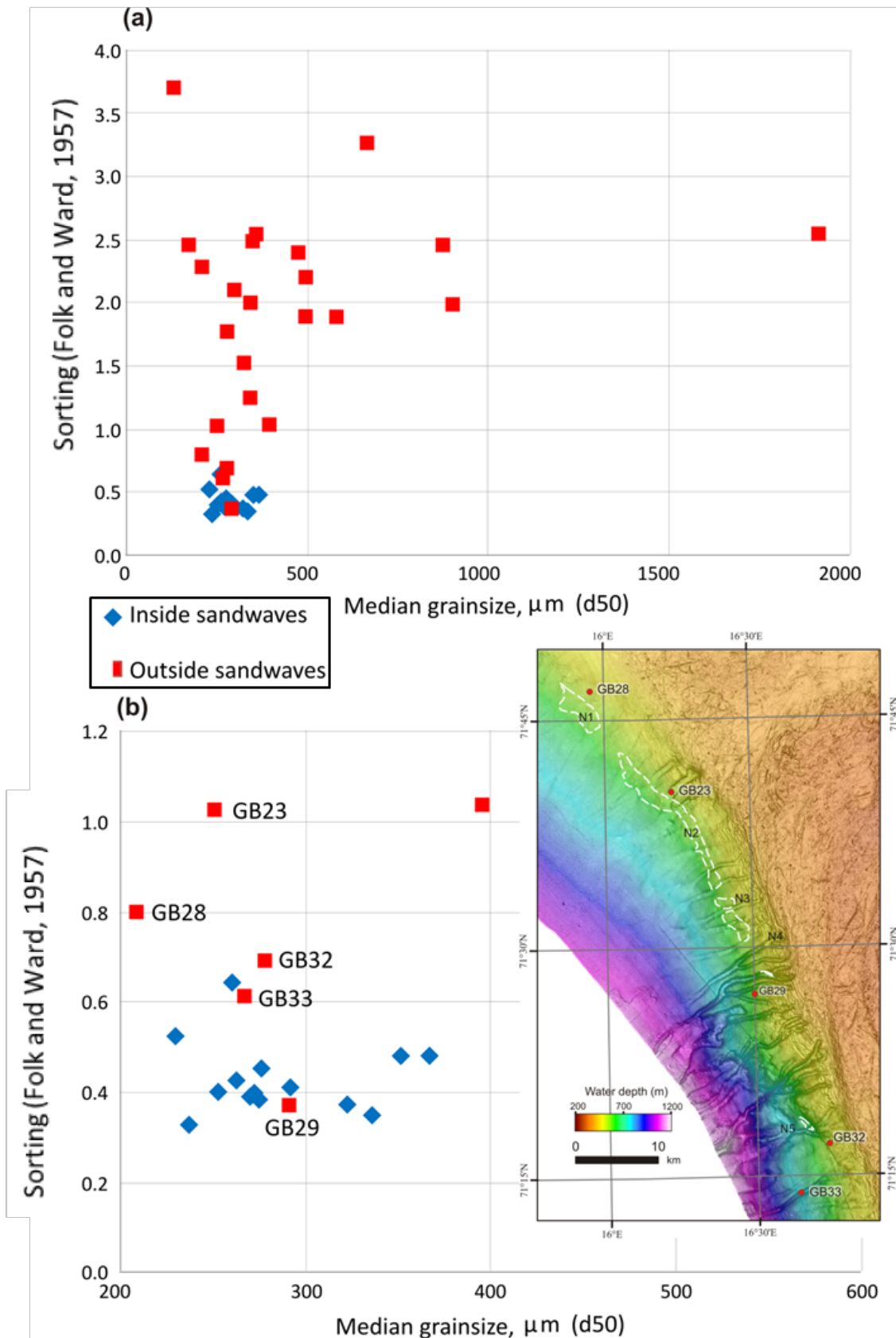


Figure 28. Plots showing relationship between median grain size and degree of sorting for (a) all samples analysed for grain-size distribution and (b) those samples showing lowest the median grains sizes and best degree of sorting.

#### 4.4.3 Comparison of grain-size parameters within sandwave fields

Median grain size ( $d_{50}$ ), mean grain size  $(d_{16}+d_{50}+d_{84})/3$  and sorting, according to the definition of Folk and Ward, are shown in Table 2. We have also included a parameter for the sorting of the main sand fraction (steepest part of curve), defined by the first part of the Folk and Ward (1957) expression:  $\text{Sorting } 2 = (\phi_{84} - \phi_{16})/4$ .

**Table 2. Average values of some sedimentological parameters within the different sandwave fields.**

<i>Sand wave field</i>	<i>No. of samples</i>	<i>Median grain size (<math>\mu\text{m}</math>)</i>	<i>Mean grain size (<math>\mu\text{m}</math>)</i>	<i>Sorting (Folk &amp; Ward, 1957)</i>	<i>Sorting 2 (main fraction)</i>
S1 (southern)	3	337	347	0.46	0.206
S1 (northern)	4	270	278	0.42	0.204
N5	1	260	266	0.64	0.244
N4	3	311	319	0.37	0.187
N2, northern part	2	235	250	0.36	0.185
N1	1	229	237	0.52	0.196
All samples	14	286	294	0.43	0.201

There are too few samples from the sandwave fields to make a confident comparison, however, a trend can be observed. Both median and mean grain size are largest in the southern part of field S1, whereas the smallest sizes are in the northern fields N2 and N1. According to the definition of Folk and Ward (1957), the sorting is best in N4 and N2. The sorting of the main fraction varies very little, but this parameter also indicates slightly better sorting in N4 and N2. The sample in N5 (GB 31) shows the poorest sorting also in the main fraction. This sample is the only one within the sandwave fields that contain particles in the silt fraction (~ 4%).

We have compared samples from areas of large sandwaves with samples from areas of small sandwaves. The number of samples is too small for confident comparison, but the data indicate that neither mean grain size nor sorting are controlled by the size of the sandwaves.

## 4.5 Calcium carbonate content

Total organic carbon (TOC) and total carbon (TC) content were measured on the same top samples that were analyzed for grain size. Assuming that all the inorganic carbon is bound to  $\text{CaCO}_3$  we have calculated the weight percentage in the different surface samples (Fig. 29). The  $\text{CaCO}_3$ -content may represent minerals, rock fragments and foraminifers/other shell material.

Figure 23a shows that samples within the sandwave fields clearly have lower calcium carbonate content (mean concentration of 1.4 wt%) than samples outside the sandwave fields (mean concentration of 13.2 wt%). It is also interesting to note that those samples outside the sandwave fields which have grain-size distribution most similar to the sandwave samples (GB 23, 28, 29, 32 and 33), also have relatively low calcium carbonate content (Fig. 29b). The highest concentrations are recorded south of the sandwave fields, where concentrations reach 42.3 wt%. The very low carbonate content of the sediments in the sandwaves contrasts strongly with that found in the Hola sandwave field in Vesterålen where carbonate content is more than 90 wt% (Bøe et al., 2009).

Interestingly, shell accumulations are clearly seen on the leeside of sandwaves on video transects taken during the MAREANO programme (Fig. 2), demonstrating that deposition of shell fragments occurs in some locations under the present current regime. Visual inspection of the grab samples shows that samples from the sandwaves tend to have the highest carbonate content (mostly comprised of shell fragments) in the coarse fraction (> 1 mm). In contrast, the samples outside the sandwaves tend to have the highest carbonate content (again mostly shell fragments) in the sand fraction (0.5-1 mm), with generally little shell in the coarser and finer fractions.

The observed pattern of calcium carbonate concentration in the sandwaves apparently results from the sediment transport on the seabed. We suggest that variations in current strength and direction may shed some light on this, something which should be possible to investigate once the current modeling is completed by IMR.

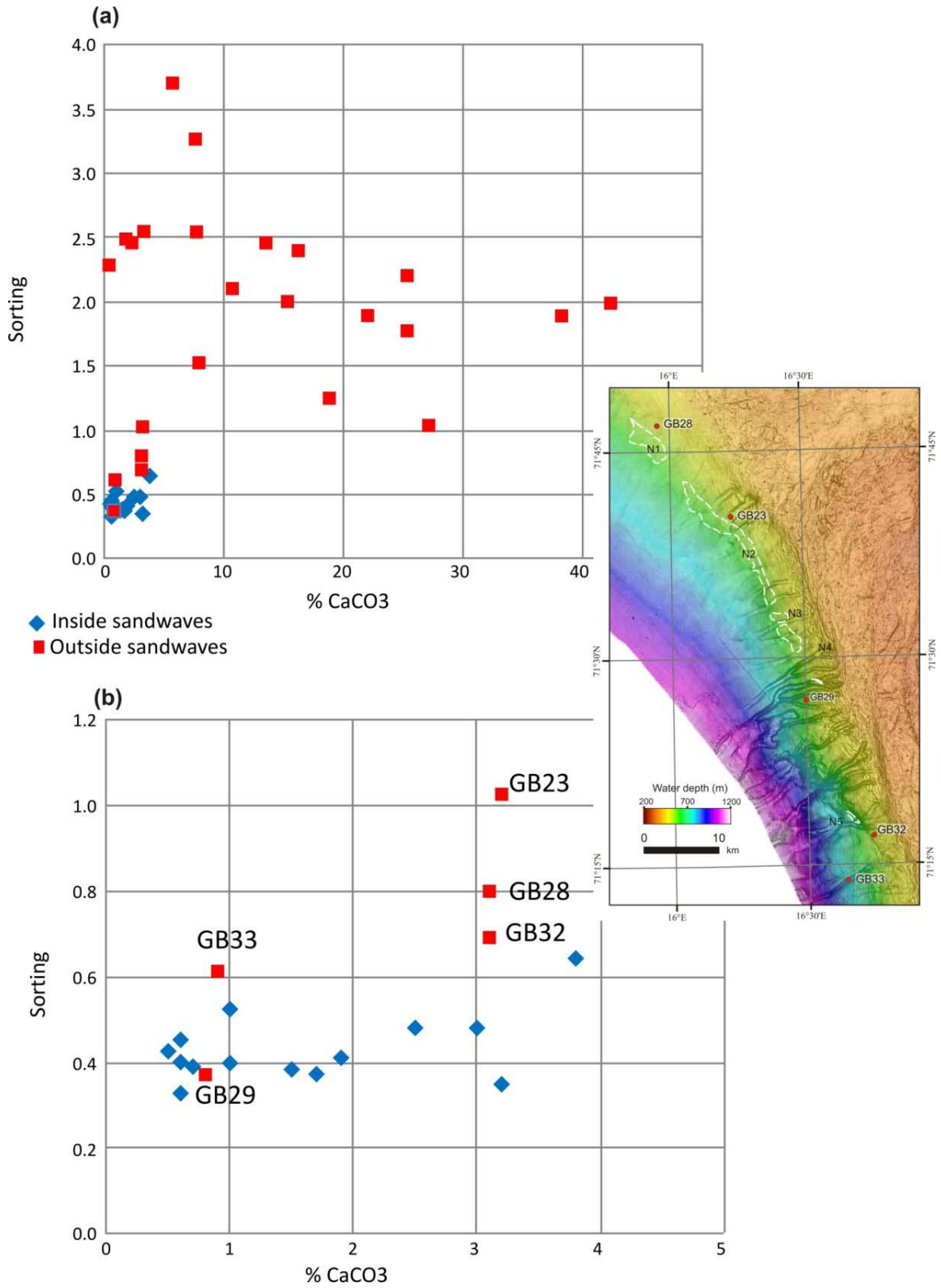


Figure 29. Plots showing the relationship between calcium carbonate content (wt%) and degree of sorting for (a) all samples analysed and (b) the samples with the lowest calcium carbonate content.



## 4.6 Petrographic analysis

Petrographic analysis of 6 of the 14 sand samples sent for thin section petrographical analysis is available. Table 3 shows the composition of these samples. Micrographs of all samples are presented in Appendix 2.

The grain size of the sand was determined by measuring the longest cross section of 30 grains per sample. The average grains size is medium sand, and the sorting is generally very good although in some samples there are outsized grains that reduce the degree of sorting.

Petrographic analysis was performed by point counting 200 points (excluding porosity) on each thin section. The dominating mineral is quartz, varying from 57% to 68%. This could suggest erosion from older sediments/sedimentary rocks. Some quartz grains have inherited quartz overgrowth. K-feldspar and plagioclase are also common. The samples from the sandwaves contain up to 5% carbonate shells while the sample from south of S1 contains up to 15% shell material, including silica fossils.

The sand samples do not contain clay or sand-sized mica grains. Glauconitic clay matrix occurs only in porous particles, mainly in the carbonate fossils. There is a wide range of bedrock fragments, including sandstone, metasandstone of quartz/muscovite/sericite/other minerals, siltstone, gneiss, granite, mica schist, dolomite, chert etc. Chert and dolomite suggest erosion of older sediments.

The heavy mineral association is dominated by amphibole and garnet. Amphibole does not survive deep burial and high content of this mineral suggests erosion from metamorphic or magmatic rocks. Several other heavy minerals are also common. It should be noted that some heavy minerals, i.e. tourmaline, spinel and rutile, are very rare suggesting low content of these in the source area.

It is hard to see systematic trends in geographical distribution of the various sand components. There is possibly an increase in quartz content northwards as the sample with lowest quartz content is located in the southern part of sandwave field S1.

**Table 3. Thin section petrographical analysis of six sand samples. GB 1 is the only sample located outside the sandwave fields. The samples have been arranged with those on the left farthest south, moving northwards across the table.**

Sample number	GB 1	GB 7	GB 34	GB 31	GB 15	GB 22
Area/sandwave field	South of S1	Southern S1	Northern S1	N5	N4	Central N2
Quartz	40.5	57.0	68.0	66.5	68.0	66.5
Chert	1.0	2.0	1.0	0.5	1.5	0.5
K-feldspar	5.0	3.5	5.5	5.5	3.0	2.5
Plagioclase	6.5	4.0	7.5	6.0	12.0	6.0
Muscovite			trace			
Biotite			0.5			
Chlorite					0.5	
Zircon		trace	trace	trace		trace
Tourmaline	trace	trace	trace	trace		?
Rutile		trace	trace		trace	trace
Apatite	0.5	trace	0.5		trace	0.5
Garnet	3.5	4.5	0.5	1.0	trace	8.0
Staurolite	?					trace
Kyanite	trace	trace	0.5	trace	0.5	1.0
Epidote	2.0	trace	0.5		trace	1.0
Clinozoisite/epidote	trace	3.0	0.5	0.5	0.5	2.0
Amphibole	3.0	5.0	5.0	3.5	1.0	6.0
Titanite	trace	trace	trace	trace		trace
Opaque iron-titanium oxides	0.5	0.5	trace	trace	trace	0.5
Glauconitic clasts				trace	trace	trace
Sedimentary rock fragments	5.5	6.5	5.0	3.5	4.0	2.5
Metamorphic rock fragments	9.5	8.5	4.5	6.5	5.5	1.5
Igneous rock fragments	4.0	5.0	0.5	2.0	2.5	1.5
Forams	2.5	0.5		1.5	trace	
Molluscs	5.5	trace		0.5	0.5	
Unidentified carbonate fossils	5.5		trace	2.5	0.5	trace
Silica fossils	3.0	trace		trace		
Glauconitic clay matrix	2.0	trace		trace	trace	trace

## 4.7 Physical and geotechnical properties

Measurements of water content ( $w$ ) and undrained shear strength ( $s_u$ ) were carried out every ten or twenty centimeters on all the 9 gravity cores described (Figs. 3-5, Appendix 1). Seven of the cores (GC 4, GC 7, GC 8, GC 11, GC 12, GC 13, and GC 14) give results indicating that the sediments are normally consolidated. Some variation in parameter values are observed, which is normal as sediment texture and depositional environment vary over such a large area.

Water content mainly varies within the range 40-55%, while undrained shear strength varies from 4 kPa to 10 kPa. Some  $s_u$ -measurements in the range 15-20 kPa are probably due to coarse sediment textures or other local sediment anomalies. Most of the samples show a normal consolidation trend, i.e. decreasing water content and increasing undrained shear strength downwards.

Two of the cores are different from the others. Core GC 10 (1.1 m long) is from the bottom of a deep, narrow slide scar; this probably explains the large variation in empiric values. The core contains resedimented slide blocks with sediments that were more deeply buried prior to sliding ( $w \sim 30\%$  and  $s_u \sim 25$  kPa), contrasting the soft sediments surrounding the blocks.

Core GC 6 (0.7 m long) was taken on a small, diapir-like high. In this core, much higher shear strength values and lower water content values than expected were measured ( $w=30-35\%$ ,  $s_u=20-39$  kPa). Multibeam bathymetry data do not show erosion phenomena or slides at the coring locality. The overconsolidated sediments in this core are thus probably not related to such processes. Overconsolidation may be related to sediment diapirism or another unknown process.

## 4.8 AMS $^{14}\text{C}$ dating

Dateable material from selected sediment cores was identified and dated at the Chrono Centre, University of Belfast by accelerator mass spectrometry (AMS) (Table 4). The  $^{14}\text{C}$  ages were  $\delta^{13}\text{C}$ -normalized, however not corrected for potential reservoir effects, usually reported to be of the order of 465 years in the study region. AMS  $^{14}\text{C}$  dating was performed on mainly bivalves and/or their fragments (Table 4). All samples yielded sufficient carbon for AMS radiocarbon dating. Because the majority of samples are from a context that is at the limit of the radiocarbon method and beyond the range of standard calibration curves, the results are presented in radiocarbon years BP.

Two samples from the upper most section of core GC 08 (UBA-21157) and GC 11 (UBA-21161) gave ages between the late Holocene and the last deglaciation ( $\sim 13\,500$   $^{14}\text{C}$  years BP). The other samples taken from the glaciomarine sections of the cores gave results between 32

000 and 52 000 <sup>14</sup>C years BP. All samples gave finite results. Since glaciomarine sediments in the southwestern Barents Sea are often reworked, and bivalves/fragments are likely transported together with ice-rafted material (IRD), we decided to date one more sample in GC 08 composed of planctonic and benthic foraminifera (UBA-21482).

The result shows that foraminifers are roughly 25-30 000 years younger than shell fragments in almost the same section. The late glacial maximum (LGM) age of this sample (~16 500 <sup>14</sup>C years BP) indicates that bivalves are not reliable for dating in this region. Further, it provides us the opportunity to study the environmental changes during the LGM/Holocene transition in more details. We are now picking foraminifer for four more age determinations in core GC 08 to validate the age model. The results are expected later this year.

**Table 4. AMS<sup>14</sup>C dating results of selected cores in the study region.**

Core	Section	Depth in cm	Composite in cm	Sample Type	Species	Lab ID	<sup>14</sup> C Age	Error
GC_8	3	34-36	34-36	coral/bivalve	<i>C. smithii</i> / <i>Thyasira</i> sp.	UBA-21157	13447	49
GC_8	2	7-9	107	fragments		UBA-21155	47137	2028
GC_8	2	36-38	136	fragments		UBA-21156	42626	1067
GC_8	2	69-71	169	mixed forams		UBA21482	16516	84
GC_8	1	18-20	218	fragments		UBA-21153	51022	3432
GC_8	1	44-46	244	fragments		UBA-21154	38966	675
GC_11	3	12	0-1	bivalves	<i>L. minuta</i>	UBA-21161	479	21
GC_11	2	4-6	92	fragments		UBA-21160	38039	602
GC_11	1	35-37	223	fragments		UBA-21159	50731	3295
GC14	1	207-208	207	fragments		UBA-21162	40326	809
GC10	2	6-7	16	shell/bivalve	<i>N. pernula</i> / <i>Antalis</i>	UBA-21165	31867	297
GC10	2	18-19	18	bivalves	<i>C. islandica</i>	UBA-21167	47098	1952
GC10	1	32-33	75	fragments		UBA-21164	46971	1920
GC10	1	81	81	fragments		UBA-21166	51993	4012

## 4.9 Multibeam data analysis

In this section we provide examples of data quality and terrain analysis performed to examine both the northern and southern sandwave areas based on multibeam bathymetry and backscatter data from MAREANO, UiT and FFI (section 3.3).

### 4.9.1 Comparison of bathymetric data quality

Before we can speculate on changes in the sandwave fields over the years from the first MAREANO survey to the most recent FFI survey, we must assess data quality achieved by the multibeam surveys. Visual comparison of shaded relief images generated from the bathymetry data is perhaps the most intuitive tool for gaining an initial feel for data quality, and allows at least a subjective assessment of the confidence that can be associated with each dataset. Figures 30 and 31 show examples of data quality from the northern (N2) and southern (S1) sandwave fields, respectively. All data are gridded at 5 m resolution but it is clear that the data quality is not equal between datasets, due to differences in sounding density/quality.

From Figure 30 we can see that the data in the N2 sandwave field are quite comparable when it comes to larger sandwaves. Each dataset has some noise/artefacts associated with it which generally appear as linear corrugations in the shaded relief image. The orientation of the artefacts is different in each dataset due to the sailing direction(s) of the survey vessel. The FFI data offer the most detailed view of the sandwaves and reveal the presence of many smaller sandwaves towards the periphery of the main sandwave field which were not detected by either the MAREANO or UiT surveys.

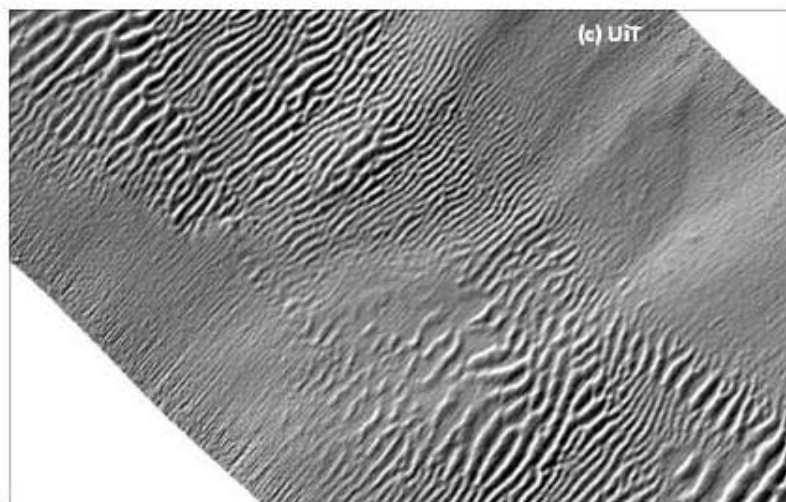
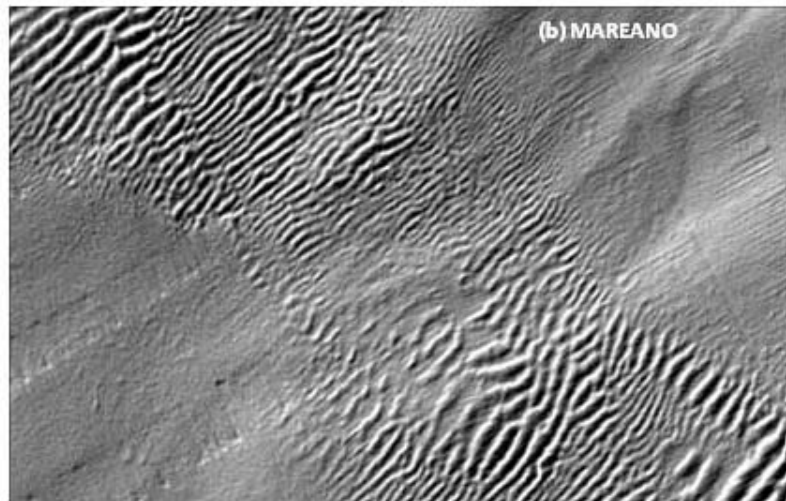
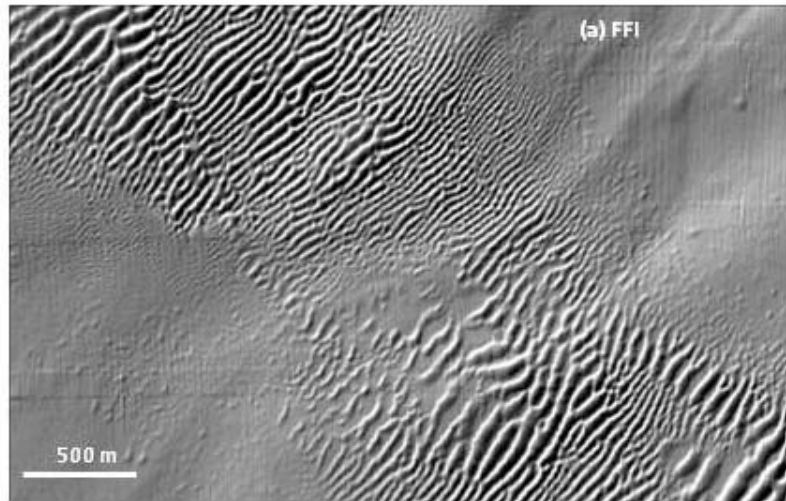


*Figure 30. Multibeam bathymetry shaded relief images from part of the N2 area showing data quality and resolution of sandwaves from (a) FFI data (b) MAREANO data (c) UiT data. Each dataset is gridded at 5 m resolution.*

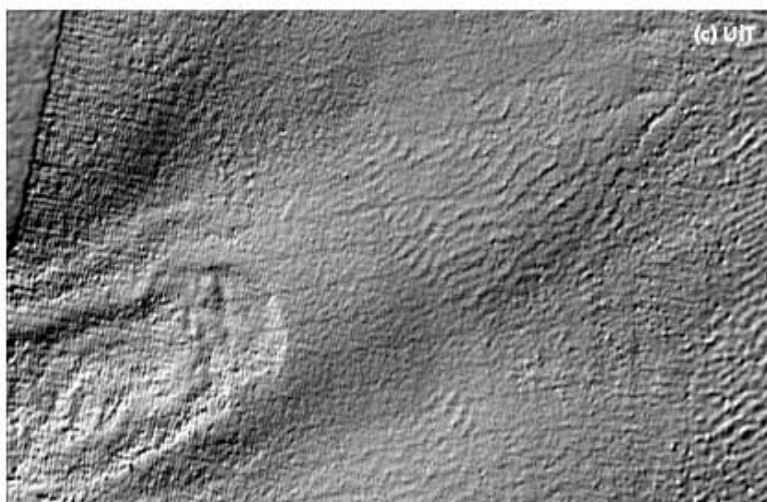
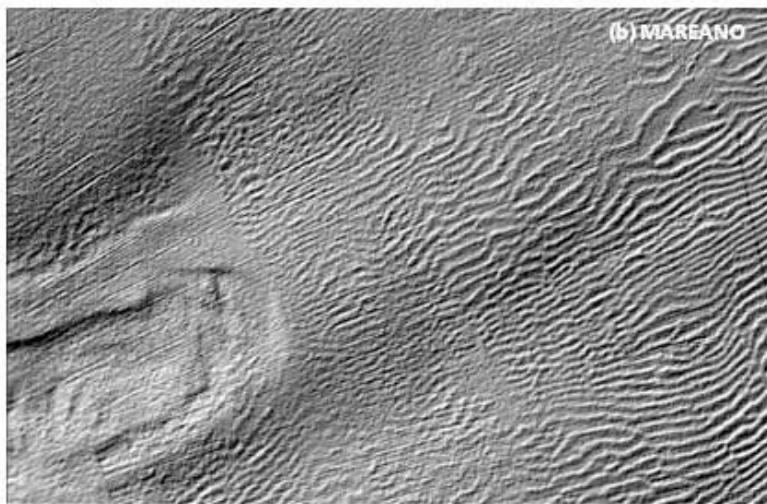
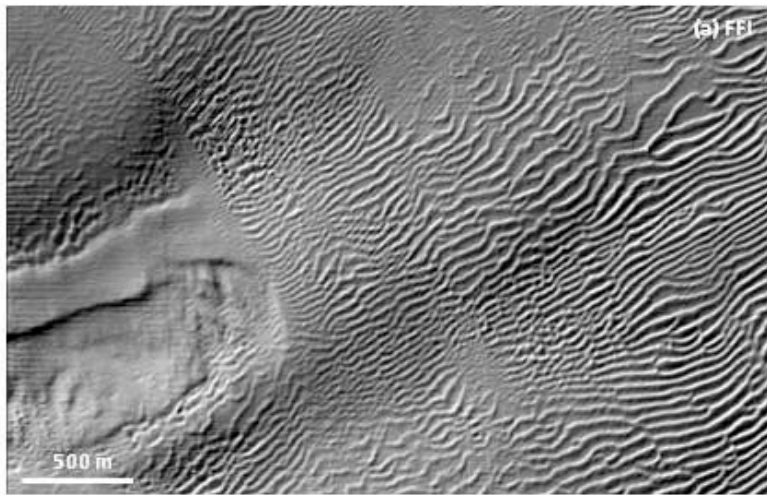


*Figure 31. Multibeam bathymetry shaded relief images from the S1 area showing data quality and resolution of sandwaves from (a) FFI data (b) MAREANO data (c) UiT data. Each dataset is gridded at 5 m resolution.*

Data quality from the S1 area is more varied. Again the FFI data show the best detail of the sandwaves revealing more extensive small sandwaves around the edge of the main sandwave area, including into the slide area on the left of Figure 31. These small sandwaves were obscured by noise in the MAREANO data. The UiT data are plagued by more noise than the data from the N2 area and from this dataset it is only the larger sandwaves which can be resolved. This additional noise could be due to interference from other sensors (note the multibeam data were collected simultaneously with 3D seismic data), sea conditions during the survey, and/or other data acquisition problems.

In addition to the horizontal differences evident from the shaded relief images we have also checked vertical differences between the datasets. These are quite frequently 1-3 m within the sandwave area – therefore of the same order of magnitude as the sandwaves themselves. This is most likely due to the fact that only the MAREANO data are corrected for tides. This makes comparison of sandwave heights difficult, at least using the data directly. In this report we focus on horizontal comparison of the sandwave datasets. Further investigation will examine additional confidence measures associated with the bathymetry data.

#### 4.9.2 Terrain analysis of bathymetry data

Terrain analysis was performed on each bathymetric dataset to help delineate the sandwave features and quantitative measures of their morphology, already proven to be useful for the MAREANO data (King et al. 2011) and UiT data (Waage 2012). The primary objective at this stage in the study was to compare potential changes in sandwave morphology/position over the time-series datasets. It was therefore especially important to minimize the influence of artefacts on the data.

One method of achieving this is to use successively larger analysis windows for extracting terrain parameters such as slope, aspect and curvature, thereby allowing derivation the terrain parameters at multiple scales (Dolan 2012, Wilson et al. 2007, Wood 2009). Landserf v.2.3 software (Wood 2009) was used for terrain analysis. Following tests on the MAREANO and FFI data it was decided that a window size of 9x9 pixels was appropriate for the present datasets. At this length scale (corresponding to a ground distance of 45 x 45 m) terrain variables could be analysed and produce results useful for the characterization of sandwaves, yet without undue interference noise from artefacts in the bathymetry data.

The UiT data contained more prominent artefacts which were often of similar size to the sandwaves themselves, therefore were unsuitable for filtering out using this approach. UiT data were therefore subject to terrain analysis at the same 9x9 window size but we note the presence of some artefact-induced features in the derived terrain variables.



Visual analysis of these derived terrain variables shows how they can help to highlight ridges and troughs in the sandwave fields, however setting of a threshold value for the transition from e.g. crest to slope of a sandwave, is more challenging and it is difficult to find values which hold across all datasets due to the differences in the level of detail mapped which has consequences for the values of terrain variables generated.

Recognizing limitations in the use of continuous terrain variables for the delineation of features (crests and troughs) we have also introduced the use of terrain feature analysis. This was not conducted by King et al. (2011) or Waage (2012) but proves effective at delineating features relevant to sandwave morphology and change detection. This approach is based on a quadratic approximation to the terrain surface and is detailed by Wood (1996). More recent applications include that of Zieger et al. (2009) who used the technique to map tropical coral reefs and who summarized the technique in to the figure below (Figure 32).

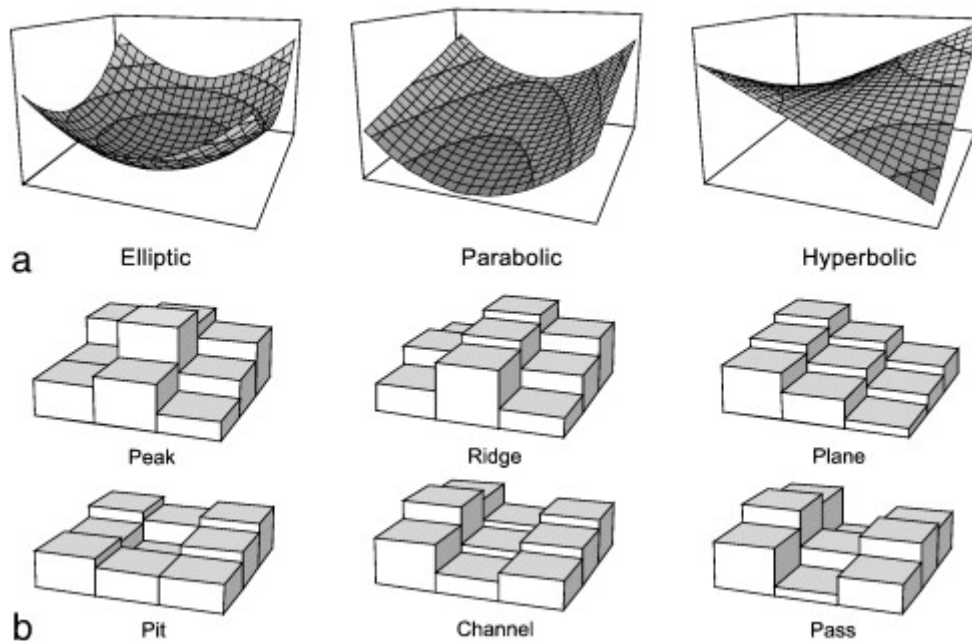


*Fig. 32. Second-degree polynomials (a) are applicable to derive six morphometric feature classes (b), simplified by a 3×3 cell raster. From Zieger et al. (2009), adapted from Wood (1996).*

Although analysis of the sandwave areas identifies each of these feature classes, it is the ridge and channel classes which are most useful in determining the location of sandwave crests and troughs respectively. Using Wood's (1996) definition we have:

- Ridge (sandwave crests) - Point that lies on a local convexity that is orthogonal to a line with no convexity/concavity.

- Channel (sandwave troughs) - Point that lies in a local concavity that is orthogonal to a line with no concavity/convexity.

An example of ridge /channel feature classification is shown in Figure 33 which shows how effective the method is at picking crests and troughs in the sandwave data.

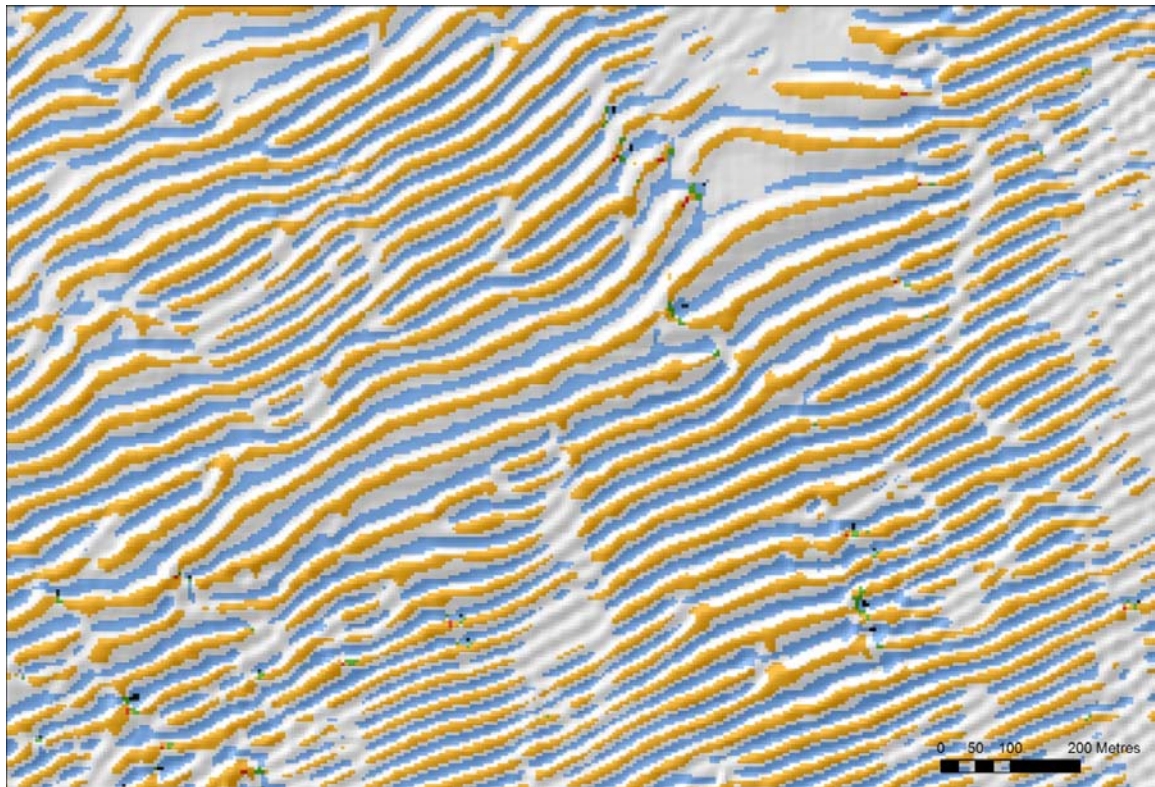


*Figure 33. Example of crests (orange) and troughs (blue) identified by automatic feature detection (Wood 2009) using a 9x9 pixel analysis window from the FFI bathymetry dataset with 5 m grid resolution (S1 field). Features are shown draped on shaded relief in order to aid interpretation.*

Both King et al. (2011) and Waage (2012) used asymmetry measures to infer migration direction. This is a reasonable approach when no time-series data are available for comparison of crest/trough positions. However, now that we have data over number of years available and a robust method for automatic crest/trough detection we selected to use visual analysis of these features across datasets in order to detect possible migration. Due to the limitations of the data (both grid resolution and quality differences) we can only detect changes that are quite large (~ over 5 metres). It is quite possible that smaller changes are taking place but these cannot be detected with available data. It is also possible that some areas which appear to be migrating based on crest/trough position are only seen as such due to difference in data quality which introduces uncertainty in subsequent feature detection.

For the northern area we compared features identified in the MAREANO dataset with those identified from the FFI data. Not all crests could be compared due to quality differences

between the datasets which meant that fewer features were detected in the MAREANO data. However, whilst it was impossible to determine change at the majority of investigated locations we observed a noticeable change in the position of crests/troughs at those locations marked with red dots (migration towards NW) and blue dots (migration towards SE) (Fig. 34). Only a few locations within the area of barchan-shaped sandwaves were checked as it proved virtually impossible to detect changes here. The more linear sinusoidal sandwaves were easier targets for migration detection. Migration distances are in the range 5-15 m though we note they could be overestimated due to pixel size and feature classification.

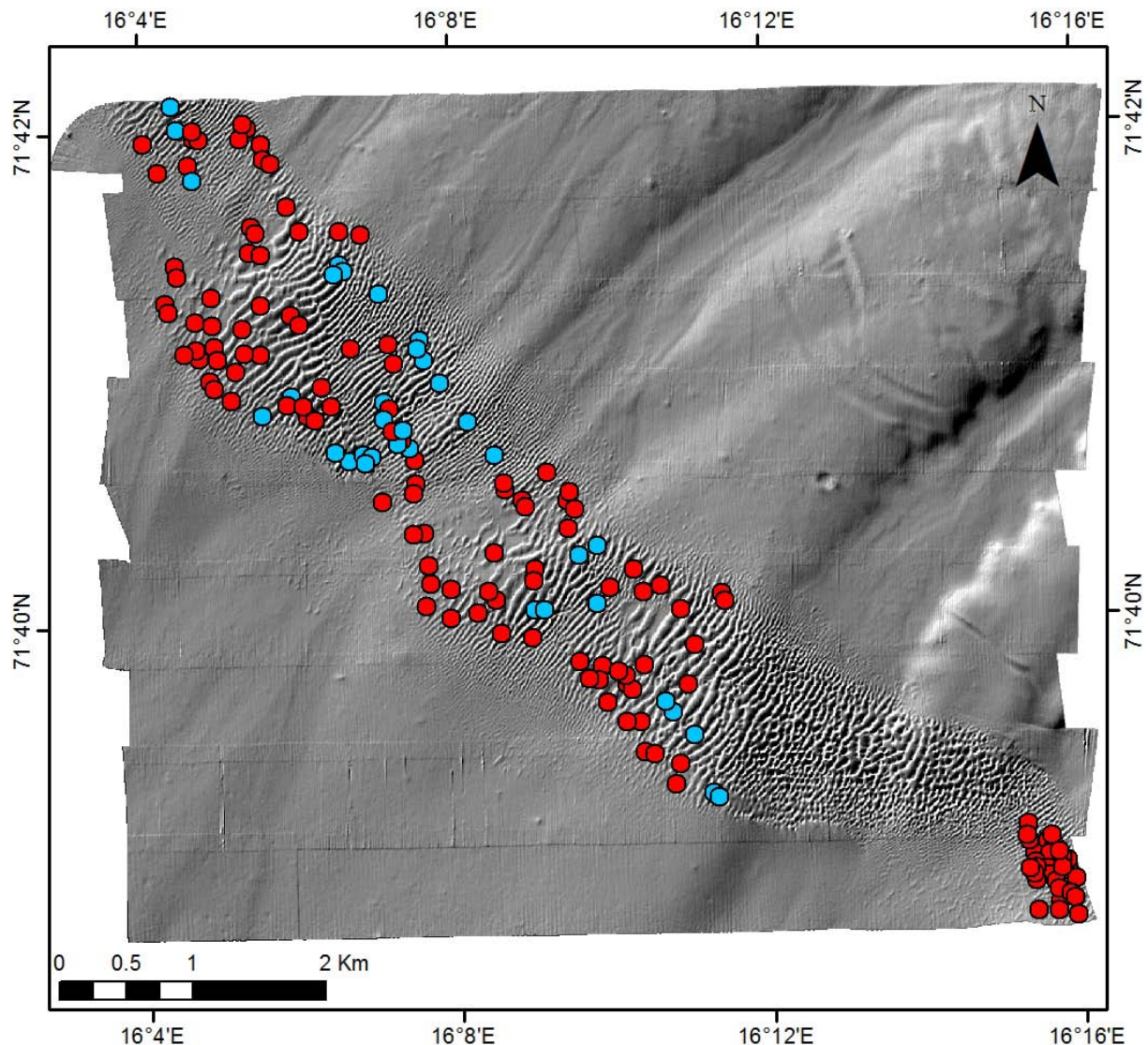


*Figure 34. Inferred directions of sandwave migration in the N2 sandwave area determined from changes in crest/trough position between the MAREANO and FFI datasets using automatic feature detection (Wood 2009). Red dots indicate a crest that has moved NW while blue dots indicate a crest that has moved SE. The sandwave area in the SE corner is shown in greater detail in Figure 35.*

In the southern part of the N2 area we observe the most prominent migration. There appears to be a successive movement NW in the position of crests over the years between the

MAREANO (yellow), UiT (purple), and FFI data (orange) bathymetry data. Some sandwaves appear to have migrated up to 10 m. A NW migration is in contradiction with the migration direction inferred by Waage (2012) from asymmetry metrics (though we also note particularly poor data quality in the UiT data used by Waage which makes interpretation challenging). We have investigated asymmetry visually from profiles which revealed that the detection of asymmetry is very sensitive to the orientation of the profile. Therefore small differences in the direction of a profile (used to calculate asymmetry) can yield very different results since the sandwaves are often slightly irregular. This sensitivity may also not be captured by analyses conducted by King et al. (2011) who followed the main axis of the sandwave field for all morphometrics calculations in order to get an overall picture of the morphology and seabed processes.

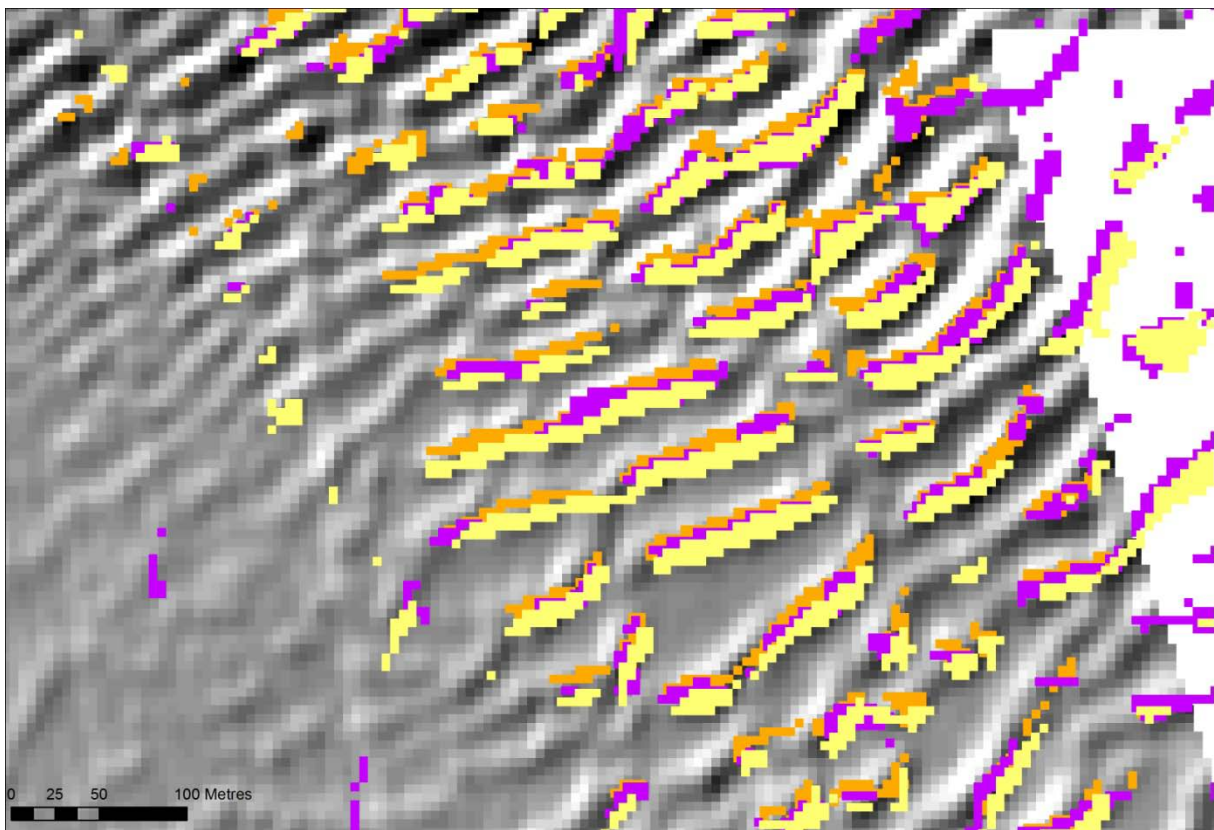


*Figure 35. Feature detection example from the SE corner of the N2 area where migration is most prominent. The figure shows the position of crests identified from MAREANO (yellow), UiT (purple), and FFI data (orange). Location indicated in Figure X above.*

The same comparison of crests/troughs was performed in the S1 area (Fig. 36), however, we found no locations where it was possible to detect migration. Data from MAREANO and FFI showed good agreement in the position of crests and troughs, while UiT data was of too poor quality to be considered. Some additional crests/troughs were identified in the FFI data due to the better data quality, however this information could not be used to assess migration as there was no basis for time-series comparison.

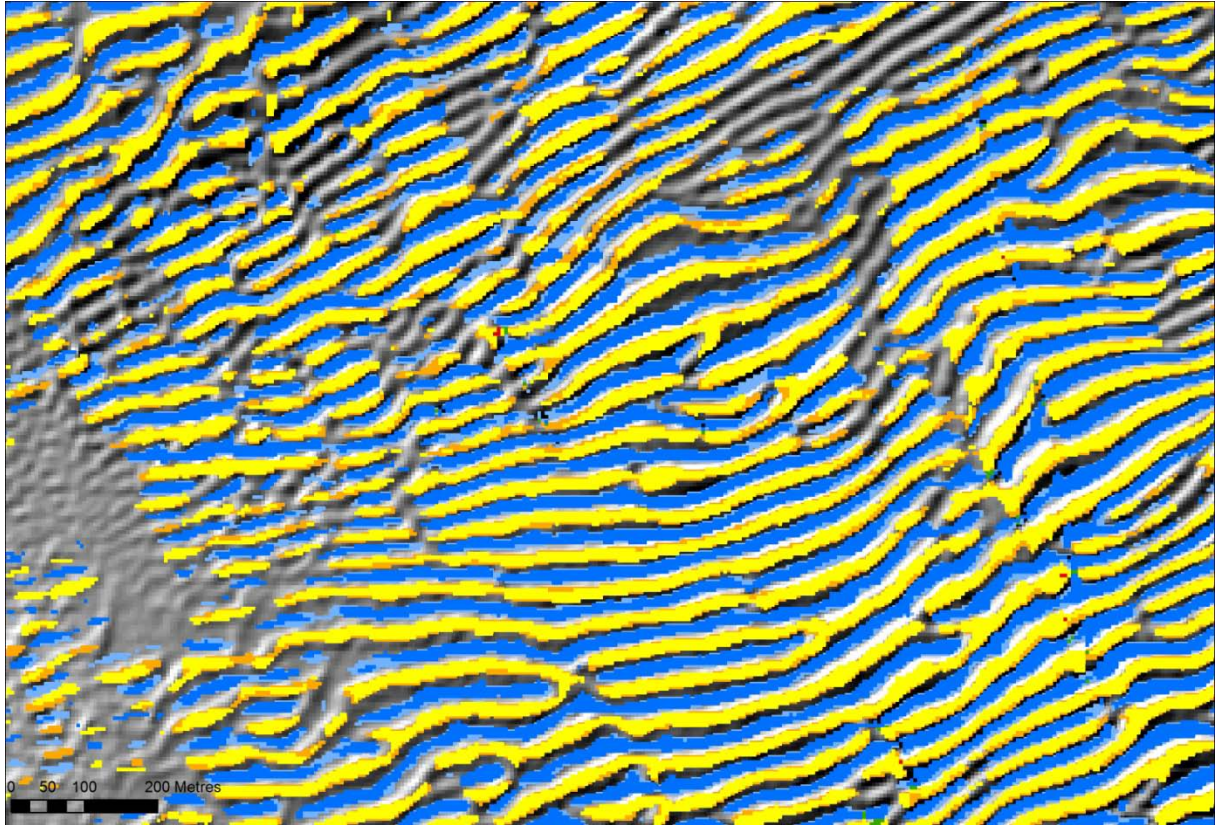


*Figure 36. Example of crests and troughs identified by automatic feature detection in the S1 area. MAREANO data are shown with yellow crests and dark blue troughs, while FFI data are shown with orange crests and lighter blue troughs.*

Using the latest data from FFI it has also been possible to reinterpret the extent of the sandwave fields. The new data reveal that both the N2 and S1 areas are more extensive than previously recognised by MAREANO multibeam and TOPAS. The newly interpreted outlines are indicated in Figures 37 and 38 and show the persistence of small sandwaves around the edge of the main, previously identified area. In both areas, the newly identified smaller sandwaves continue right to the edge of the dataset so it is not possible to determine their full extent, therefore this re-interpreted boundary should be considered a provisional boundary until new detailed data may become available.

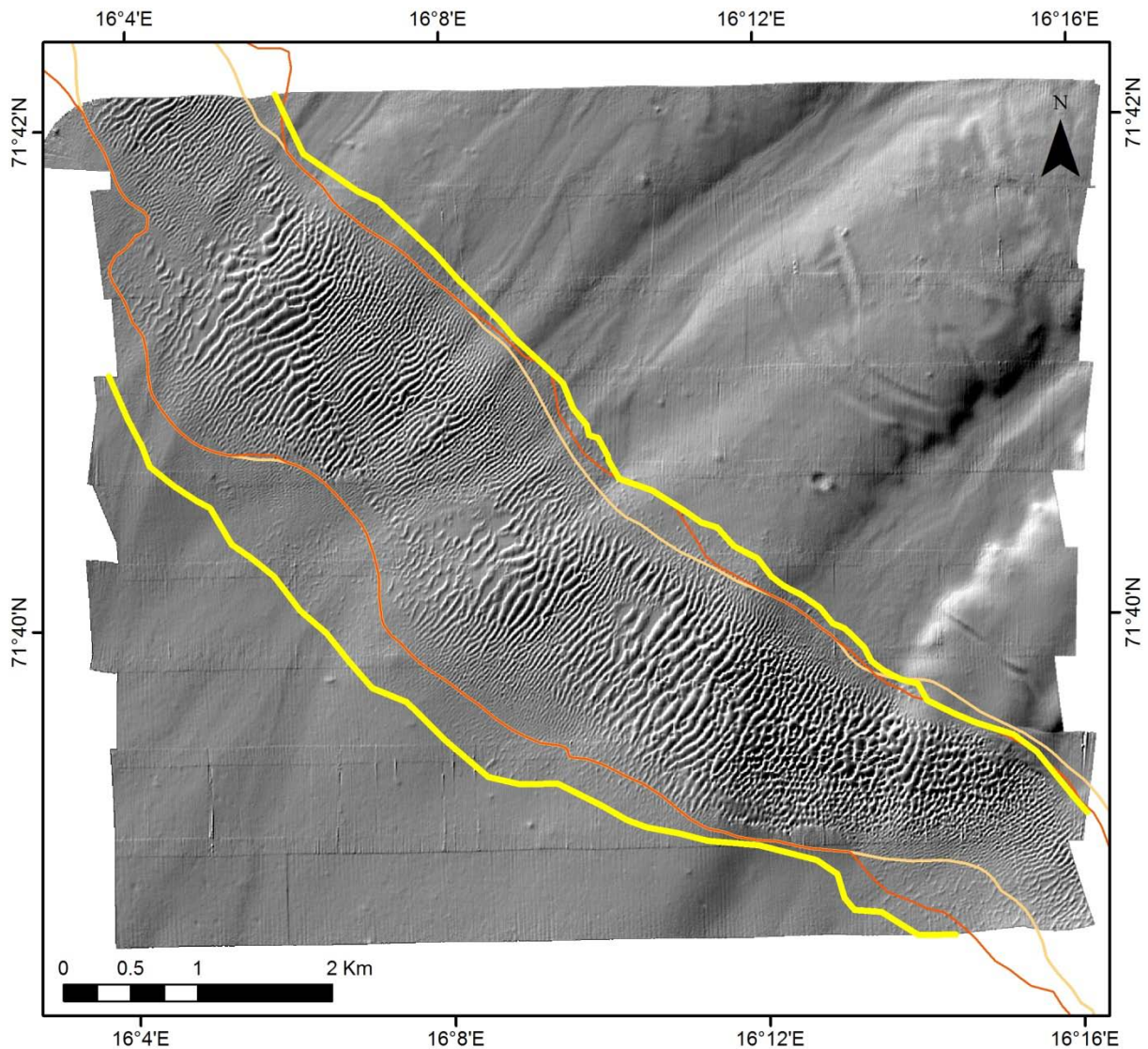


Figure 37. Extent of N2 sandwave area inferred from FFI multibeam bathymetry data (yellow). Previous interpretations from MAREANO multibeam bathymetry (light orange) and from TOPAS data (dark orange) are shown for comparison.

#### 4.9.3 Analysis of backscatter data

Only FFI and MAREANO backscatter data have been considered for comparative analysis since these data were all acquired using an EM710 multibeam echosounder. The UiT data were acquired using a different multibeam echosounder (EM300) operating at a different frequency; therefore the backscatter signal is not directly comparable in terms of penetration and scattering at the seabed.

Backscatter data were processed using QPS-Fledermaus FMGT to produce raster mosaics at 3 m resolution. This was an increase in resolution over the original MAREANO processed multibeam data studied by King et al. (2011), which were processed using Geological Survey of Canada software. Nevertheless the re-processing of MAREANO data using FMGT did not yield any noticeable difference in quality over the original data processing which was used by

King et al. (2011), and which is available on [www.mareano.no](http://www.mareano.no). From Figure 39 however, we see clearly that the MAREANO data remain significantly poorer quality than FFI data in terms of their ability to resolve fine-scale differences in acoustic response (an indicator of sediment composition) associated with the sandwaves.

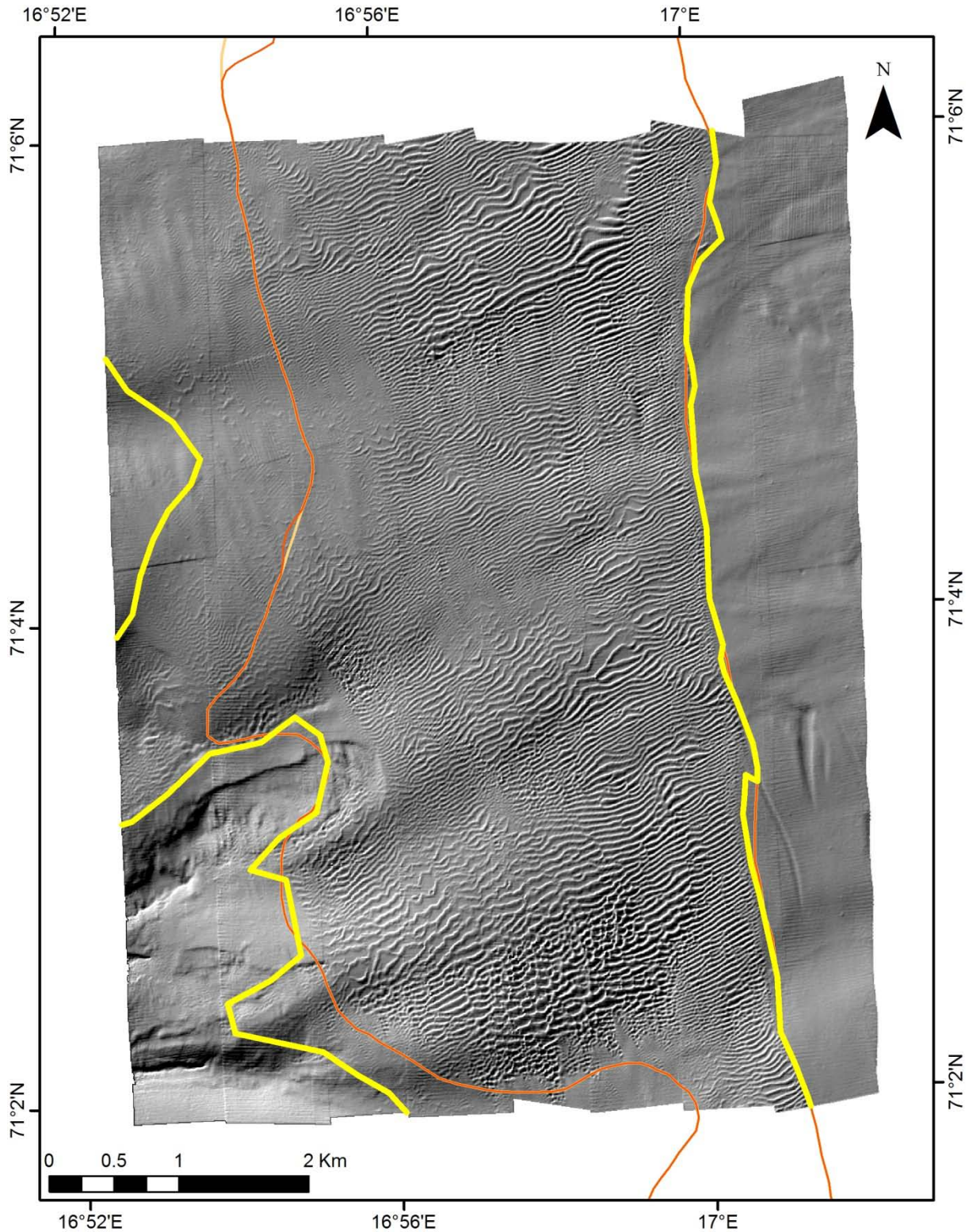


*Figure 38. Extent of S1 sandwave area inferred from FFI multibeam bathymetry data (yellow). Previous boundaries from MAREANO multibeam bathymetry (light orange) and from TOPAS data (dark orange) are shown for comparison - these are very similar.*

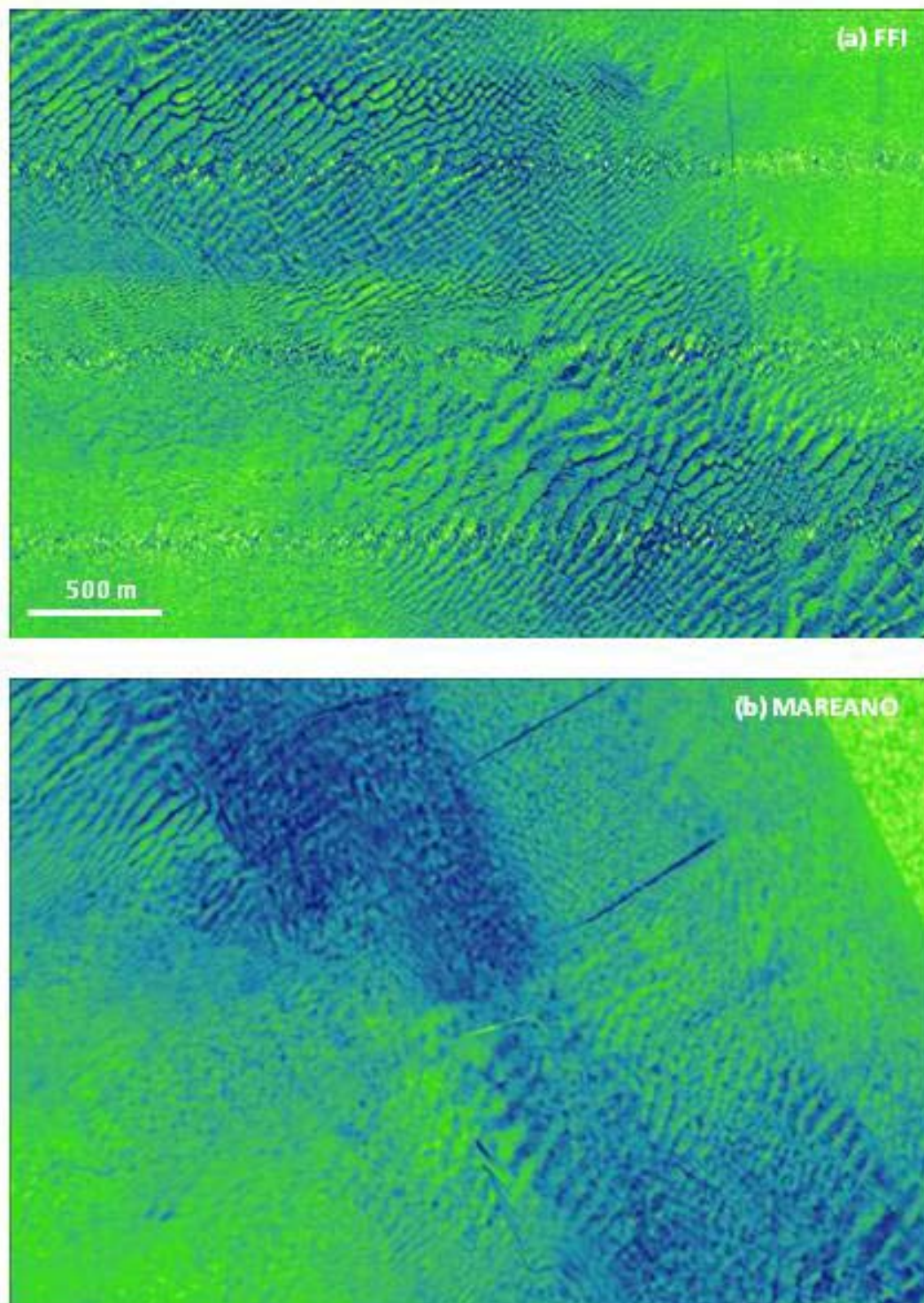


*Figure 39. Examples of EM710 multibeam backscatter imagery from the N2 area. (a) FFI data, (b) MAREANO data. Both datasets have been mosaiced to 3 m resolution. Higher values (coarser/compact sediments) are shown in green while lower backscatter values (finer/less compact sediments) are shown in blue. Different colour ramps are used for each image as the primary purpose of the figure is to illustrate differences in resolution.*



The FFI data offer an excellent view of the sandwaves and may thereby help better understand sediment accumulation processes within the study areas. The 3D visualization in Figure 40 shows FFI backscatter data draped on bathymetry data. This visualization highlights the differences in backscatter signature between crests and troughs and also reveals differences between the acoustic responses of sandwaves with different morphological characteristics e.g. the dark area towards the centre of the image is an area of barchan-shaped dunes within an area otherwise dominated by sinusoidal sandwaves of various sizes.

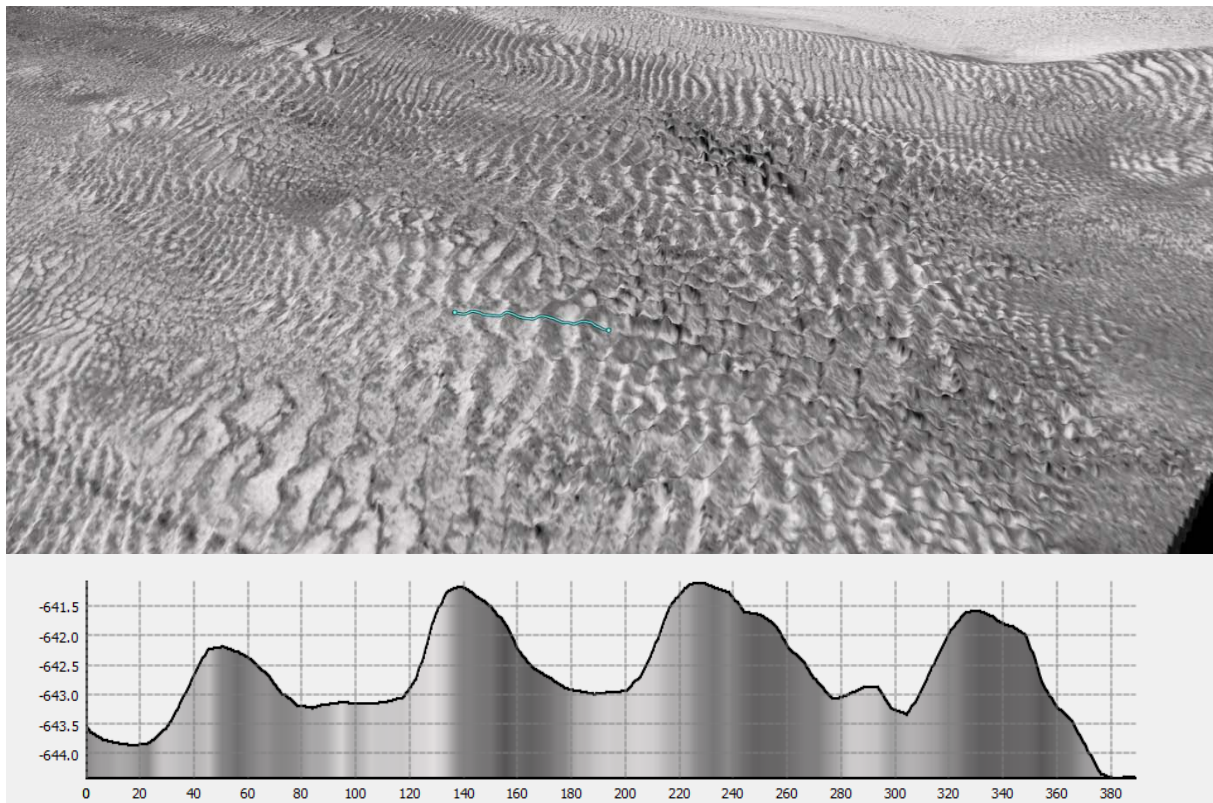


*Figure 40. 3D visualization of FFI backscatter from the N2 sandwave area draped on bathymetry (6 x vertical exaggeration). Lighter colours indicate coarser/more compact sediments, while darker colours indicate finer/less compact sediments. This is highlighted in the profile which shows backscatter variation across several large sandwaves.*

## 5. DISCUSSION OF SAND SOURCE AND TRANSPORT DIRECTION

The sandwave fields overly glaciogenic sediments both from times when the ice margin grounded at the shelf break some kilometres up-slope (until c. 15 000 years ago) and when it retreated to supply hemipelagic muds and ice rafted material (King et al. 2011). A number of gravity mass failures occurred afterward, some within the sandwave fields and stratigraphic relations suggest that even these pre-date the sandwave field initiation. The sand source may be local, from current washing of the uppermost glacial sediments and the sink may be within the sandwave fields themselves, preserved as immobile sand beneath more active forms. It is

also possible that the sand originates from further south on the slope, from lower on the slope, or from higher on the slope/ bank areas.

King et al. (2011) concluded, from statistical analyses, that there are several indices suggesting a clustering or domains of bedforms which are somewhat tuned to the meso-morphology of the terrain in which they lie, a terrain inherited from glacial processes and actively shaped up to the end of the last glaciation. This suggested that there is a much more complex hydrologic regime than a simple continuous northward contour current which drives the bedforms. Local steering, current acceleration and perhaps induced turbulence were suggested. An upward driving hydrologic component must be able to balance mid-term tendencies of down-slope grain migration. The complexity suggested provided support for the initial hypothesis that relatively unique and poorly understood oceanic conditions are at play, possibly including tidal-wave driven internal waves channelled on the thermocline and tied to interaction with the slope near the shelf break. All indications suggested active bedform mobility.

Visual observations based on existing data indicate that small ripples are nearly ubiquitous, superimposed on the sandwaves (King et al. 2011). Orientations are largely unknown but starkly contrasting directions at the sharp transition from bedform stoss to lee slopes suggests local hydraulic regimes which are important to transport direction and magnitude and must be better understood. Most indications are that the sandwave crests are sharp and lee sides steep. All these indications suggest active bedform mobility, both in a mobile layer several centimetres thick and, at a much slower pace in the larger bedforms.

The results in this report, from the study of bathymetry datasets collected over a 4-year time period, show that sandwaves are migrating. The resolution of the bathymetry data is not high enough to observe small changes but, especially in the N2 area, migration is evident. Sandwaves migrating NW are common in this area, especially in the southern part of N2, where sandwaves may have migrated up to 10 m. In N2, there are also sandwaves migrating SSE.

Our grain-size data suggest that within the sandwave fields, better sorted sand occurs towards the north. This is consistent with a sand source towards the south and transport towards the north. It is difficult to see a consistent pattern in the rounding of sand grains. Also median and mean grain sizes decrease in northerly direction, indicating the same general transport direction towards the north.

Although there are too few samples for confident comparison, the petrographic analysis indicate that the samples with the lowest quartz content occur in the south. This could indicate wearing down of less resistant material and concentration of quartz grains as bottom currents transport material gradually towards the north. It should be noted however, that preliminary results from IMR's modelling work indicate gyres and local variations in bottom currents direction and velocity. Mineralogical and geochemical analyses show that the sands have low

carbonate content (average 1.4%), mainly shell fragments/foraminifers/fossils. This may suggest that the sand is actively migrating on the sea floor, possibly back and forth, and that less resistant carbonate is being worn down.

From the data in this report it is not possible to conclude whether there is sand transport into or out of the sandwave fields along the downslope channels. However, current measurements and preliminary modeling results conducted by IMR in the present project suggest a daily migrating thermocline in the sandwave area. It is thus possible that active sand transport occurs along the channels into or out of the sandwave areas from the upper slope/adjacent banks or from areas lower on the slope.

## **6. SUMMARY AND FURTHER WORK**

The following preliminary conclusions can be drawn:

- There is no clear relationship between the location of sandwaves and the location of seafloor channels/slide scars.
- From the sub-bottom profiler dataset we see no indication of a sand unit beneath the sandwaves, nor do we see buried or partially buried sandwaves.
- Mean sand thickness, estimated from sub-bottom profiler data, ranges from 1.2 to 2.3 m within the sandwave fields; this correlates well with sandwave height estimated from multibeam bathymetry data. Maximum sandwave thickness, estimated from sub-bottom profiler data, is 6.2 m and found within one of the channels south of N4.
- No clear trends in sand thickness are observed across the sandwave fields, although some downslope channels are associated with thicker sand.
- Within the sandwave fields the particles predominantly comprise well-sorted, medium-grained sand.
- Sediment samples taken outside of the sandwave field show a lower degree of sorting, with a larger percentage of coarse sand and gravel, than sample from within the sandwave fields.
- A weak trend towards better sorted sand with lower median and mean grain size northwards is observed within samples from the sandwave fields.
- No clear trend in sand maturity (e.g. degree of rounding) can be observed although the sample with the lowest quartz content occurs in the south.
- No correlation between sandwave height or wavelength and mean grain size or degree of sorting is observed.
- A clear trend for lower calcium carbonate concentrations within the sandwave fields (mean 1.4 wt%) compared with outside the sandwave fields (mean 13.2 wt%) is seen. The highest calcium carbonate concentrations are observed immediately south of the sandwave fields, reaching 42.3 wt%.

- Results from repeated multibeam surveys show that the sandwaves migrate, mainly towards the NW, but also towards the SE. Migration distances up to 10 m in northerly direction are indicated.

The data and preliminary interpretations in this report will be integrated with IMRs bottom current measurements and modelling work and UiTs 3D seismic data. Results and interpretations will be published in scientific journals.

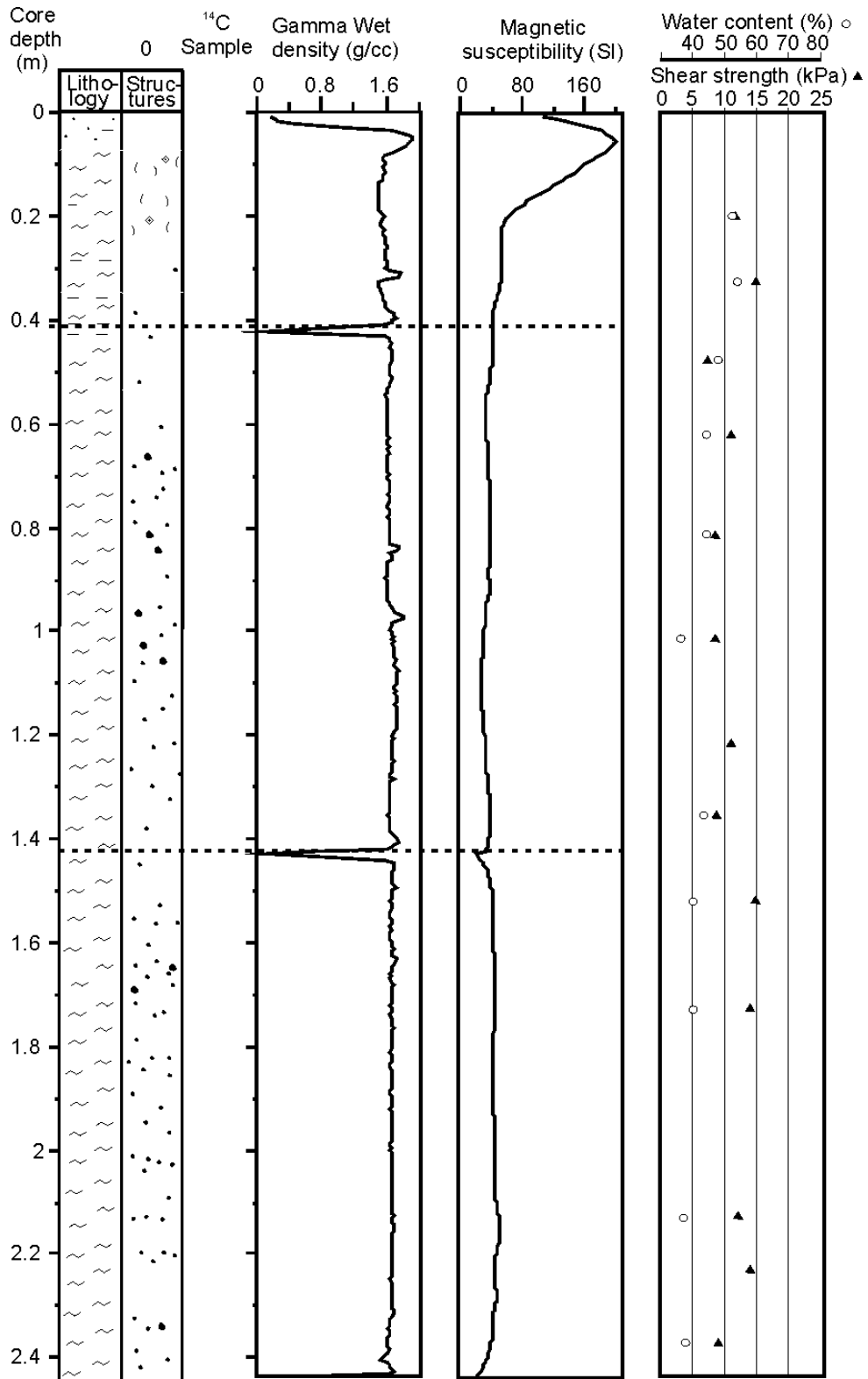
## 7. REFERENCES

- Blott, S.J. and Pye, K., 2001: Gradistat- A grain size distribution and statistics package for the analysis of unconsolidated sediments. *Earth Surface Processes and Landforms* 26, 1237-1248.
- Bøe, R., Bellec, V., K., Dolan, M.F.J., Buhl-Mortensen, P., Buhl-Mortensen, L., Slagstad, D. and Rise, L. 2009: Giant sandwaves in the Hola glacial trough off Vesterålen, North Norway. *Marine Geology* 267, 36-54.
- Dolan, M.F.J. 2012: Calculation of slope angle from bathymetry data using GIS - effects of computation algorithms, data resolution and analysis scale. NGU Report 2012.041.
- Faugères, J.C., Stow, D.A.V., Imbert, P. and Viana, A. 1999: Seismic features diagnostic of contourite drifts. *Marine Geology* 162, 1-38.
- Folk, R.L. and Ward, W.C. 1957: Brazos River bar: a study in the significance of grain size parameters. *Journal of Sedimentary Petrology* 37, 3-26.
- King, E., Bøe, R., Bellec, V.K., Rise, L., and Dolan, M. 2011: Contour current driven sandwaves on the upper slope of the continental margin offshore northern Norway - setting and morphometrics. NGU Report 2011.073, 93 pp.
- Laberg, J.S., Andreassen, K., Knies, J., Vorren, T.O. and Winsborrow, M.C.M. 2010: Late Pliocene-Pleistocene development of the Barents Sea Ice Sheet. *Geology* 38 (2), 107-110.
- Laberg, J.S., and Vorren, T.O. 1995: Late Weichselian submarine debris flow deposits on the Bear Island trough mouth fan. *Marine Geology* 127, 45-72.
- Landvik, J.Y., Bondevik, S., Elverhøi, A., Fjeldskaar, W., Mangerud, J., Salvigsen, O., Siegert, M.J., Svendsen, J.I. and Vorren, T.O. 1998: The last glacial maximum of Svalbard and the Barents Sea area: Ice sheet extent and configuration. *Quaternary Science Reviews* 17 (1-3), 43-75.
- Norwegian Mapping Authority Hydrographic Service (NHS) 2009: Technical Specifications Seabed Mapping. MAREANO programme.  
[http://www.mareano.no/\\_\\_data/page/9162/Technical\\_Specifications.pdf](http://www.mareano.no/__data/page/9162/Technical_Specifications.pdf)
- Ottesen, D., Stokes, C.R., Rise, L. and Olsen, L. 2008: Ice-sheet dynamics and ice streaming along the coastal parts of northern Norway. *Quaternary Science Reviews* 27 (9-10), 922-940.
- Rise, L., Olsen, L., Bøe, R. and Ottesen, D. 1996: Thickness, distribution and depositional environment of Holocene sediments in the Norwegian part of Skagerrak. *Norges geologiske undersøkelse Bulletin* 430, 5-16.
- Rüther, D.C., Mattingsdal, R., Andreassen, K., Forwick, M. and Husum, K. 2011: Seismic architecture and sedimentology of a major grounding zone system deposited by the Bjørnøyrenna Ice Stream during Late Weichselian deglaciation. *Quaternary Science Reviews* 30, 2776-2792.
- Sættem, J., Poole, D.A.R., Ellingsen, L. and Sejrup, H. P. 1992: Glacial geology of outer Bjørnøyrenna, southwestern Barents Sea. *Marine Geology* 103, 15- 51.

- Svendsen, J.I., Gataullin, V., Mangerud, J. and Polyak, L. 2004: The glacial history of the Barents and Kara Sea Region. In: Ehlers, J. and Gibbard, P. L. (eds.): Quaternary Glaciations- Extent and Chronology, Vol 1 Europe. Amsterdam, Elsevier, 369-378.
- Vorren, T.O., Hald, M. and Lebesbye, E. 1988: Late Cenozoic environment in the Barents Sea. *Paleoceanography* 3, 601-612.
- Vorren, T. O. and Kristoffersen, Y. 1986: Late Quaternary glaciation in the south-western Barents Sea. *Boreas* 15, 51-59.
- Vorren, T.O. and Laberg, J.S. 1996: Late glacial air temperature, oceanography and ice sheet interactions in the southern Barents Sea region. In: Andrews, J.T., Austin, W.E.N., Bergsten, H. and E., J.A. (eds.): Late Quaternary Palaeoceanography of the North Atlantic margins. Geological Society Special Publication 111. London, Geological Society of London, 303-321.
- Waage, M. 2012: Sand Waves and Sediment Transport on the SW Barents Sea Continental Slope. MSc Thesis, University of Tromsø.
- Wilson, M.F.J., O'Connell, B., Brown, C., Guinan, J.C. & Grehan, A.J. 2007: Multi-scale terrain analysis of multibeam bathymetry data for habitat mapping on the continental slope. *Marine Geodesy* 30 (1-2), 3-35.
- Winsborrow, M.C.M., Andreassen, K., Corner, G.D. and Laberg, J.S. 2010: Deglaciation of a marine-based ice sheet: Late Weichselian palaeo-ice dynamics and retreat in the southern Barents Sea reconstructed from onshore and offshore glacial geomorphology. *Quaternary Science Reviews* 29, 424-442.
- Winsborrow, M.C.M., Bøe, R., Rise, L. and Chand, S. 2012: Cruise report- Sandwaves and sand transport on the Barents Sea continental margin offshore Norway. NGU report 2012.038, 75 p.
- Ådlandsvik, B. and Ostrowski, M. 2010: Fysiske forhold utenfor kysten av nordnorge. In: Buhl-Mortensen, L., Hodnesdal, H. and Thorsnes, T. (eds.): Til bunns i Barentshavet og havområdene utenfor Lofoten: Trondheim, Norges geologiske undersøkelse.

**APPENDIX 1**

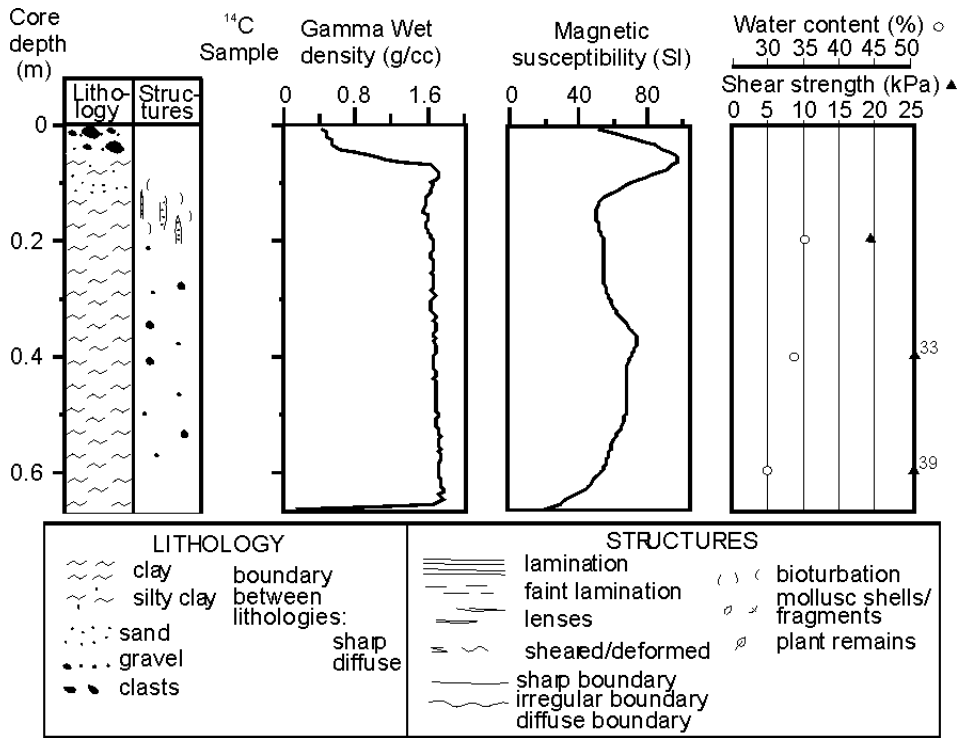
**GRAVITY CORE LOGS**



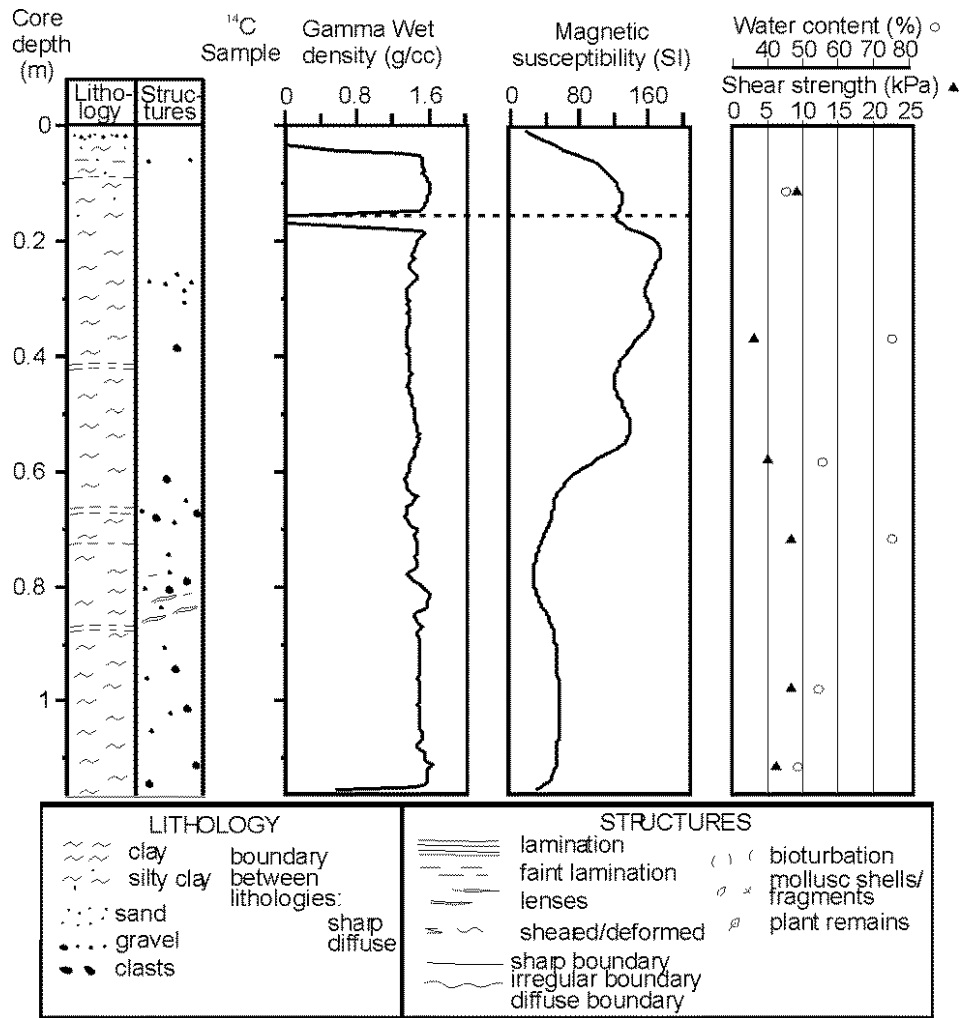
LITHOLOGY		STRUCTURES	
~ ~ ~	clay	=====	lamination
~ ~ ~ .	silty clay	- - - - -	faint lamination
. . . . .	sand	— — —	lenses
. . . . .	gravel	~ ~ ~	sheared/deformed
● ● ●	clasts	— — —	sharp boundary
	boundary between lithologies:	— — —	irregular boundary
	sharp	~ ~ ~	diffuse boundary
	diffuse	( ) (	bioturbation
		o x	mollusc shells/fragments
		∅	plant remains

GC 4

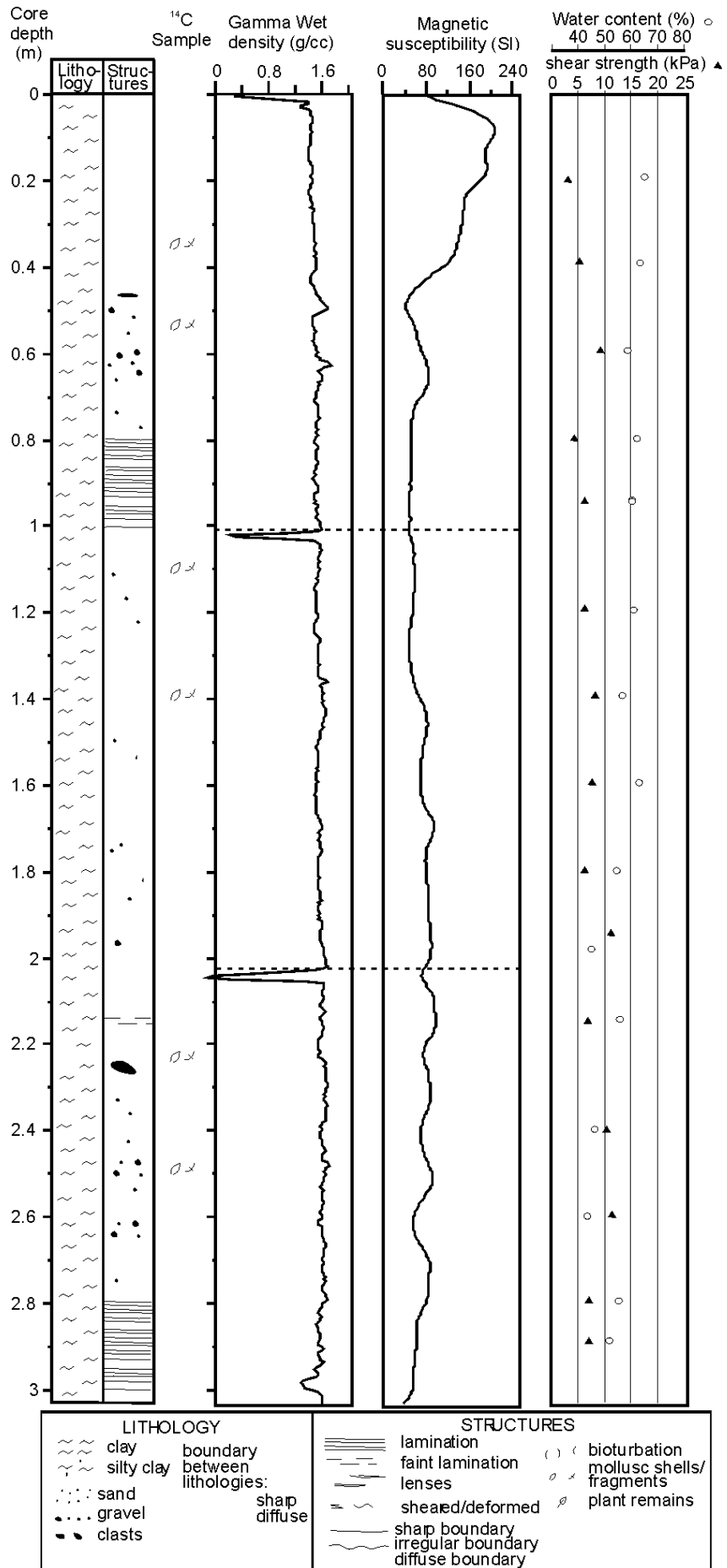




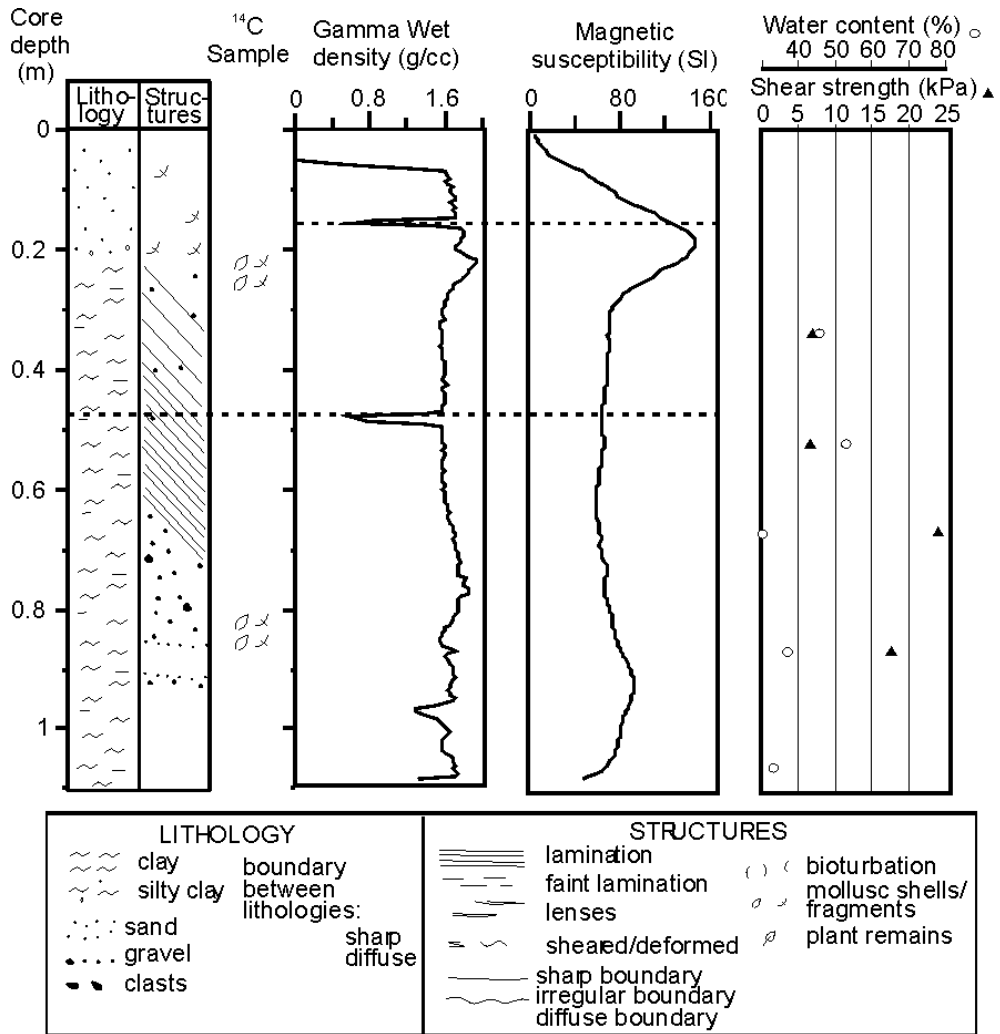
GC 6



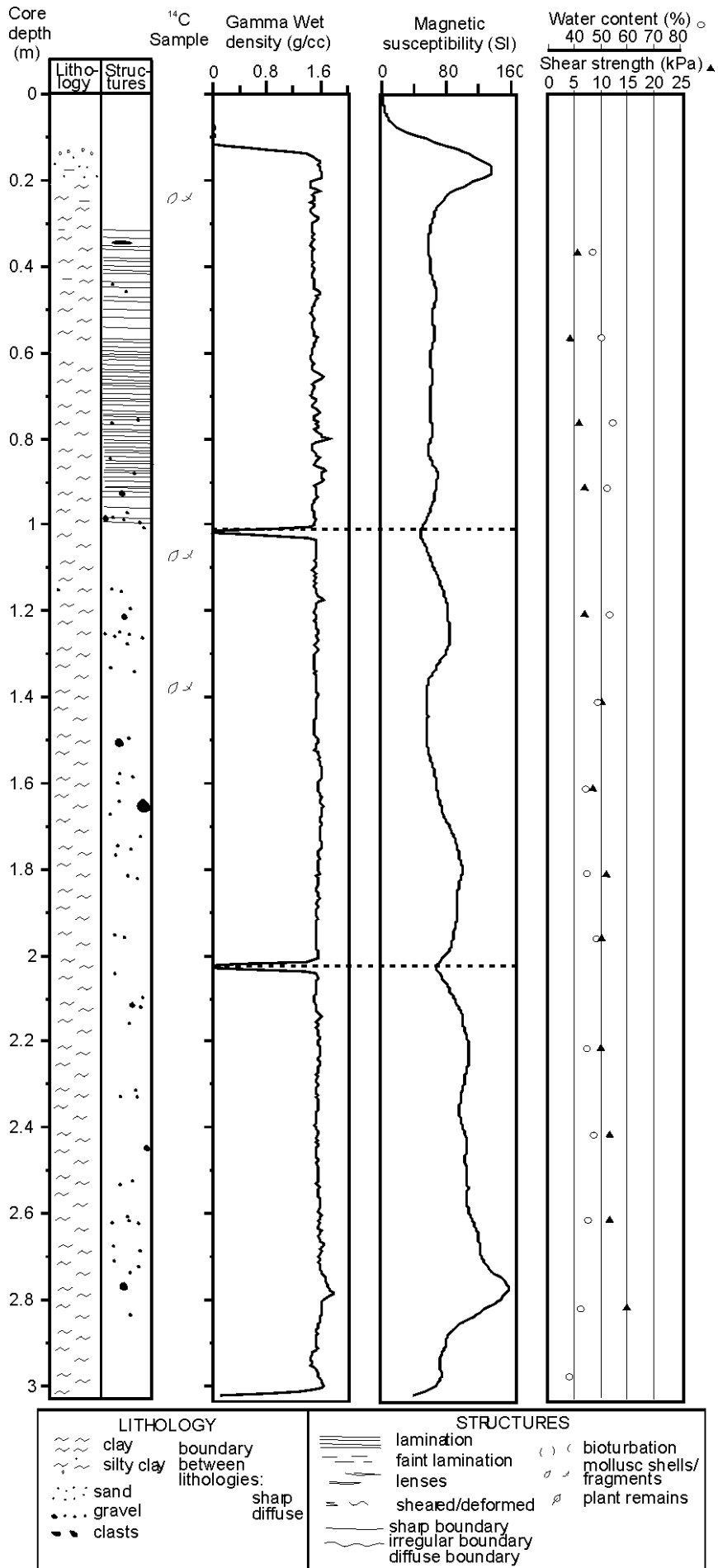
GC 7



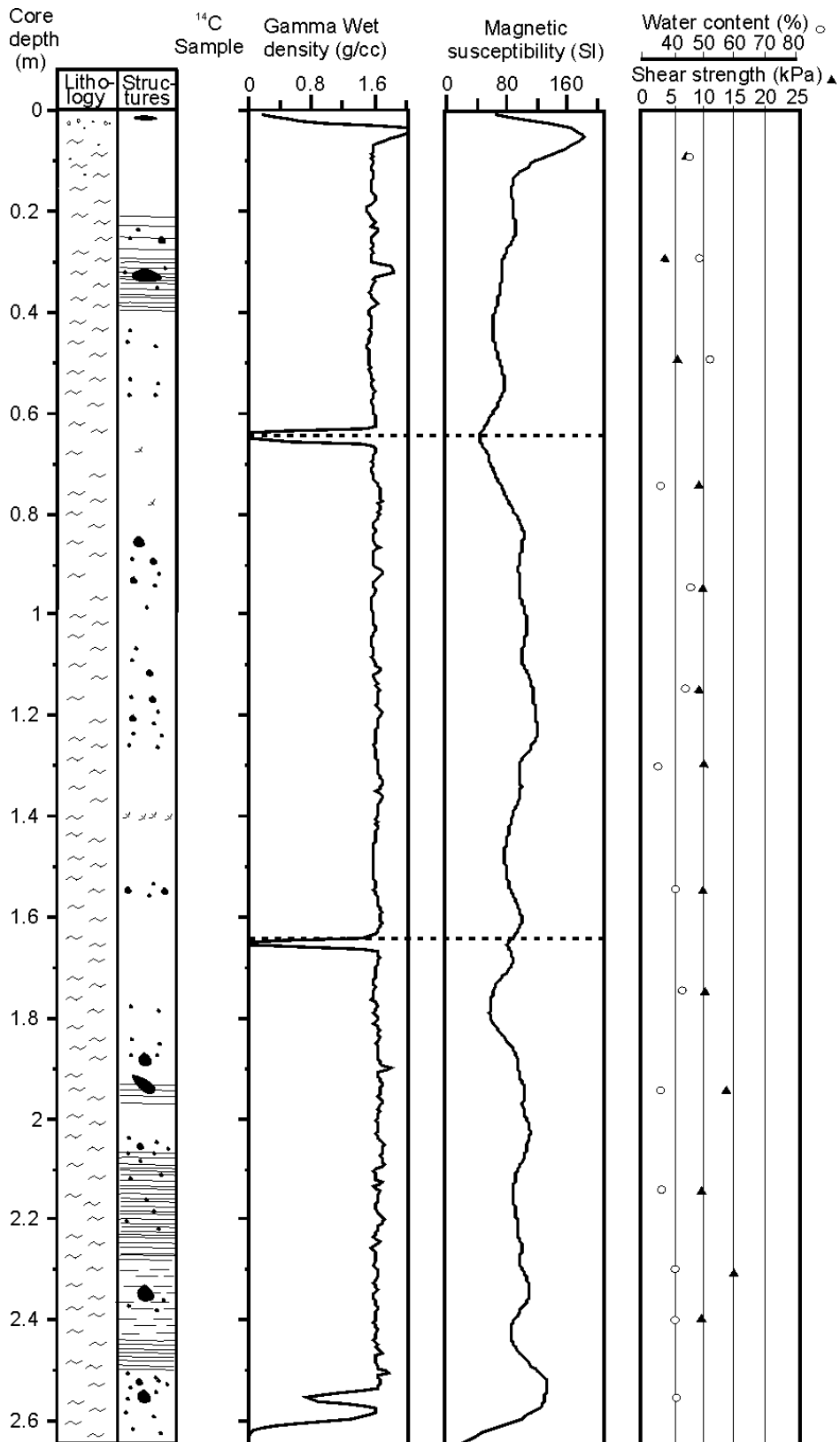
GC 8



GC 10

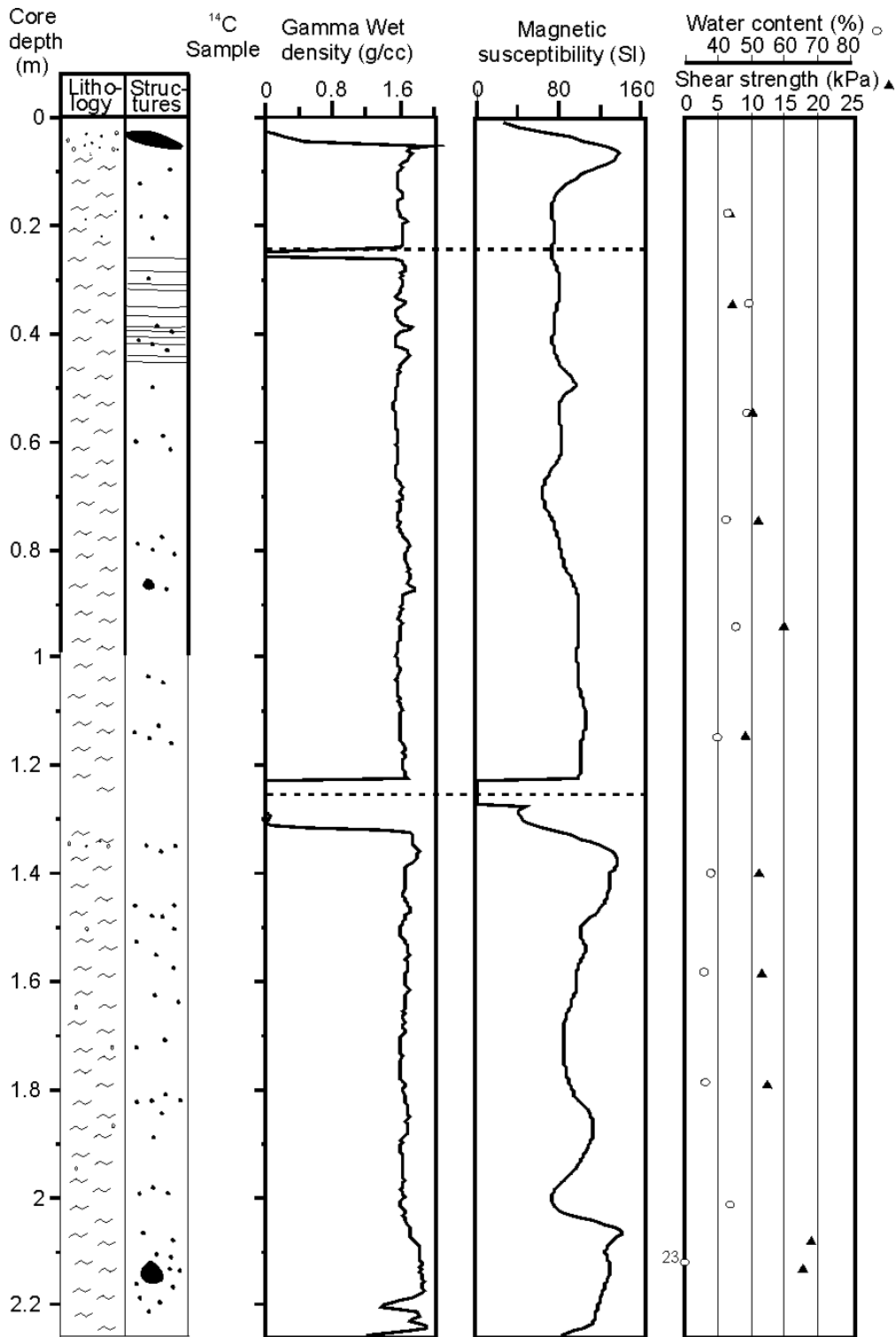


# GC 11



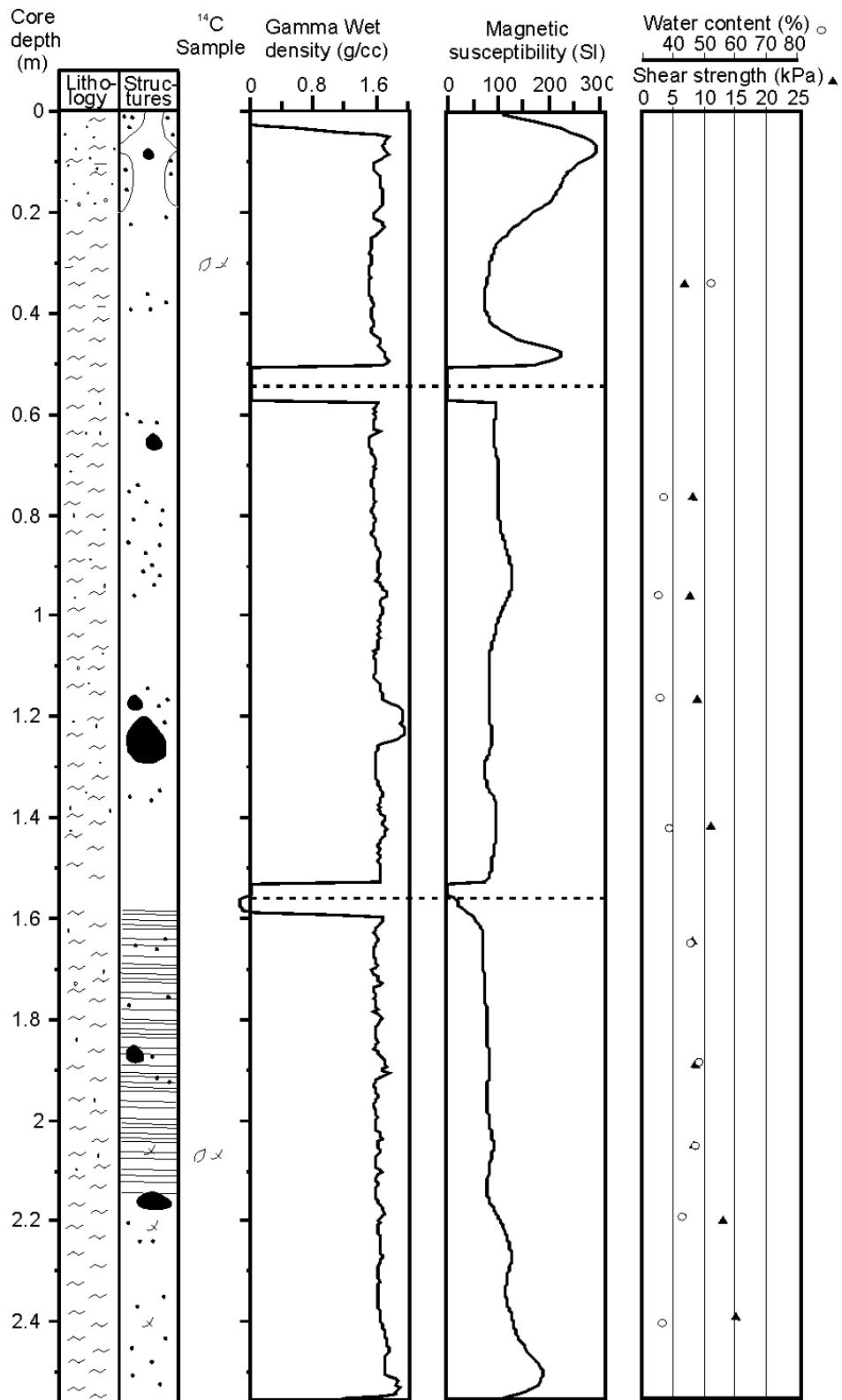
LITHOLOGY		STRUCTURES	
~ ~ ~	clay	=====	lamination
~ ~ ~	silty clay	-----	faint lamination
. . . . .	sand	=====	lenses
. . . . .	gravel	= ~ ~	sheared/deformed
● ● ●	clasts	———	sharp boundary
	boundary between lithologies:	- - - - -	irregular boundary
	sharp	~ ~ ~	diffuse boundary
	diffuse	( ) (	bioturbation
		o x	mollusc shells/fragments
		p	plant remains

### GC 12



LITHOLOGY	STRUCTURES
~ ~ ~ clay ~ ~ ~ silty clay . . . . sand . . . . gravel ● clasts	lamination - - - faint lamination — lenses = ~ sheared/deformed — sharp boundary ~ irregular boundary ~ diffuse boundary
boundary between lithologies: shape diffuse	( ) ( bioturbation o x mollusc shells/fragments ø plant remains

### GC 13



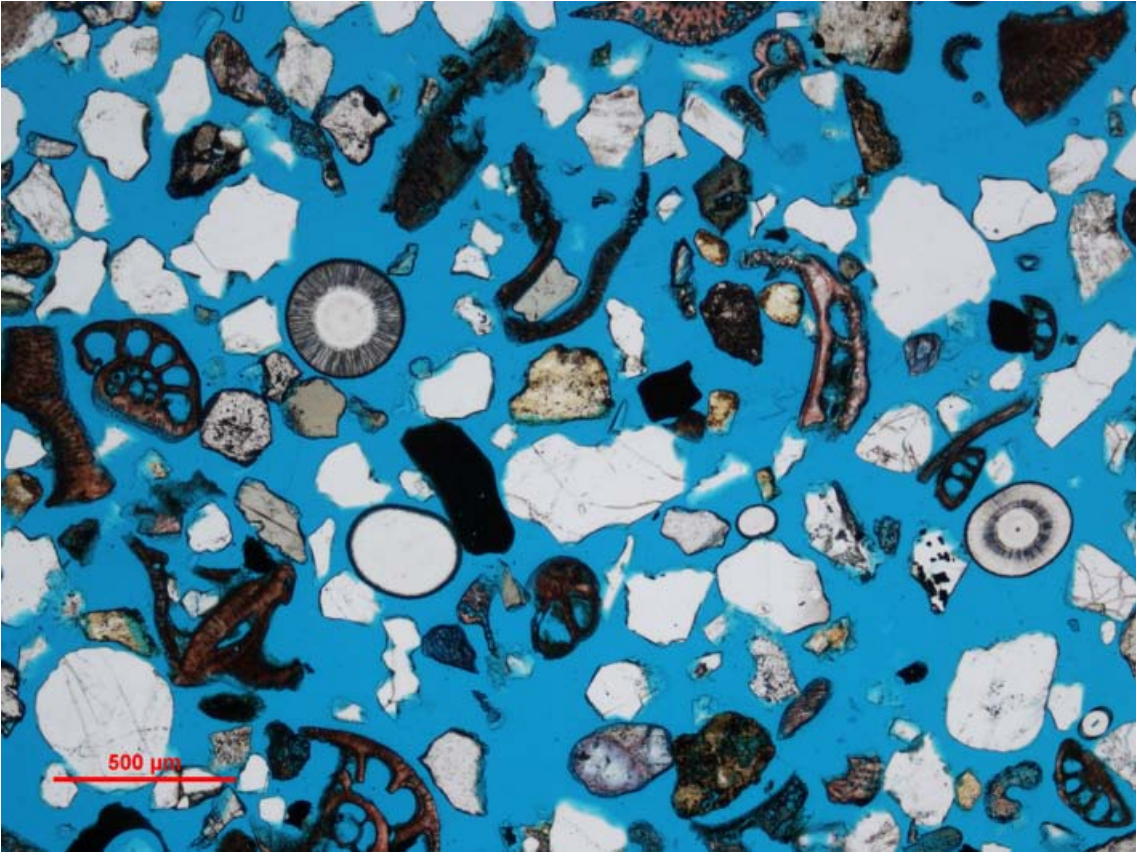
LITHOLOGY		STRUCTURES	
~ ~ ~	clay		lamination
~ ~ ~	silty clay	— — —	faint lamination
· · · ·	sand	— — —	lenses
· · · ·	gravel	≡ ~ ~	sheared/deformed
● ●	clasts	— — —	sharp boundary
	boundary between lithologies:	— — —	irregular boundary
	sharp	~ ~ ~	diffuse boundary
	diffuse	( ) (	bioturbation
		β x	mollusc shells/fragments
		β	plant remains

GC 14

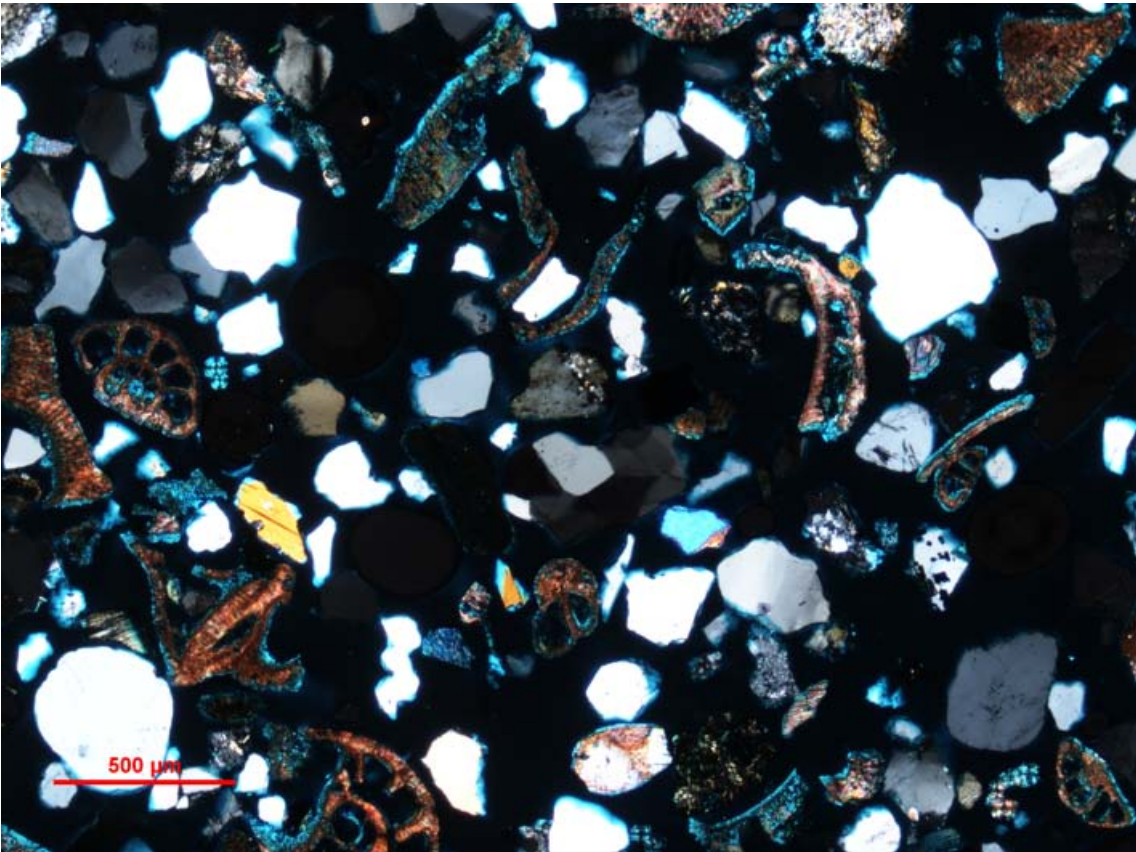


**APPENDIX 2**

**PHOTO MICROGRAPHS OF SEDIMENT SAMPLES**



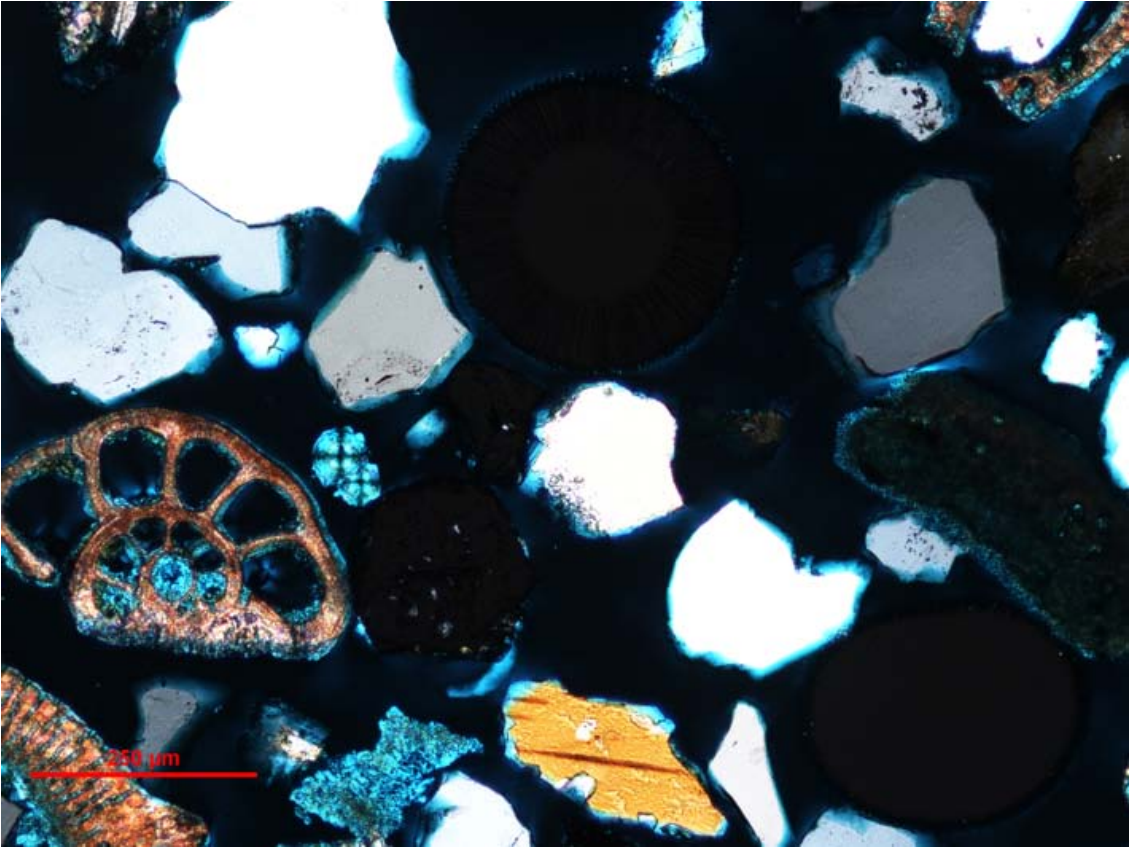
GB 1. Overview showing fossils, plane polarized light.



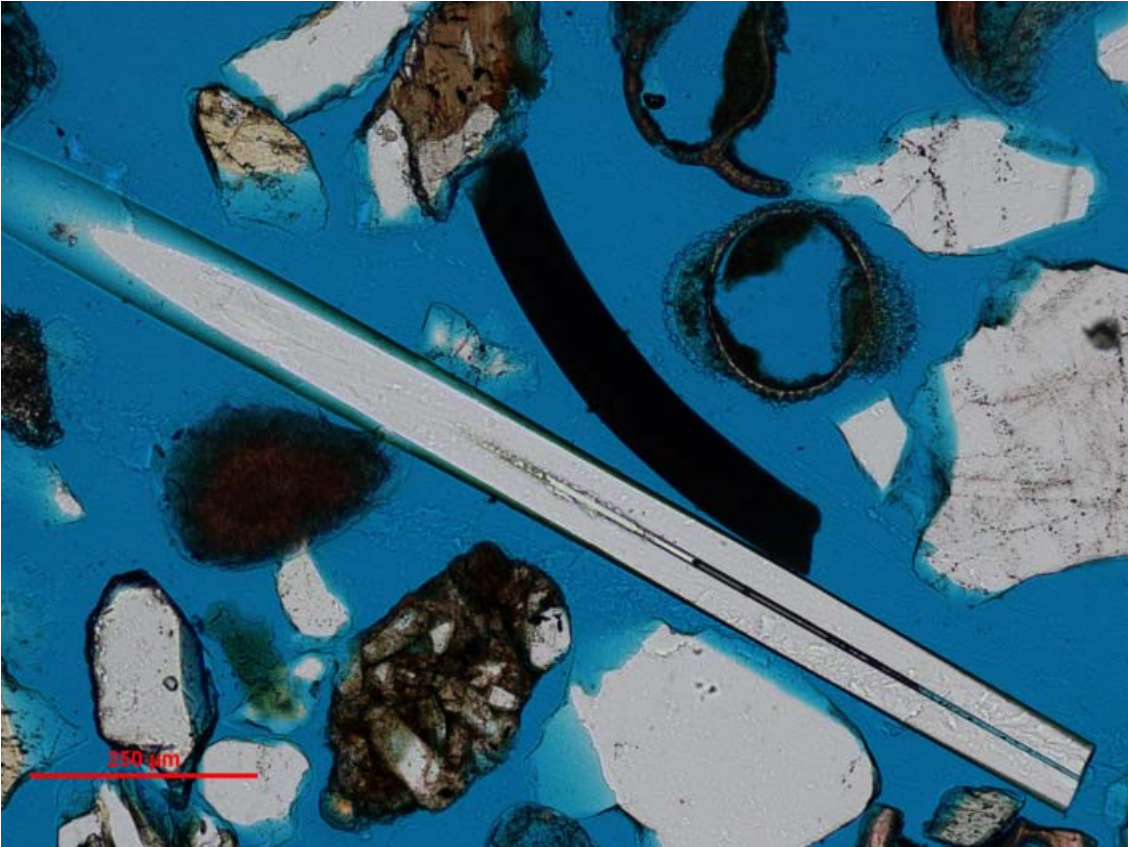
GB 1. Overview showing fossils, crossed Nicols.



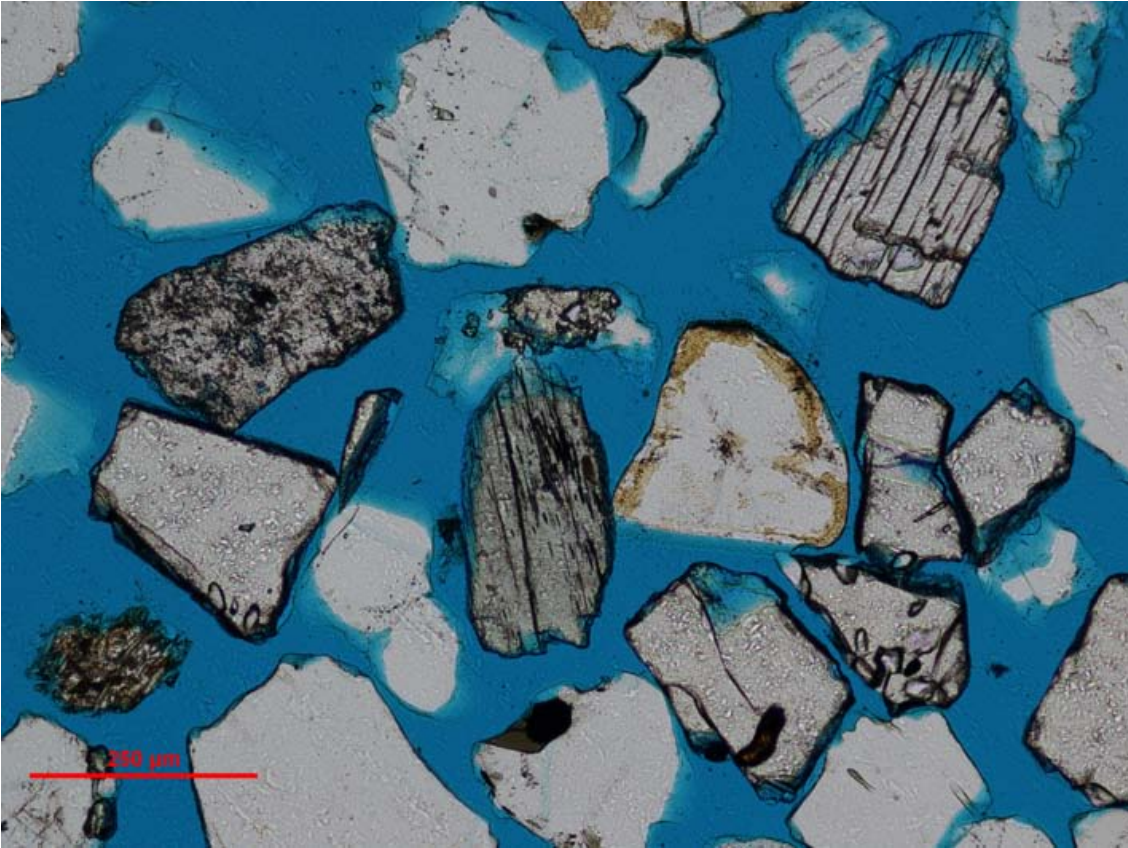
GB 1. Fossils and heavy minerals, plane polarized light.



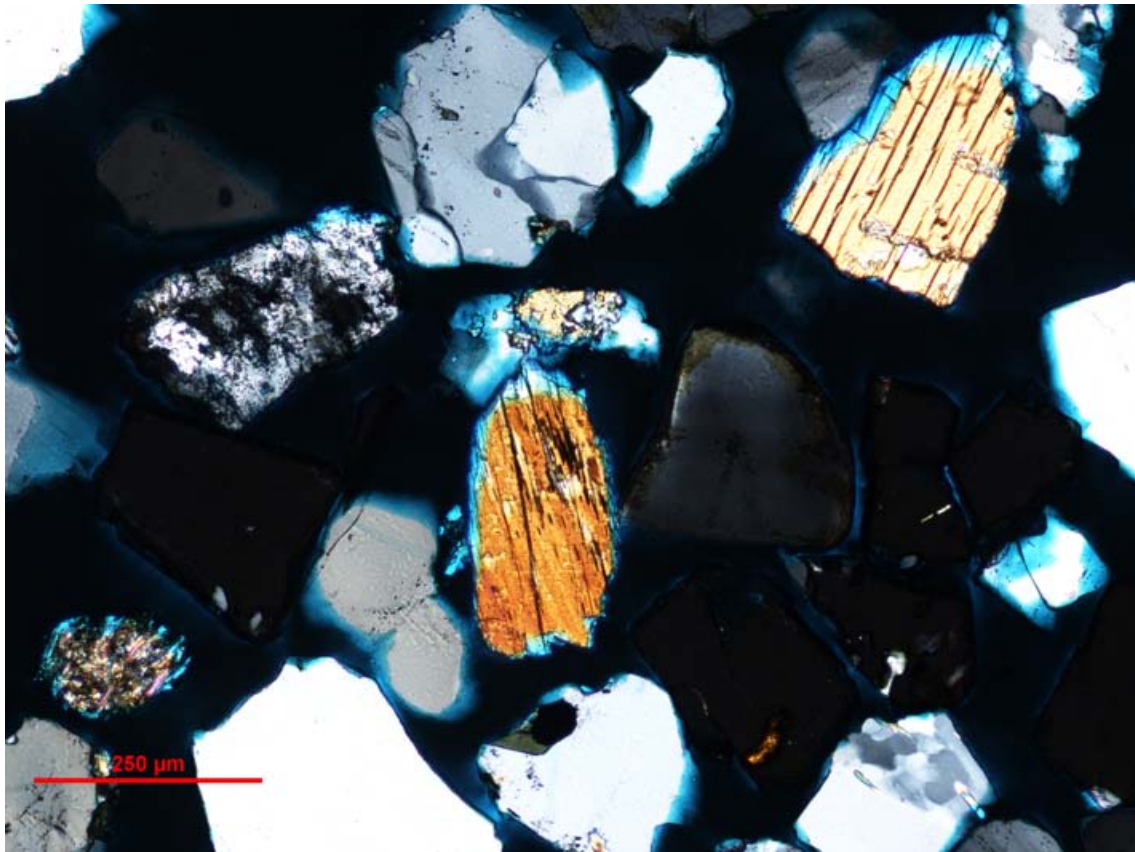
GB 1. Fossils and heavy minerals, crossed Nicols.



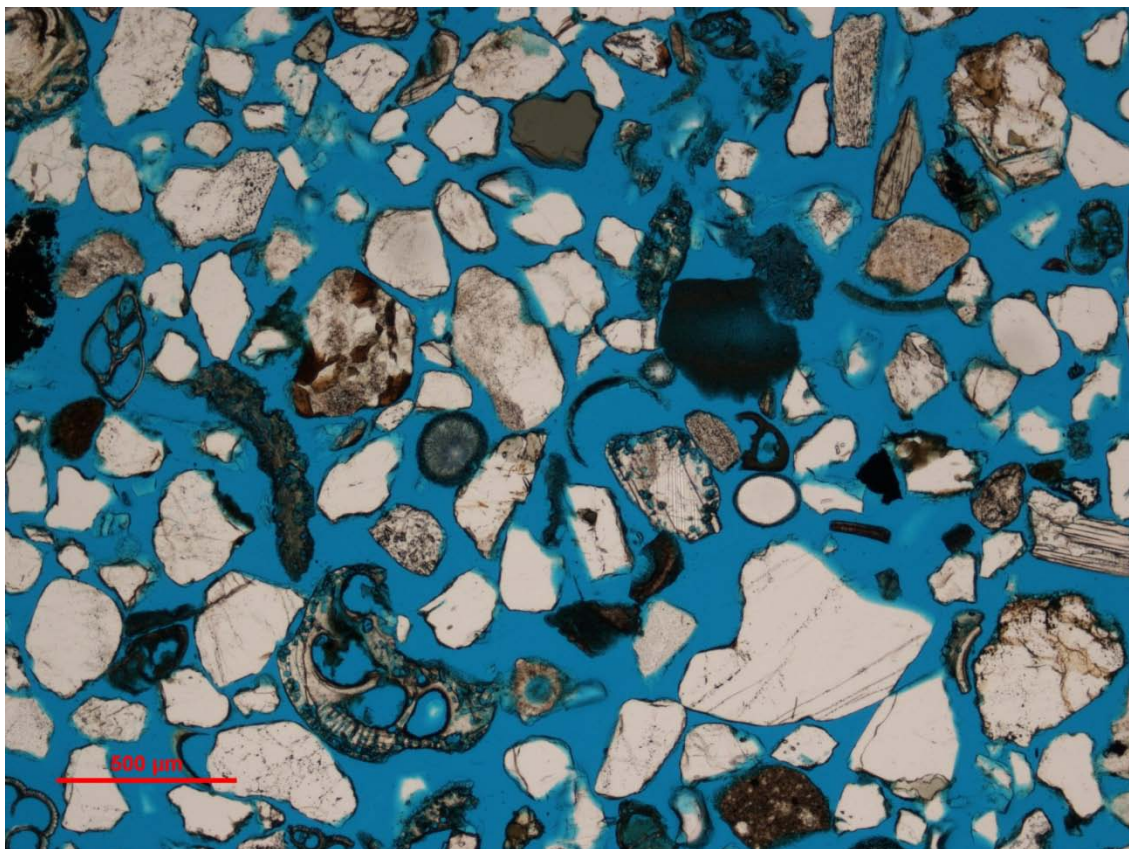
GB 1. Sponge spicule, plane polarized light.



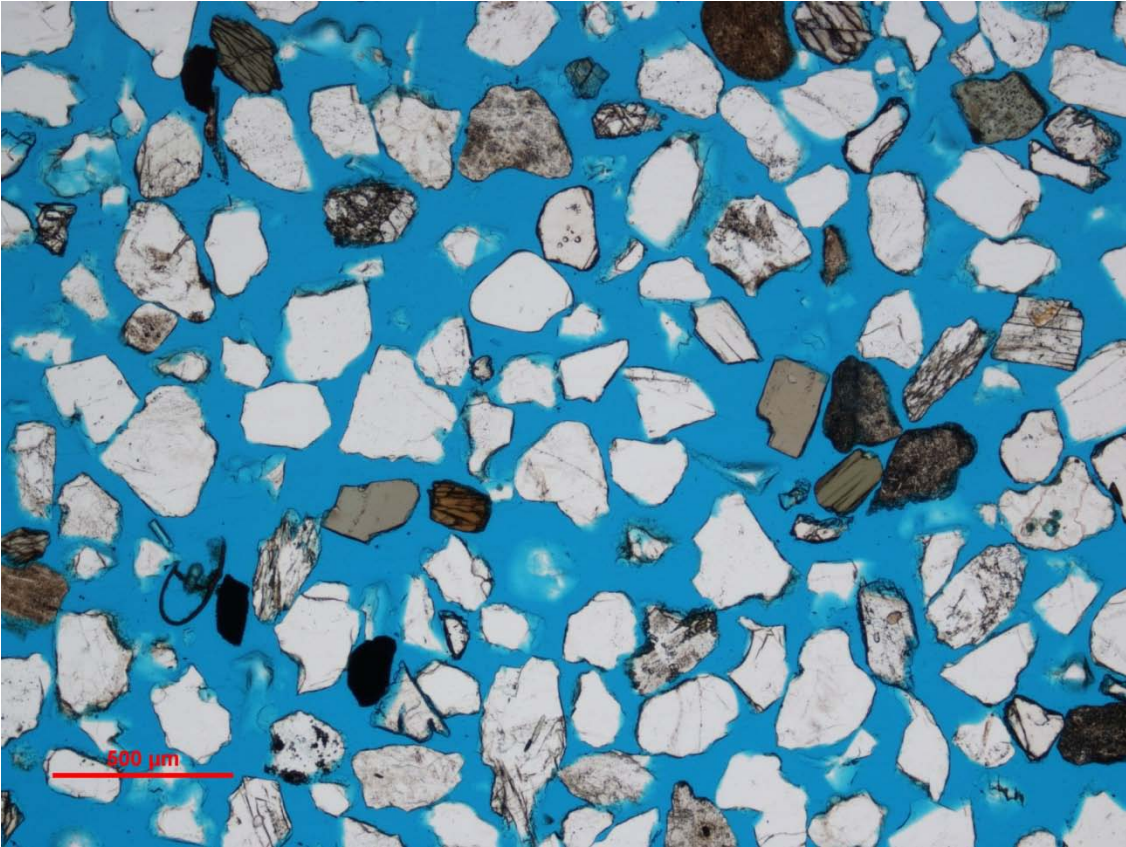
GB 7. Garnet and amphibole grains, plane polarized light.



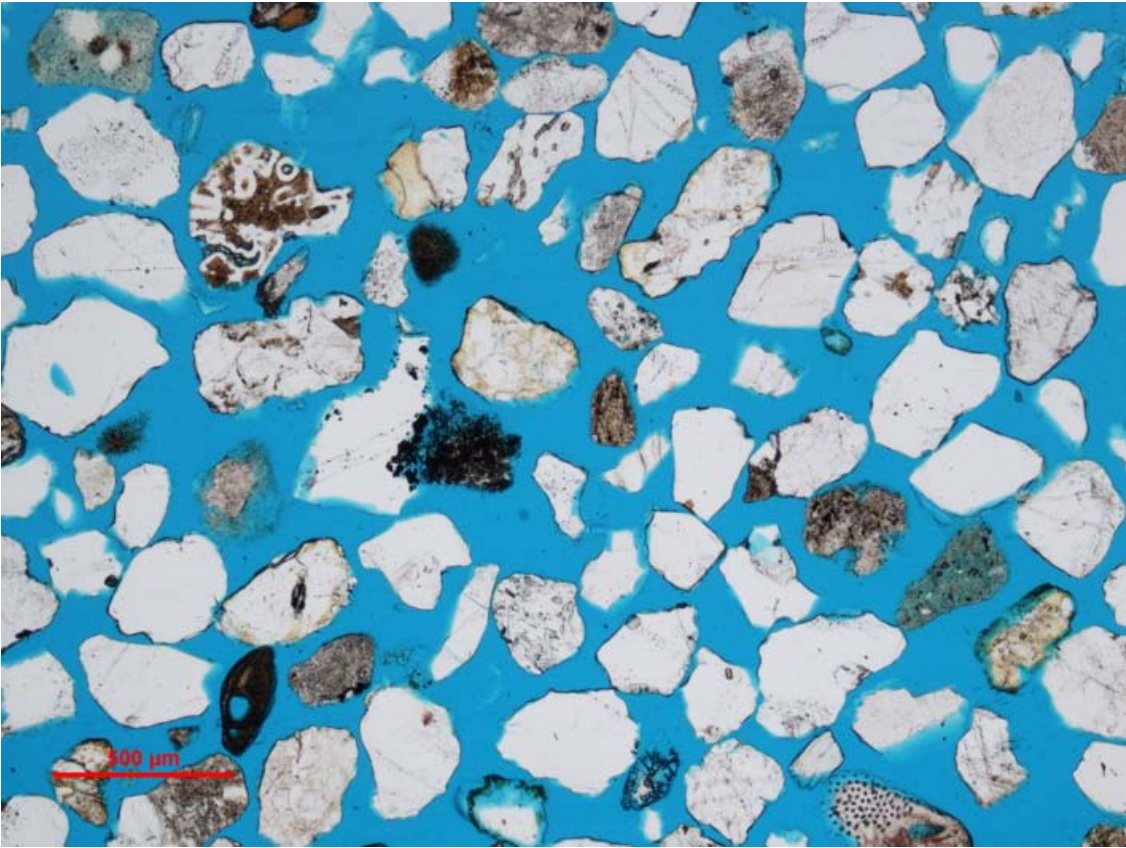
GB 7. Garnet and amphibole grains, crossed Nicols.



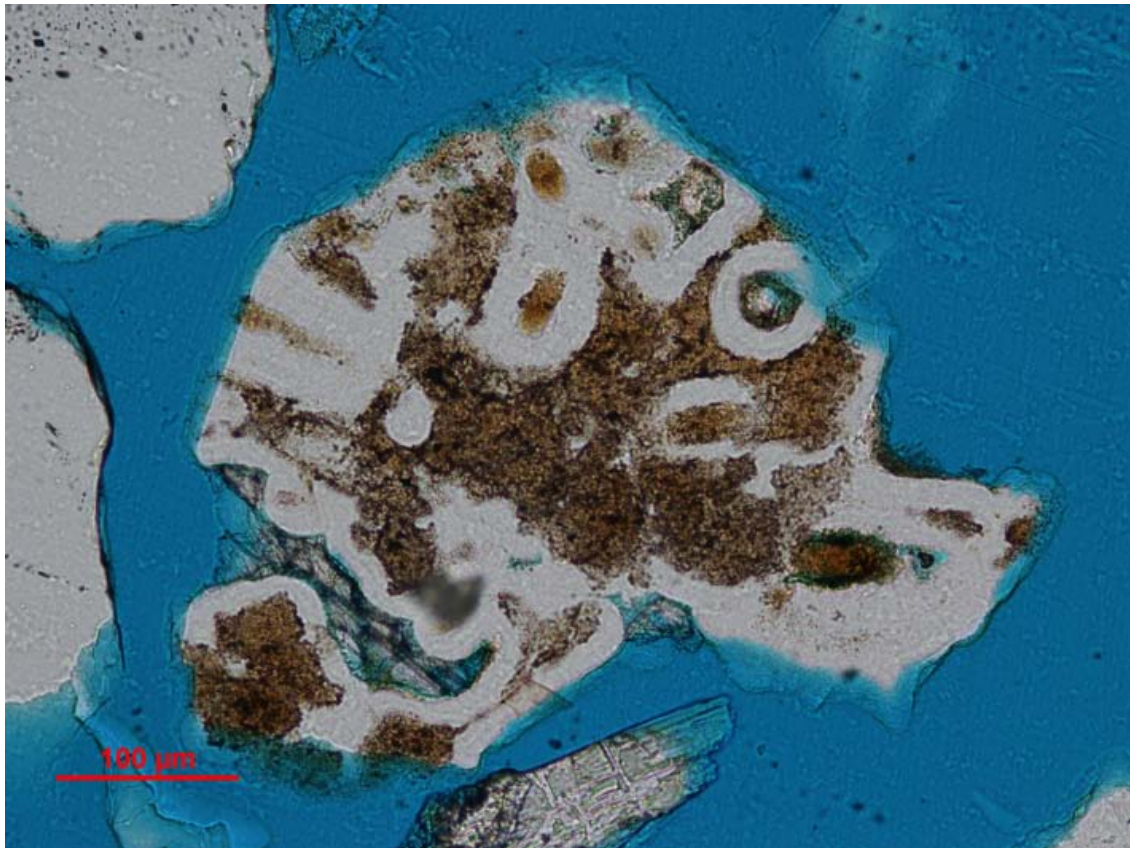
GB 10. Fossiliferous sand, plane polarized light.



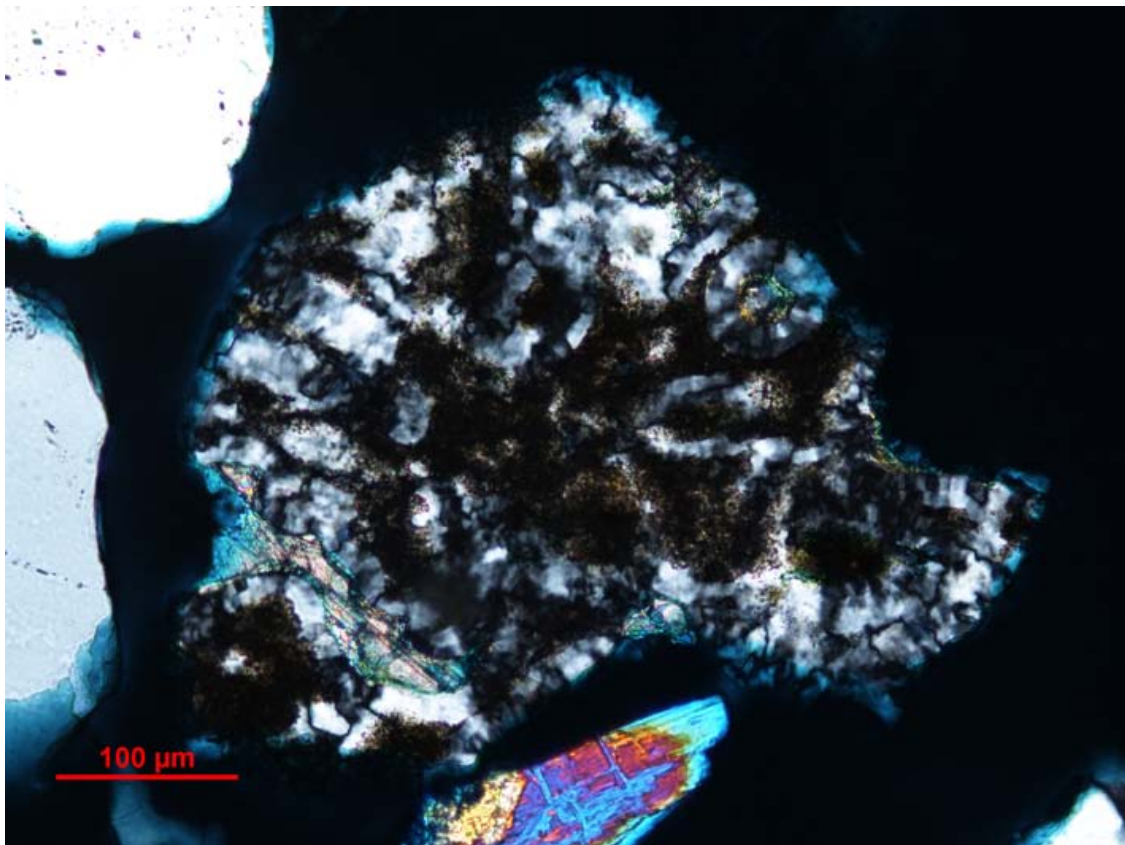
GB 12. Quartz-rich sand, plane polarized light.



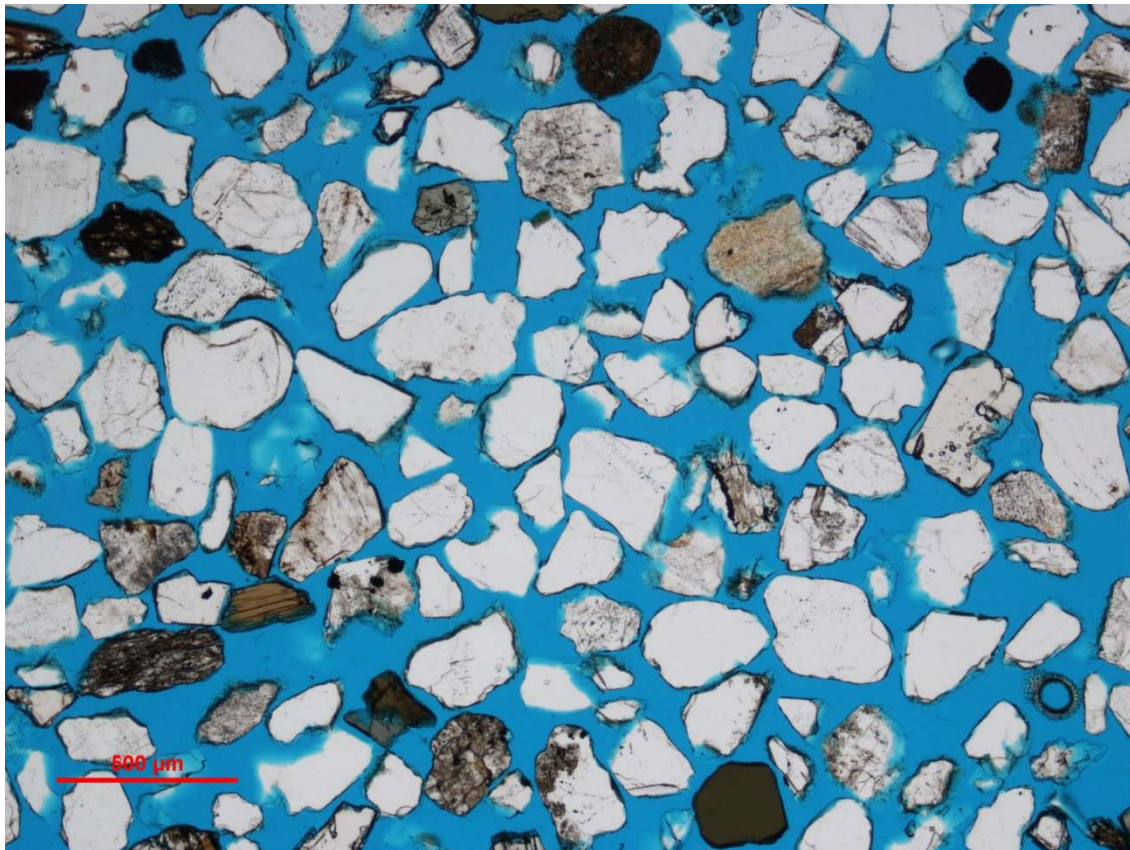
GB 15. Quartz-rich sand, plane polarized light.



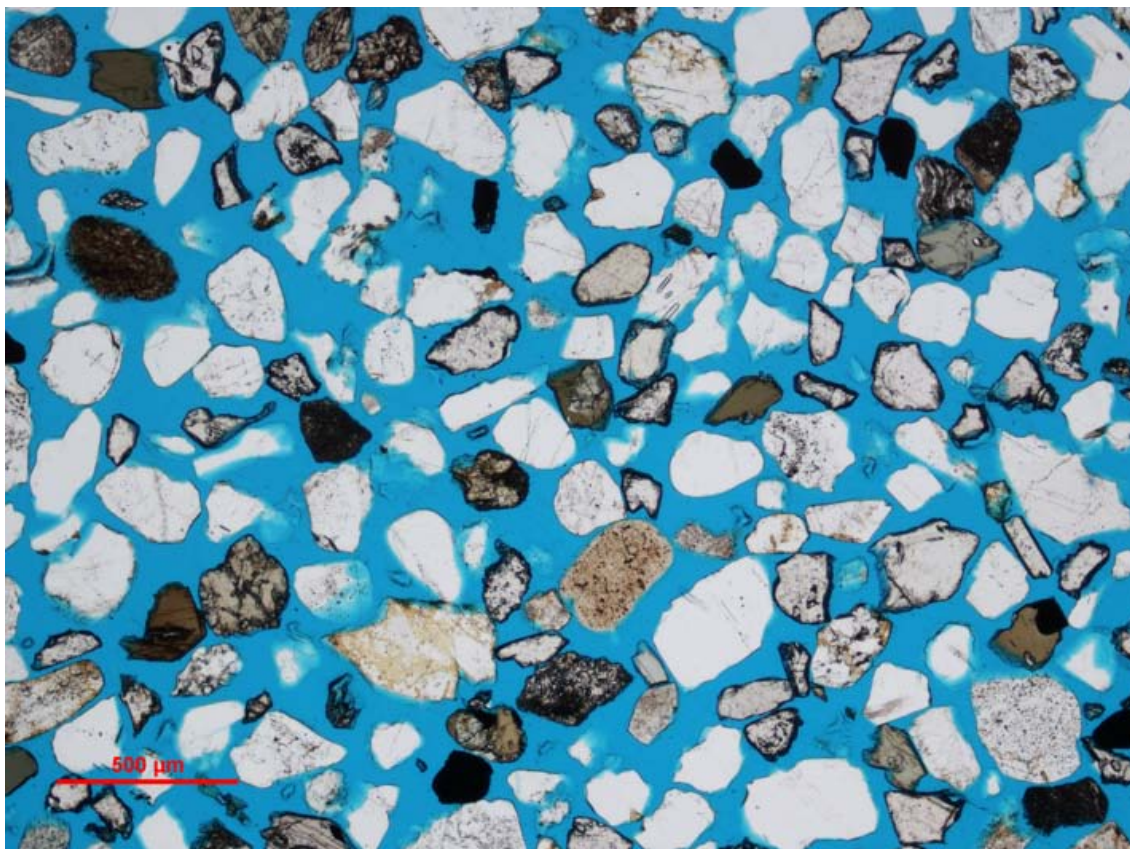
GB 15. Chert grain, plane polarized light.



GB 15. Chert grain, crossed Nicols.

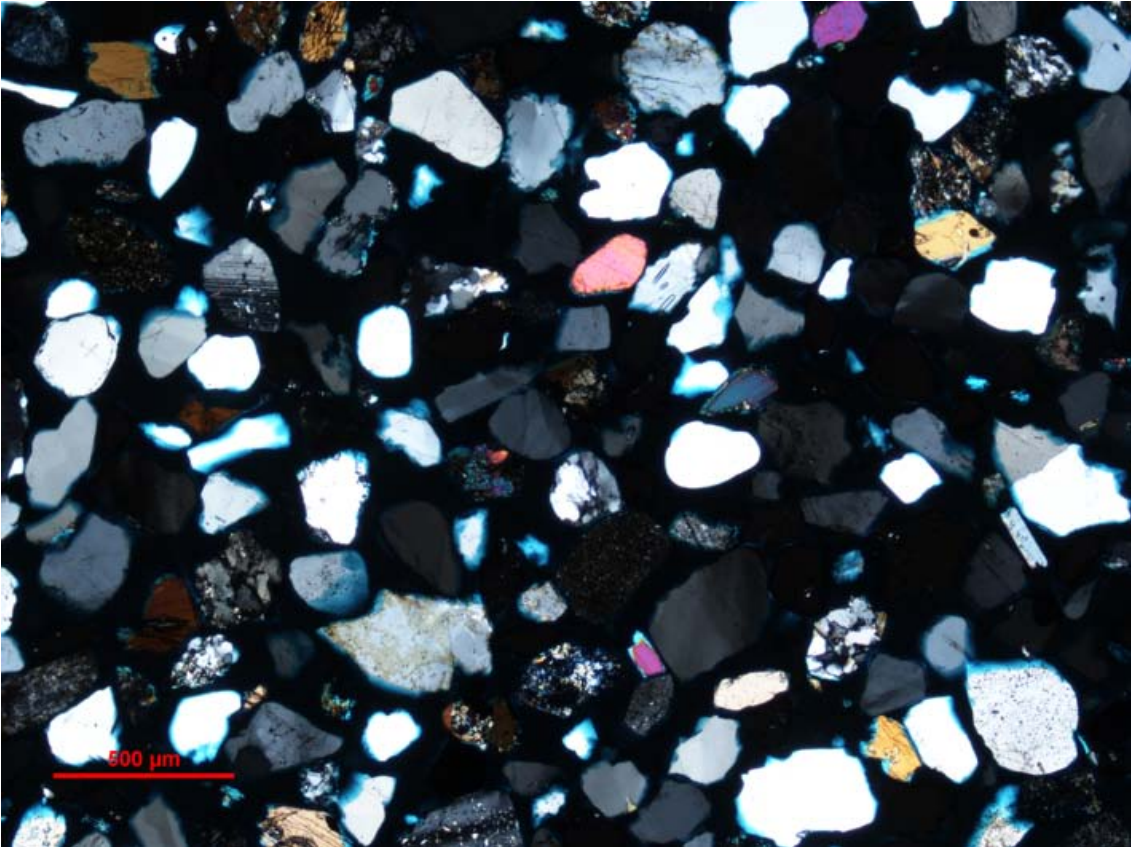


GB 18. Quartz rich sand with heavy minerals, plane polarized light.

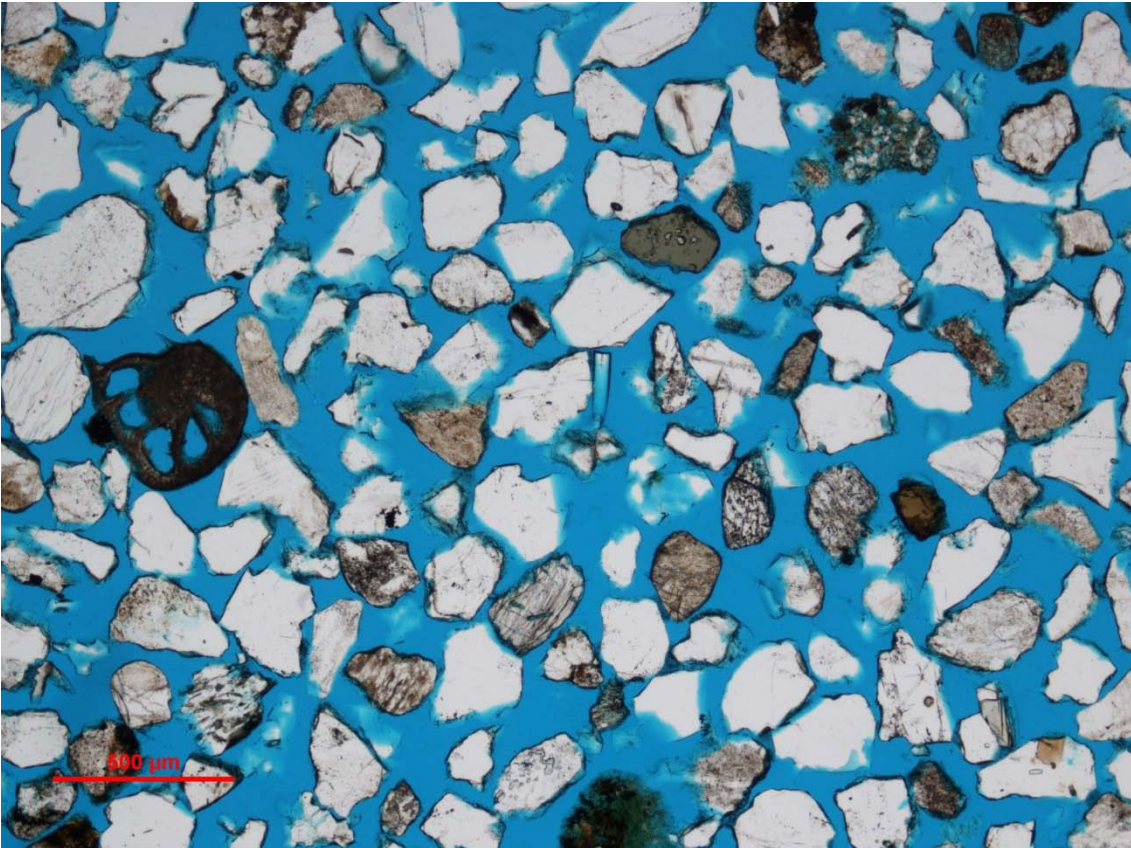


GB 22. Heavy mineral rich sand, plane polarized light.

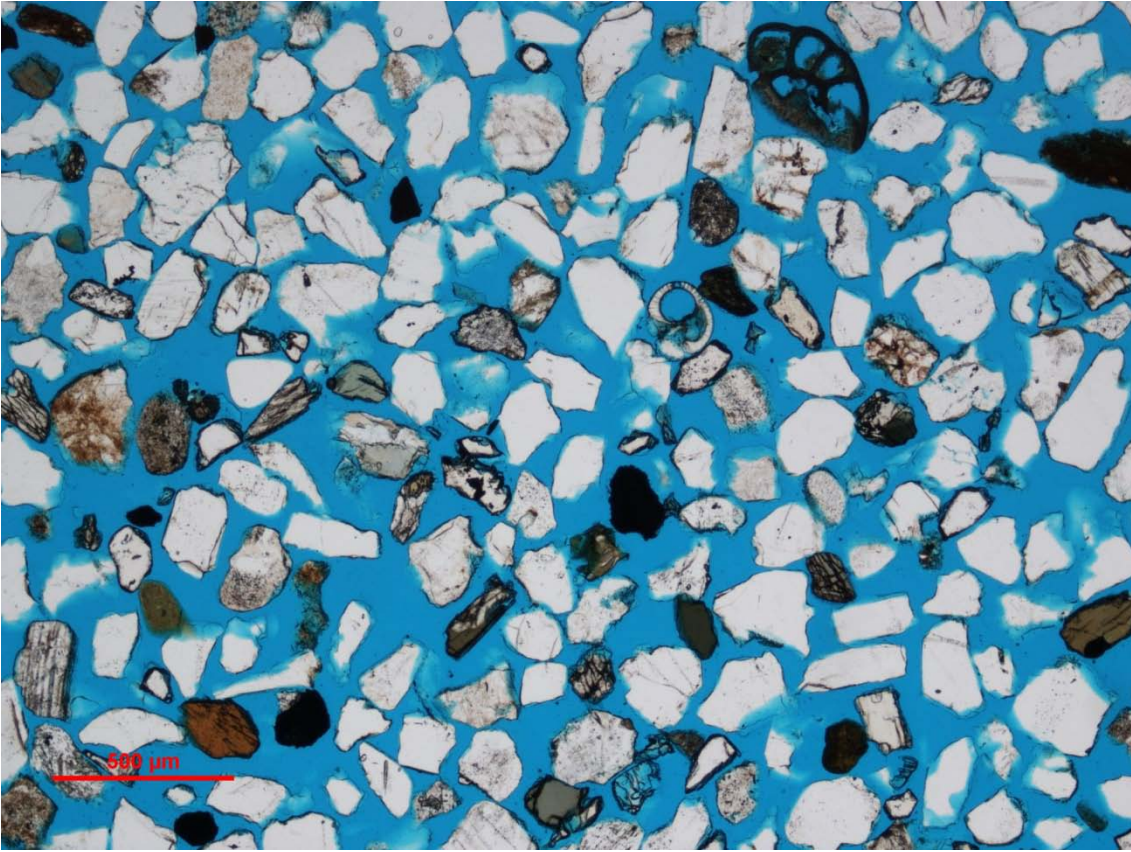




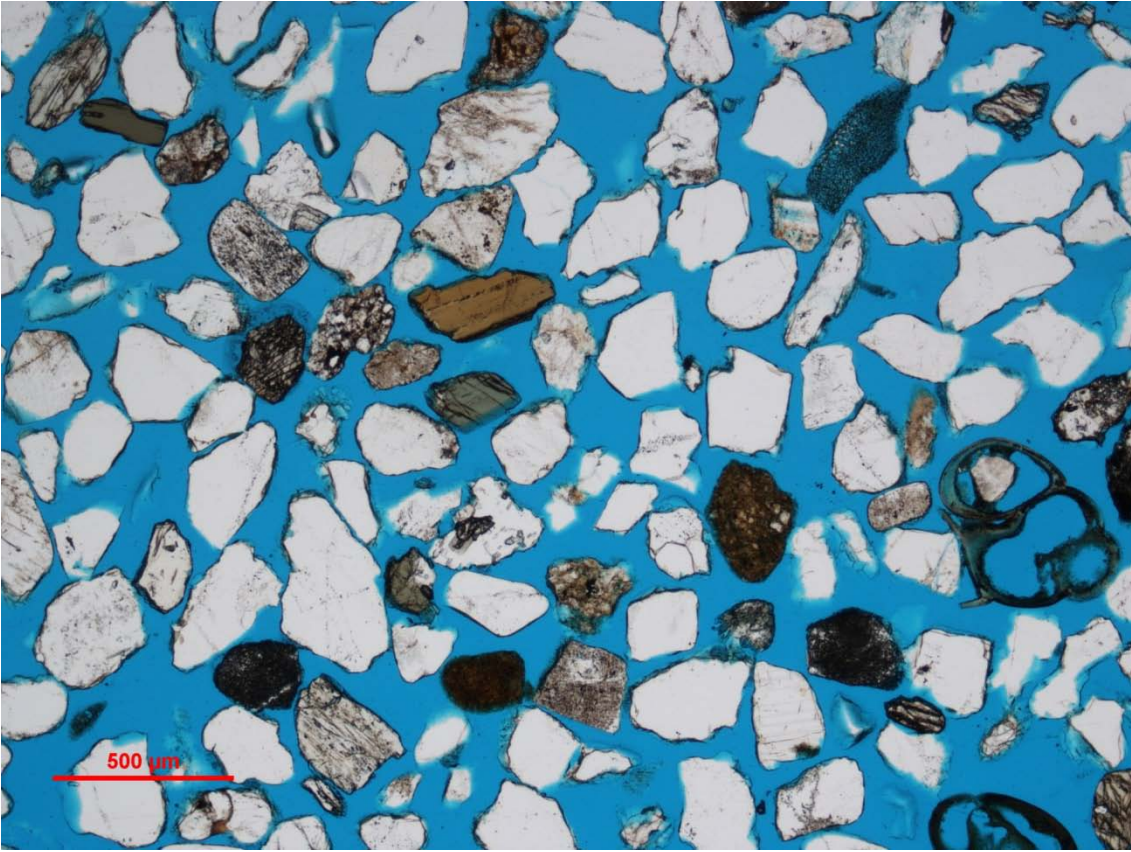
GB 22. Heavy mineral rich sand, crossed Nicols.



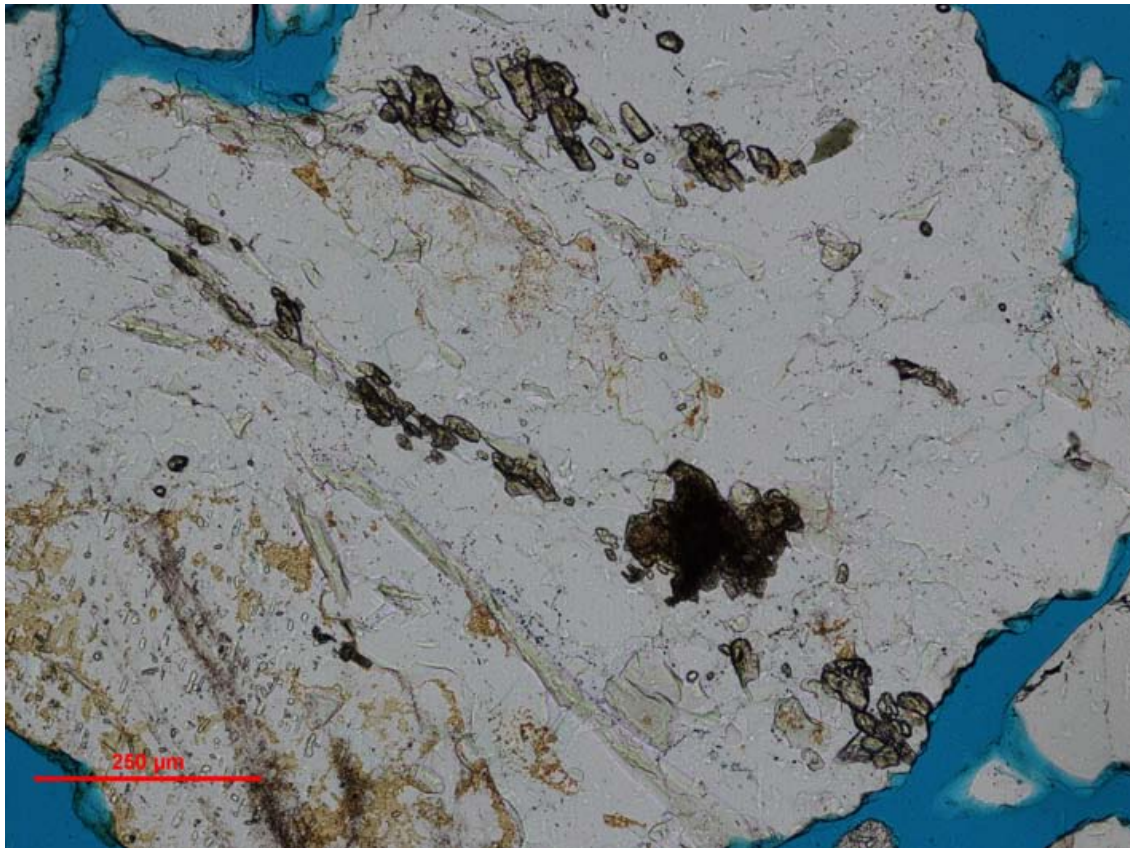
GB 26. Quartz rich sand, plane polarized light.



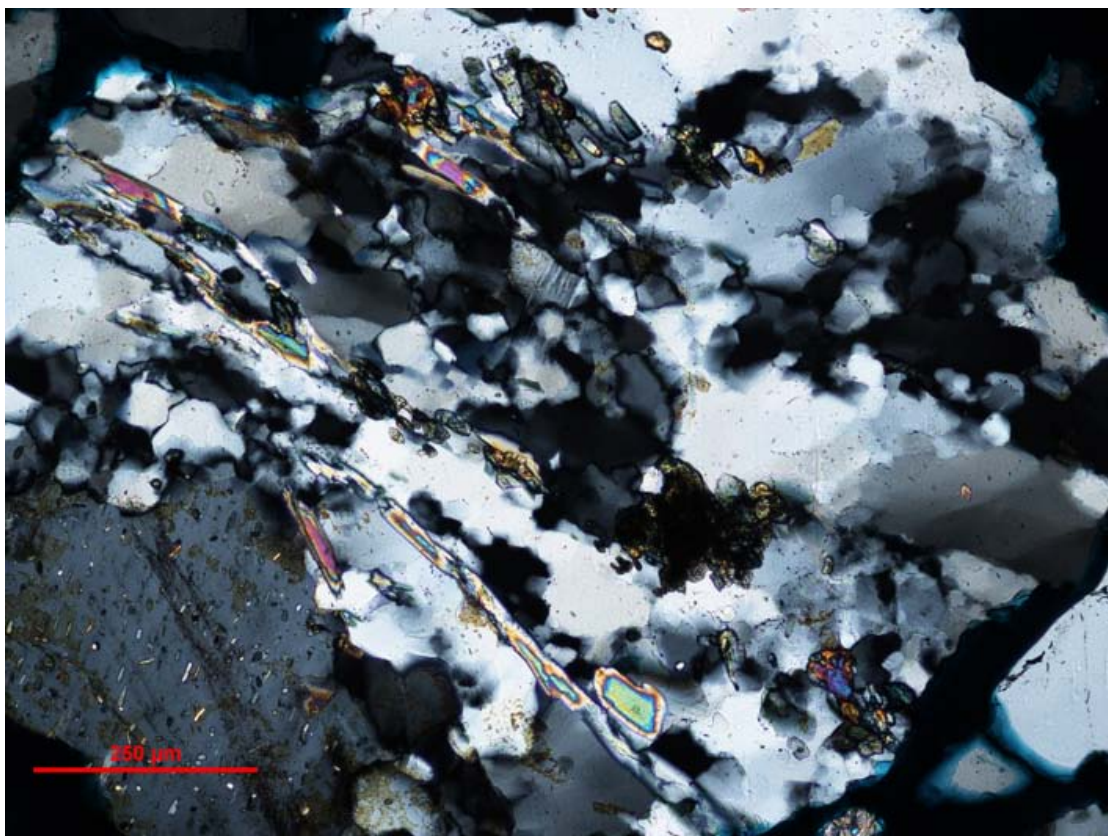
GB 27. Quartz rich sand, plane polarized light.



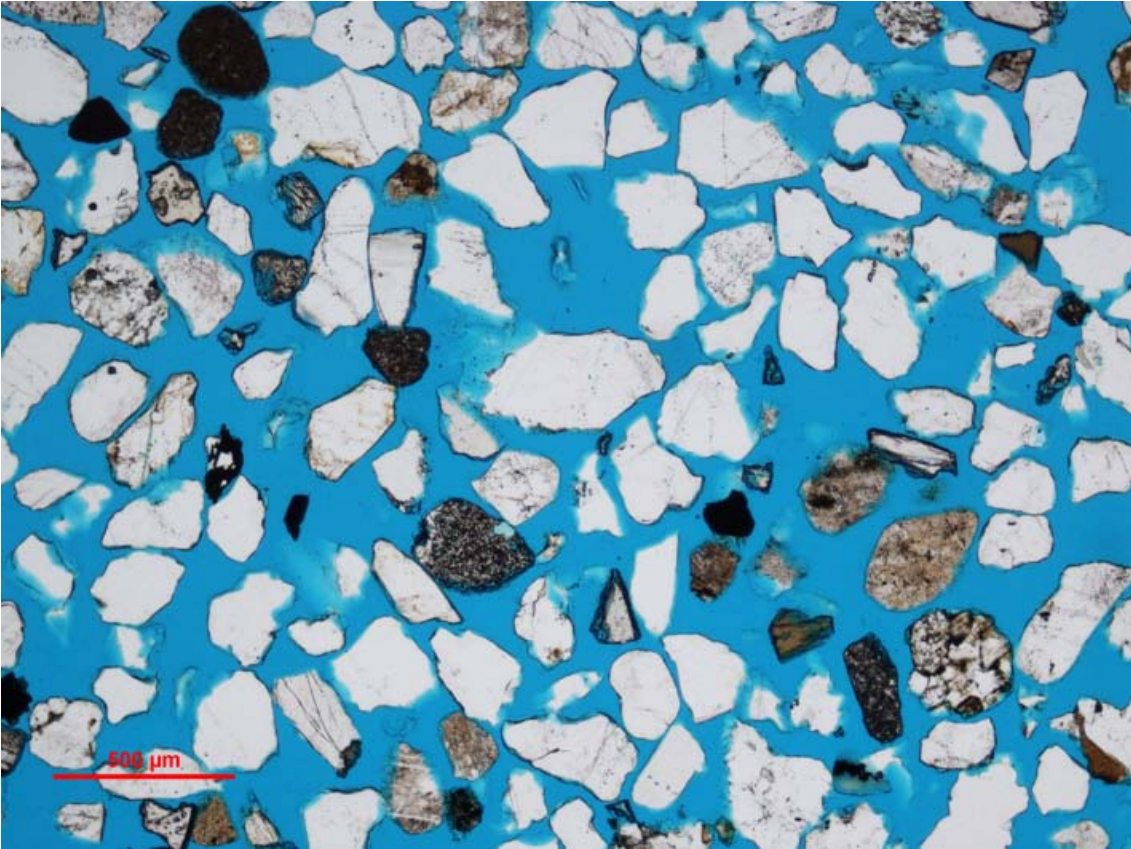
GB 29. Quartz rich sand, plane polarized light.



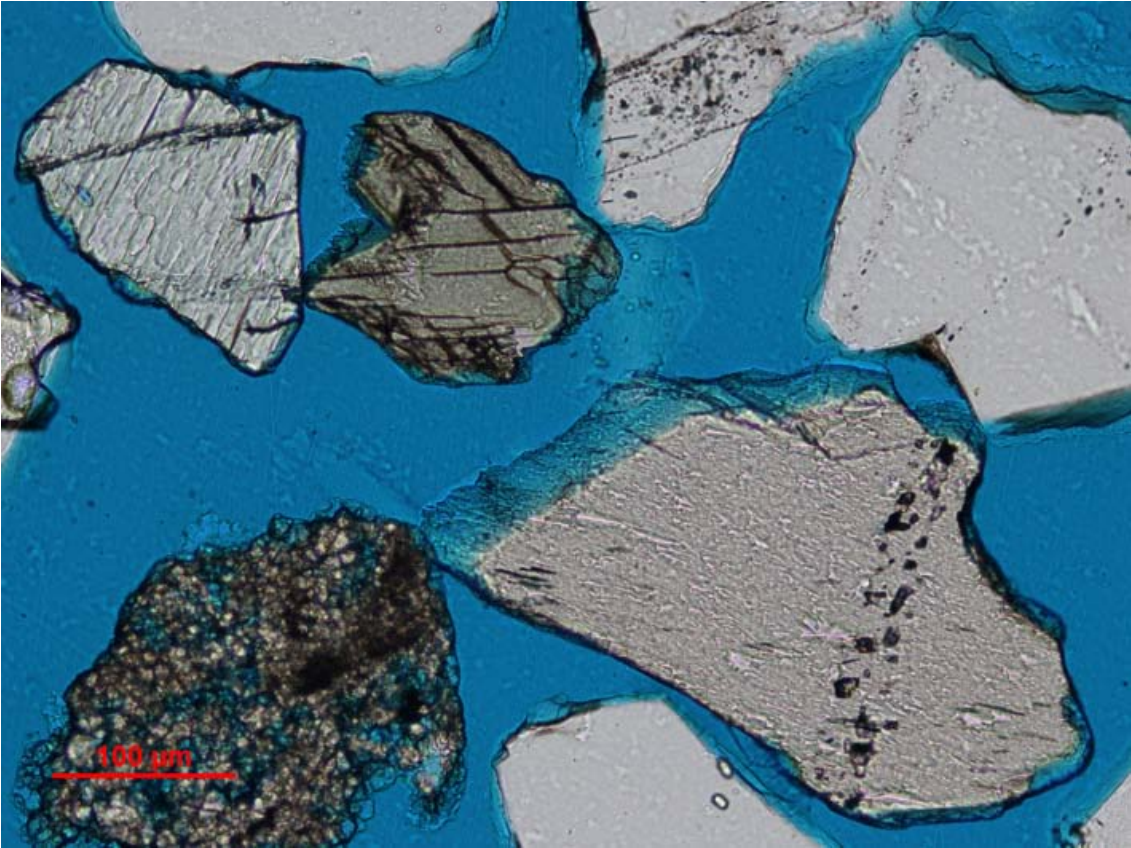
GB 31. Metamorphic bedrock fragments, plane polarized light.



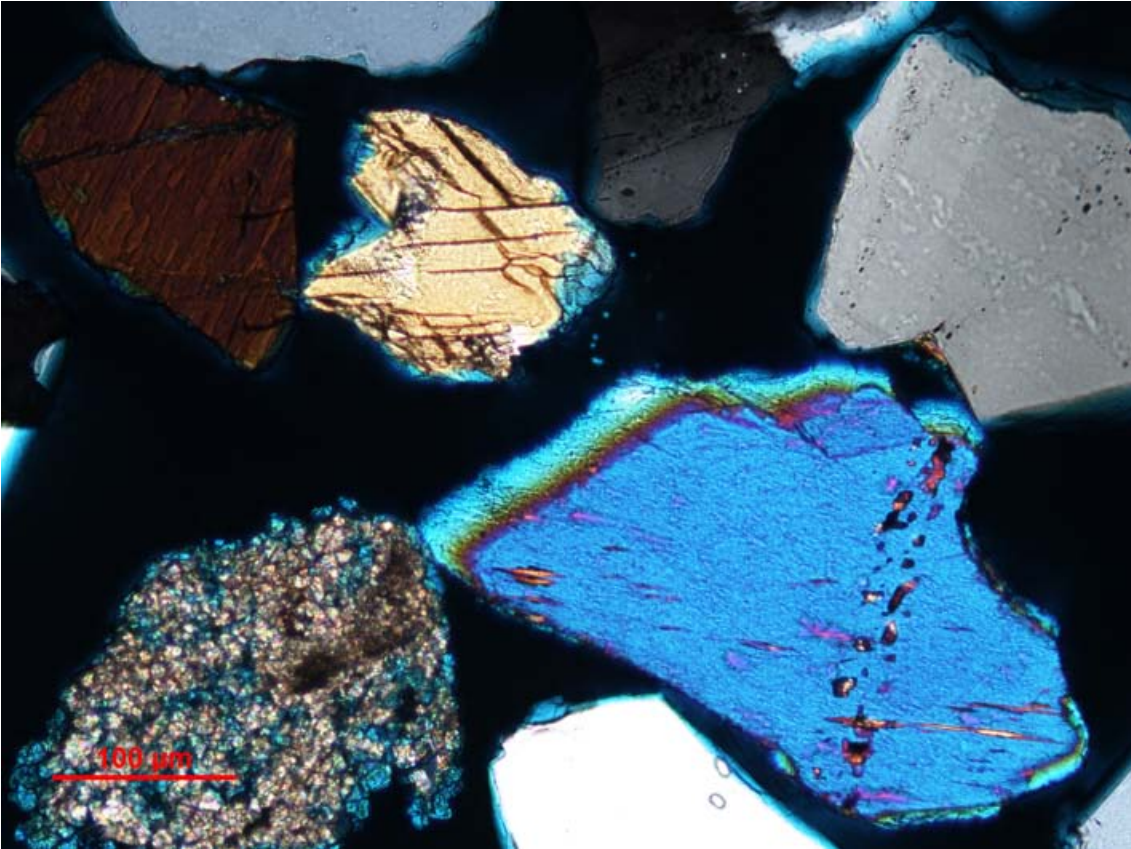
GB 31. Metamorphic bedrock fragments, crossed Nicols.



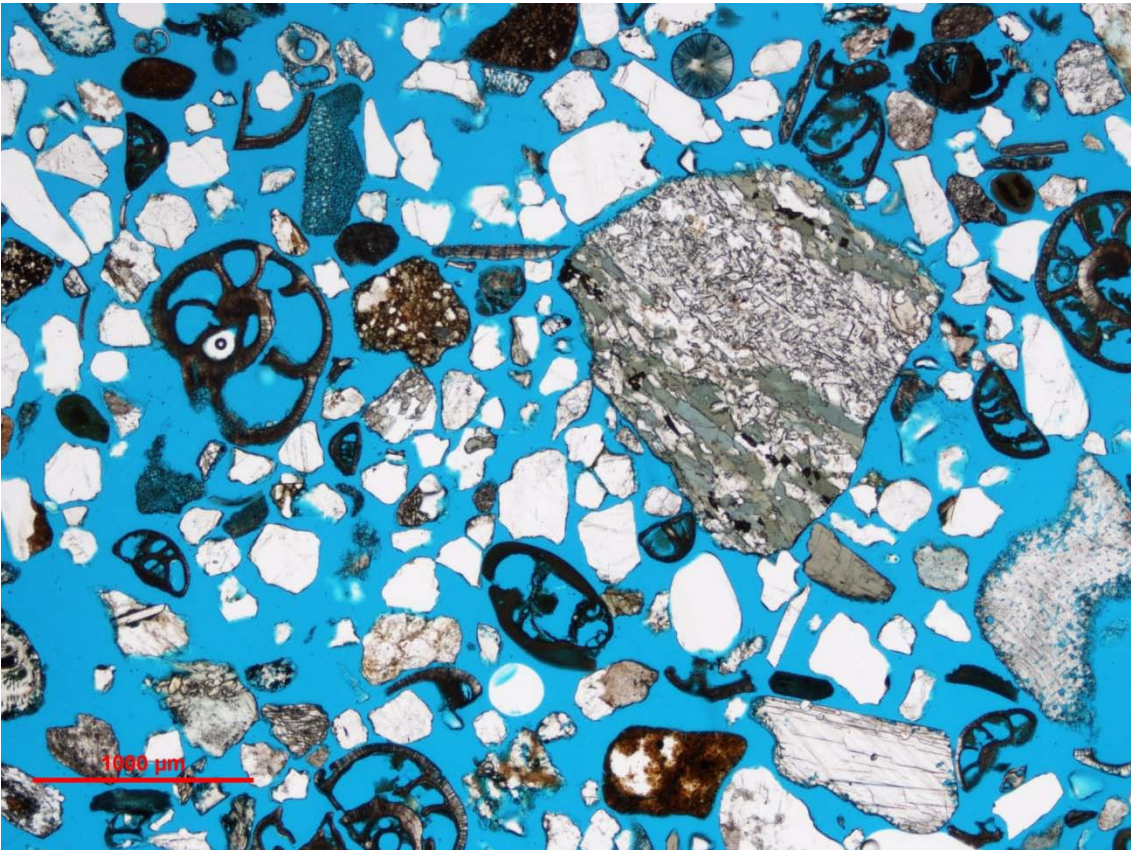
GB 34. Overview with quartz-rich sand, plane polarized light.



GB 34. Amphibole grains, plane polarized light.



GB 34. Amphibole grains, crossed Nicols.



GB 37. Overview with forams and rock fragments, plane polarized light.



Norges geologiske undersøkelse  
Postboks 6315, Sluppen  
7491 Trondheim, Norge

Besøksadresse  
Leiv Eirikssons vei 39, 7040 Trondheim

Telefon 73 90 40 00  
Telefax 73 92 16 20  
E-post [ngu@ngu.no](mailto:ngu@ngu.no)  
Nettside [www.ngu.no](http://www.ngu.no)

*Geological Survey of Norway  
PO Box 6315, Sluppen  
7491 Trondheim, Norway*

*Visitor address  
Leiv Eirikssons vei 39, 7040 Trondheim*

*Tel (+ 47) 73 90 40 00  
Fax (+ 47) 73 92 16 20  
E-mail [ngu@ngu.no](mailto:ngu@ngu.no)  
Web [www.ngu.no/en-gb/](http://www.ngu.no/en-gb/)*